

DESIGN AND OPTIMIZATION OF A FSAE VEHICLE

Submitted to the Faculty of
WORCESTER POLYTECHNIC INSTITUTE
In partial fulfilment of the requirements for this
MAJOR QUALIFYING PROJECT

By:

Matthew Chareth, ME

Eduardo Fernandez, ME

Eric Gehrken, ME

William Grebe, ME

Camden Mallette, ECE

Vincent McMahon, ME

Tyler Moser, ME

Justin Paprota, ECE

Date: May 1, 2014

Approved By:

Professor David C. Planchard, ME Advisor

Professor William R. Michalson, ECE Advisor

Abstract

The purpose of the Formula SAE Competition is to provide students the opportunity to design and build a prototype racecar for an amateur autocross racer and then demonstrate its performance in a competition setting. The project team built upon a car that was originally intended for use in the 2013 FSAE Collegiate Competition. The team performed component evaluation and reviewed past project teams' reports to determine what systems needed to be completed to make the car both operational and competitive. The areas that were addressed included the rear suspension, exhaust, continuously variable transmission (CVT), the body, and the wiring harness. All of the systems addressed were designed and validated. These subsystems were manufactured and integrated with the existing car.

Executive Summary

The Formula SAE (FSAE) competition is an annual collegiate design competition organized by the Society of Automotive Engineers (SAE). For this event, teams design and fabricate a prototype Formula style racecar targeted for use by autocross racers. The prototype car is then evaluated in a variety of static and dynamic competition events.

The static competition events evaluate the design of the car, the overall cost to manufacture the vehicle, and the team's ability to create a business case to mass produce their final product. The dynamic events evaluate the vehicle's performance characteristics. These include acceleration, cornering, handling, and reliability. In each dynamic event, the team's prototype car is driven by a student member of the team.

The 2014 MQP project team built upon a car that was originally intended for use in the 2012 FSAE Collegiate Competition. Initially, the team performed component evaluation and reviewed past project team's reports to determine which systems needed to be addressed in order to make the car both operational and competitive. At the conclusion of this analysis, it was determined that the rear suspension, continuously variable transmission (CVT), body, exhaust and wiring harness needed to be addressed. Additionally a dash and data acquisition system needed to be created for this project.

During the FSAE competition dynamic events, different forces come into play when driving these types of vehicles. An FSAE car is a highly dynamic system; forces seen in different components of the car vary greatly during its operation. These forces apply a significant load to the variety of subsystems on the vehicle, affecting its overall performance. In order to design a competitive rear suspension that would withstand these loads, extensive research was done to gain a full understanding of these forces. Furthermore, various computer aided designs were created, analyzed and improved in an iterative process. In order to test the different suspension designs, several finite element analysis (FEA) simulation models were used. To make these models as accurate as possible, the loads created during these dynamic events were calculated. By calculating these different events, the highest possible load on each component was found and was then used as an input for FEA simulations. As a result of this analysis, the final rear suspension design met the dynamic performance specifications and was implemented in the vehicle.

While analyzing of the vehicle, it was found that the current CVT system needed to be documented in depth and tuned properly to improve the vehicle's drivetrain. As a result, the CVT system was analyzed to gain an understanding of how this unique drivetrain functioned. Furthermore, various performance specifications for tuning the transmission were determined. Based on the subsystem's analysis, equations were derived and various calculations were completed in order to determine which CVT tuning components best met the performance specifications. Once the adequate CVT components were selected, these were integrated in the transmission. Lastly, performance testing was carried out in order to verify the previous calculations and confirm that the component selection was done effectively.

During the analysis of the vehicle, it was found that the rear subframe was poorly designed and manufactured. This previous design used aluminum box tubing as its main material, resulting in high stress concentrations on the box tubing corners. These high stress concentrations caused the subframe to deflect under normal driving loads. Due to poor welding, the aluminum pieces were tempered. Therefore, the aluminum did not meet its desired mechanical properties, making the previous rear subframe unusable.

To address this issue, a subframe made from round Chromoly steel tubing was designed and manufactured. Chromoly steel was selected to increase ease of welding and to meet the static and dynamic load design specifications. Additionally, using round tubing reduced the stress concentrations in the frame. Once the design was complete, it was successfully validated using Solidworks FEA. Then, it was manufactured by two outside vendors to ensure that it was properly put together. Finally, once the subframe was delivered, it was integrated with the chassis and rear suspension components.

To provide real-time telemetry and feedback to the driver, a dash mounted heads up display was developed. This system uses the information generated by the engine control unit (ECU) to display telemetry on the dash mounted screen. The monitor primarily displays the engine rpm, vehicle speed, air fuel ratios in each cylinder, and coolant temperature. Additionally, a data acquisition system was created which records the data output from the ECU. This information is commonly used by FSAE teams in order to tune and optimize the vehicles for the dynamic competition events.

Another subsystem that was identified as an area of improvement for the 2014 FSAE project was the vehicle's bodywork. The design and fabrication of a fiberglass body that would cover the front of the car's chassis was carried out in collaboration with the WPI SAE club. The body was designed to meet all FSAE requirements, provide protection to the driver against wind and other debris found on a typical autocross course, and maintain its aesthetics appeal. Issues regarding material selection, common practice, manufacturing, painting and mounting techniques were addressed. Fiberglass was used to create the designed body due to its low cost.

At the conclusion of this project, each subsystem was successfully completed and integrated with the FSAE vehicle. This resulted in a running car that can competitively complete all of the FSAE Competition dynamic events. The car was also inspected by a group not affiliated with the project team to verify that it complies with all of the competition regulations. Though the project was considered successful, the team has variety of recommendations to guide future project teams in building upon this project.

Table of Contents

| | |
|--|----------|
| DESIGN AND OPTIMIZATION OF A FSAE VEHICLE | i |
| Abstract..... | ii |
| Executive Summary | iii |
| Table of Contents..... | v |
| Table of Figures | xii |
| Table of Tables | xix |
| Overview of Formula SAE Competition | 1 |
| Rear Suspension | 2 |
| 2013 MQP Suspension Design | 2 |
| Suspension Dynamics and Loads | 4 |
| Calculating Center of Gravity..... | 4 |
| Calculating Roll Center..... | 7 |
| Dynamic Event Forces | 7 |
| Dynamic 1.5g Braking | 8 |
| Dynamic 1.5g Acceleration | 10 |
| Dynamic 1.5g Lateral Load..... | 12 |
| Dynamic 3.5g Bump | 14 |
| SolidWorks Validation | 16 |
| Subframe | 17 |
| Overview | 17 |
| Initial State | 17 |
| Objective | 18 |
| Research..... | 18 |
| Design..... | 19 |
| Preliminary Design Concepts | 21 |

| | |
|--|----|
| Concept 1: Aluminum Frame and Vertical Shocks..... | 21 |
| Concept 2: Aluminum Frame and Horizontal Shocks..... | 22 |
| Concept 3: Steel Frame and Vertical Shocks..... | 23 |
| Concept 4: Steel Frame and Horizontal Shocks | 23 |
| Concept Selection | 24 |
| Final Design | 26 |
| Analysis of Final Design | 27 |
| Refinement of Design | 31 |
| Manufacturing | 31 |
| Integration | 35 |
| Conclusion | 36 |
| Future Recommendations | 36 |
| Pushrod | 37 |
| Overview | 37 |
| Initial State | 37 |
| Objective | 38 |
| Research..... | 38 |
| Design..... | 39 |
| Preliminary Design/Concepts | 40 |
| Concept Selection | 41 |
| Final Design | 41 |
| Refinement of Design | 42 |
| Analysis of Final Design | 43 |
| Manufacturing | 49 |
| Integration | 49 |
| Conclusion | 51 |

| | |
|-----------------------------------|----|
| Future Recommendations | 51 |
| Rocker | 52 |
| Overview | 52 |
| Initial State | 52 |
| Objective | 52 |
| Research..... | 53 |
| Design..... | 53 |
| Preliminary Design/Concepts | 56 |
| Concept Selection | 57 |
| Final Design | 57 |
| Analysis of Final Design | 58 |
| Refinement of Design | 60 |
| Manufacturing | 62 |
| Integration | 63 |
| Testing | 64 |
| Final Design Revision..... | 64 |
| Conclusion | 65 |
| Future Recommendations | 66 |
| Differential..... | 67 |
| Overview | 67 |
| Initial Condition..... | 67 |
| Research..... | 68 |
| Design..... | 69 |
| Preliminary Design | 69 |
| Final Design | 70 |
| Manufacturing | 71 |

| | |
|--|----|
| Integration | 73 |
| Conclusion | 73 |
| Summary | 73 |
| Future Recommendations | 73 |
| Continuously Variable Transmission (CVT) | 74 |
| Overview | 74 |
| Initial Condition and Past Work | 74 |
| Objectives & Criteria | 76 |
| Background Research | 76 |
| Olav Aaen's Clutch Tuning Handbook | 76 |
| Tuning the Primary/Driver Clutch | 77 |
| Tuning the Secondary/Driven Clutch: | 81 |
| Efficiency: Drive Ratio and Belt Tension | 81 |
| Drive Ratio | 82 |
| CVT Belt Pressure | 83 |
| Design | 85 |
| Current CVT Components | 85 |
| Calculations | 86 |
| Other CVT Equations | 90 |
| New Secondary Clutch vs Old Secondary Clutch | 91 |
| CVT Primary Verification | 92 |
| Testing | 92 |
| Integration | 92 |
| Summary/Conclusion | 93 |
| Electrical | 94 |
| Heads up Display (HUD) | 94 |

| | |
|------------------------------------|-----|
| Introduction | 94 |
| Previous Design | 94 |
| Hardware Research and Design..... | 95 |
| The CAN Bus | 95 |
| Arduino CAN Bus Interface..... | 97 |
| Engine Parameters..... | 98 |
| RPM | 98 |
| Road Speed | 99 |
| Coolant Temperature..... | 100 |
| Fuel Pressure | 101 |
| Air Fuel Ratios | 102 |
| Synchronization | 102 |
| Software Research and Design | 103 |
| Architecture | 104 |
| Artist's Rendition | 105 |
| Implemented Code | 106 |
| Integration | 108 |
| Wiring Harness | 110 |
| Overview/Background | 110 |
| Initial Condition..... | 110 |
| Objective | 110 |
| Research and Design..... | 110 |
| Integration | 116 |
| Battery Mount..... | 122 |
| Overview | 122 |
| Initial Condition..... | 122 |

| | |
|----------------------------------|-----|
| Research..... | 122 |
| Design..... | 123 |
| Preliminary Design | 123 |
| Concept Selection | 124 |
| Final Design | 124 |
| Manufacturing | 124 |
| Integration | 125 |
| Testing | 126 |
| Conclusion | 126 |
| Summary..... | 126 |
| Future Recommendations | 127 |
| Body | 128 |
| Overview | 128 |
| Initial Condition | 128 |
| Objectives | 129 |
| Research..... | 129 |
| Hand Lay-Up | 130 |
| Vacuum Bagging..... | 131 |
| Spray-Up..... | 131 |
| Body Design Specifications | 132 |
| Integration with Frame..... | 133 |
| Body Design..... | 133 |
| Preliminary Design | 133 |
| Concept Selection | 134 |
| Final Design | 135 |
| Manufacturing | 135 |

| | |
|--|-----|
| Creating the Mold | 136 |
| Preparation for Fiberglass Molding | 138 |
| Fiberglass Molding | 140 |
| Painting | 142 |
| Integration | 143 |
| Testing | 143 |
| Conclusion | 143 |
| Exhaust | 144 |
| Exhaust System | 144 |
| Overview/Background | 144 |
| Initial Condition | 144 |
| Objective | 144 |
| Research | 144 |
| Design | 145 |
| Sound Design Analysis | 145 |
| Preliminary Design/Concepts | 145 |
| Designing a Muffler Bracket | 147 |
| Refinement of Design | 148 |
| Conclusion | 149 |
| Outside Vendors | 150 |
| References | 151 |
| Appendix | 152 |
| Display Code | 152 |
| Serial Port Code | 158 |
| Arduino Code | 162 |

Table of Figures

| | |
|--|----|
| Figure 1: Arm Lengths and Camber Gain (2013 MQP)..... | 3 |
| Figure 2: Pushrod Design (2013 MQP) | 3 |
| Figure 3: Rear Subframe (2013 MQP) | 4 |
| Figure 4: FSAE Car Corner Weights | 4 |
| Figure 5: Static CoG Location | 5 |
| Figure 6: Front Weight at 5.27° | 6 |
| Figure 7: Height of CoG | 6 |
| Figure 8: Suspension Roll Center Calculation | 7 |
| Figure 9: Load Transfer during 1.5g Braking..... | 8 |
| Figure 10: Suspension Coordinates | 9 |
| Figure 11: Suspension Arm and Pushrod Forces Under 1.5g Deceleration..... | 10 |
| Figure 12: Load Transfer during 1.5g Acceleration..... | 11 |
| Figure 13: Suspension Arm and Pushrod Forces under 1.5g Acceleration..... | 12 |
| Figure 14: Load Transfer during 1.5g Lateral Load | 13 |
| Figure 15: Suspension Arm and Pushrod Forces under 1.5g Lateral Acceleration | 14 |
| Figure 16: Load Transfer during 1.5g Lateral Load | 15 |
| Figure 17: Suspension Arm and Pushrod Forces under 1.5g Lateral Acceleration | 16 |
| Figure 18: Welded Aluminum Rear Subframe on Car..... | 18 |
| Figure 19: Subframe Aluminum Box Design Concept..... | 20 |
| Figure 20: Round Tube Concept Subframe..... | 20 |
| Figure 21: Tube Subframe Concept Mounted Onto Chassis | 21 |
| Figure 22: Visual Representation of Concept One | 22 |
| Figure 23: Visual Representation of Concept Two | 22 |
| Figure 24: Visual Representation of Concept Three..... | 23 |
| Figure 25: Visual Representation of Concept Four..... | 24 |

| | |
|---|----|
| Figure 26: Final Subframe Design..... | 27 |
| Figure 27: Subframe Mesh..... | 27 |
| Figure 28: Applied Loads and Fixtures..... | 28 |
| Figure 29: Factor of Safety for Subframe | 29 |
| Figure 30: Stresses on Subframe..... | 30 |
| Figure 31: Displacement Subframe | 30 |
| Figure 32: View of Camber Adjustment Tabs and Max Negative Camber | 31 |
| Figure 33: Subframe Drawing | 32 |
| Figure 34: Frame Tabs during Manufacturing | 32 |
| Figure 35: Welded Frame | 33 |
| Figure 36: Welding of Subframe..... | 33 |
| Figure 37: Final Subframe with Tabs..... | 34 |
| Figure 38: Painted Suspension Parts..... | 35 |
| Figure 39: Subframe Installed | 35 |
| Figure 40: Top View of Angled Push Rod..... | 37 |
| Figure 41: Sheared Off Mounting Tabs | 38 |
| Figure 42: Example of Pushrod Suspension | 39 |
| Figure 43: Pullrod vs Pushrod..... | 39 |
| Figure 44: Pushrod Design | 40 |
| Figure 45: Pushrod | 41 |
| Figure 46: Final Pushrod with Thin Rib | 42 |
| Figure 47: Refined Pushrod Design | 43 |
| Figure 48: Pushrod without Rib Mesh | 43 |
| Figure 49: Applied Loads and Fixtures..... | 44 |
| Figure 50: Factor of Safety for Pushrod without Rib | 45 |
| Figure 51: Stresses on Pushrod without Rib | 45 |

| | |
|--|----|
| Figure 52: Displacement Pushrod without Rib..... | 46 |
| Figure 53: Pushrod with Rib Mesh | 46 |
| Figure 54: Applied Loads and Fixtures..... | 47 |
| Figure 55: Factor of Safety for Pushrod with Rib | 47 |
| Figure 56: Stresses on Pushrod with Rib | 48 |
| Figure 57: Displacement Pushrod with Rib..... | 48 |
| Figure 58: Machined Pushrod and Rib | 49 |
| Figure 59: Pushrod Assembly | 50 |
| Figure 60: Pushrod System..... | 50 |
| Figure 61: Suspension at Ride Height..... | 51 |
| Figure 62: Rocker Angles..... | 52 |
| Figure 63: Example of Single Plane Flat Rockers | 53 |
| Figure 64: Rocker Design Concept One..... | 53 |
| Figure 65: Top View of the New Pushrod Design | 54 |
| Figure 66: Second Rocker Design Concept | 55 |
| Figure 67: Top View of the Second Design | 55 |
| Figure 68: Rocker Design One..... | 56 |
| Figure 69: Rocker Design Two..... | 56 |
| Figure 70: Rocker Design Three | 57 |
| Figure 71: Final Rocker Design..... | 58 |
| Figure 72: Rocker Mesh..... | 58 |
| Figure 73: Applied Loads and Fixtures..... | 59 |
| Figure 74: Factor of Safety for Rocker | 59 |
| Figure 75: Stresses on Rocker..... | 60 |
| Figure 76: Displacement Rocker | 60 |
| Figure 77: Ride Height | 61 |

| | |
|--|----|
| Figure 78: Full Bump..... | 61 |
| Figure 79: Full Droop | 62 |
| Figure 80: Rocker Assembled on Car | 63 |
| Figure 81: Rocker Assembly | 63 |
| Figure 82: Pushrod System..... | 64 |
| Figure 83: Factor of Safety for Rocker Revision..... | 65 |
| Figure 84: Welded Rocker | 65 |
| Figure 85: Old Differential Bearing | 67 |
| Figure 86: Gap between Housing and Bearing..... | 68 |
| Figure 87: Sprocket Mount before Machining..... | 68 |
| Figure 88: Preliminary Design of Output Shaft Bushing..... | 69 |
| Figure 89: Preliminary Design of Sprocket Mount Hole | 70 |
| Figure 90: Shaft Bushing Pressed into Place | 72 |
| Figure 91: Sprocket Mount with New Counterbored Holes | 72 |
| Figure 92: Differential Assembly | 73 |
| Figure 93: FSAE Speed Diagram CVT Graph (2011 MQP)..... | 75 |
| Figure 94: Spring Height vs. Spring Rate | 78 |
| Figure 95: Ideal CVT Performance Curve | 78 |
| Figure 96: Free Body Diagram of Flyweight | 79 |
| Figure 97: CVT Curve Plot - RPM vs Speed | 80 |
| Figure 98: Manual Transmission | 81 |
| Figure 99: Efficiency Curve | 82 |
| Figure 100: Low Ratio 3:1 | 83 |
| Figure 101: Secondary and Primary at Equal Speed - 1:1 Ratio | 83 |
| Figure 102: High Ratio Overdrive | 83 |
| Figure 103: Shift Ratio vs. Max Belt Tension..... | 84 |

Figure 104: Moveable Sheave Free Body Diagram.....88

Figure 105: SolidWorks Model of Flyweight89

Figure 106: Dimensioned Flyweight in mm.....89

Figure 107: Custom Made Secondary Pretension Capabilities.....92

Figure 108: System Flow Chart.....95

Figure 109: CAN Bus Output Protocol.....96

Figure 110: Haltech CAN Protocol Bit Breakdown.....96

Figure 111: Arduino Uno with CAN Bus Shield.....97

Figure 112: Preliminary Software Architecture104

Figure 113: Artist Rendition 1- Digital Dash Display105

Figure 114: Artist Rendition 2- Digital Dash Display106

Figure 115: Implemented Code 1- Digital Dash Display107

Figure 116: Implemented Code 2- Digital Dash Display108

Figure 117: System Interface109

Figure 118: Male 9 Pin D-Sub Connector.....109

Figure 119: Concept Layout.....112

Figure 120: ECU Harness Pigtails.....113

Figure 121: ECU Output Harness Breakdown.....114

Figure 122: ECU Input Harness Breakdown.....115

Figure 123: Final ECU Harness Pigtails117

Figure 124: Final ECU Output Harness Breakdown118

Figure 125: Final ECU Input Harness Breakdown119

Figure 126: Preliminary Battery Mount Design123

Figure 127: Installed Battery (Side View)125

Figure 128: Installed Battery (Top View)126

Figure 129: Body (2013 MQP)129

| | |
|--|-----|
| Figure 130: Body Structure (2013 MQP) | 129 |
| Figure 131: Nose Mold with Epoxy Stiffener..... | 130 |
| Figure 132: Advanced Bodywork | 130 |
| Figure 133: Vacuum Bagging Process | 131 |
| Figure 134: Spray-up Molding | 132 |
| Figure 135: Definition 1 of Open Wheel | 132 |
| Figure 136: Definition 2 of Open Wheel | 132 |
| Figure 137: Quick Release Quarter Turn Fastener..... | 133 |
| Figure 138: Initial Body Design | 134 |
| Figure 139: Final Body Design | 135 |
| Figure 140: Mold Manufacturing Calculations | 136 |
| Figure 141: Pre-Sanded Body..... | 137 |
| Figure 142: Heat Blade | 137 |
| Figure 143: Sanding with the Grinder..... | 138 |
| Figure 144: Initial Shaping Complete | 138 |
| Figure 145: Before Curing..... | 139 |
| Figure 146: Test Piece after Curing..... | 139 |
| Figure 147: Melted Foam | 139 |
| Figure 148: Nose Mold with Sanding Complete..... | 140 |
| Figure 149: Cut Fiberglass Weave | 140 |
| Figure 150: Finished First Layer..... | 141 |
| Figure 151: Body Removed from Mold..... | 141 |
| Figure 152: Filled Surface Defects | 142 |
| Figure 153: Painted Body..... | 142 |
| Figure 154: Frame Foam and Mounting Position..... | 143 |
| Figure 155: Exhaust Header Pipe | 145 |

Figure 156: Header Pipe Measurement145

Figure 157: The Two Mufflers and Two Reducers.....146

Figure 158: Reducer on the Header Pipe147

Figure 159: Muffler on the Header.....147

Figure 160: Steel Bar Connected to the Rear Subframe148

Figure 161: Vibration Dampening Sandwich Mount.....148

Figure 162: Picture of Final Setup149

Table of Tables

| | |
|--|-----|
| Table 1: Corner Weights | 5 |
| Table 2: Rear Subframe Design Matrix | 26 |
| Table 3: Subframe Loads under 1.5g Acceleration (force in Newton)..... | 28 |
| Table 4: Pushrod Loads under 3.5g Bump (force in Newton) | 44 |
| Table 5: Rocker Loads under 3.5g Bump (Force in Newton)..... | 59 |
| Table 6: Advantages of CVTs over a Manual Transmission | 74 |
| Table 7: CVT Tuning Objectives | 76 |
| Table 8: CVT Ratios..... | 83 |
| Table 9: Current CVT Inventory | 86 |
| Table 10: Definition of Variables | 87 |
| Table 11: Character Identifiers | 103 |
| Table 12: Electrical Parts List..... | 116 |
| Table 13: 34-Pin Connector | 120 |
| Table 14: 26-Pin Connector | 121 |
| Table 15: Battery Mount Design Matrix | 124 |
| Table 16: Body Design Matrix | 135 |
| Table 17: Exhaust Design Matrix | 146 |

Overview of Formula SAE Competition

The Formula SAE (FSAE) competition is an annual collegiate design competition organized by the Society of Automotive Engineers (SAE). In this competition, teams design and fabricate a prototype Formula style race car targeted for use by amateur weekend autocross racers. The prototype car is then evaluated in a variety of static and dynamic competition events.

The static competition events include design, cost, and presentation. The design event evaluates how well the design of the car meets the needs of the target market. The cost event assesses the overall cost of manufacturing the team's prototype. The presentation event evaluates the team's ability to create and deliver a business case that convinces the executives of a corporation that the team's design best meets the needs of the target customer and can be profitably manufactured.

The dynamic events include acceleration, skid-pad, autocross, and endurance. In each dynamic event, the team's prototype car is driven by a student member of the team to evaluate a particular aspect of the prototype's performance. The acceleration event evaluates the car's acceleration in a straight line on flat pavement. The skid pad event evaluates the prototype's cornering ability while making a constant-radius turn. The autocross event assesses the car's maneuverability and handling characteristics on a course. The endurance event evaluates the all-around performance and reliability of the car.

Rear Suspension

2013 MQP Suspension Design

The primary goal of the redesign of the 2013 suspension was to first understand the design choices that were made during its creation. During the 2013 FSAE MQP the 2012 FSAE car was changed from a solid, live rear swing axle to an unequal length double A-arm suspension setup. The original 2012 car used a live swing axle and it had several advantages such as low weight, low cost, and mechanical simplicity; however it did not provide optimal handling characteristics. To improve these characteristics, the main purpose of the 2013 MQP suspension design was to improve vehicle handling, responsiveness, and adjustability of suspension dynamics while maintaining serviceability and low vehicle weight. To do this, the team performed baseline testing of the car with the solid rear axle. The ultimate goal was to compare it to the new suspension design which they were planning on implementing.

After testing of the live axle was completed, the team looked into several rear suspension setups and eventually decided upon an independent rear suspension design. This setup was chosen in order to minimize unsprung weight and also to help resolve packaging issues. Another advantage of a rear independent suspension setup is improved rear tire grip and vehicle stability due to an improved tire contact patch and rear camber control. After a comparison of semi-trailing and unequal length double A-arm setups, the double A-arm setup was chosen because of its ability to control camber gain in both bump and droop independently.

Once an unequal length double A-arm setup was decided upon, the 2013 team worked towards designing a system that would provide the best overall control of camber during suspension travel. The main restriction in the design of the upper and lower control arms was packaging constraints caused by the differential and other drivetrain components. The final length of the lower arm was found to be around 18" in length. Next, the spacing between the lower and upper control arms was found to be 8" due to the height of the tires used. For defining the length of the upper arm, the team consulted "Milliken & Milliken's Race Car Vehicle Dynamics" and found that the arm ratios should be between 50-80%. For the best possible packaging, the upper arm was determined to be around 11.60". These arm lengths translated into a very reasonable camber gain. During bump, the suspension gained -2.06° of camber and under droop it gained 1.79° of camber. The final control arms were manufactured from 4140 Chromoly steel and TIG welded.

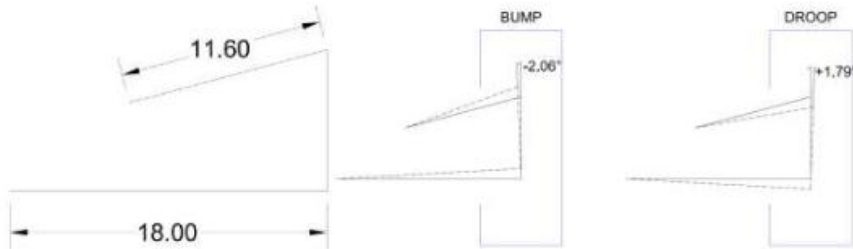


Figure 1: Arm Lengths and Camber Gain (2013 MQP)

The next step in the suspension design was to formulate a method of actuating the shocks. Due to the long length of the lower control arm, the use of direct shock actuation would not be possible and a direct method would add additional unsprung weight. To solve this problem, a pushrod actuation method was used. The use of a pushrod system allowed the shocks to be moved inside the sub frame. The final pushrod setup allowed for shock actuation with less material and lower unsprung weight than a direct acting system. The use of a rocker design also allowed for the motion ratio of the suspension to be optimized to meet FSAE requirements.

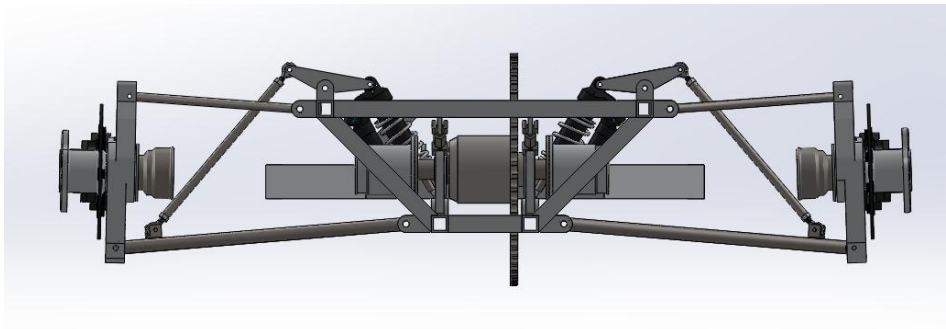


Figure 2: Pushrod Design (2013 MQP)

The 2013 rear subframe was designed to bolt directly in place of the solid rear axle used on the 2012 car by using the mounting tabs for the main swing arm pivots and shock mounting points. It provided suspension mounting points for the control arms and differential. This frame was constructed of 6061-T6 aluminum square tubing and was TIG welded.

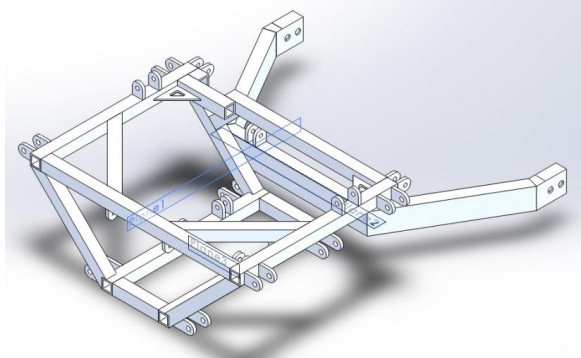


Figure 3: Rear Subframe (2013 MGP)

Suspension Dynamics and Loads

Calculating Center of Gravity

For the new rear suspension to be designed and tested before manufacturing, a full understanding of the forces and loads seen during different dynamic events needs to be known. By knowing this information, designs can be analyzed and improved. An FSAE car is a highly dynamic system. Forces seen in different components of the car under acceleration, braking, and cornering vary greatly during its operation. To test the new suspension design during these dynamic situations several finite element analysis (FEA) simulation models were used. To make these models as accurate as possible, the loads created during these dynamic events must be known.

To find the suspension loads, the first task was to understand the car's weight distribution. The weight distribution is very important since it allows for the center of gravity (CoG) to be found. Using corner weight scales, the car was weighed with a driver to find the corner weights on each tire.

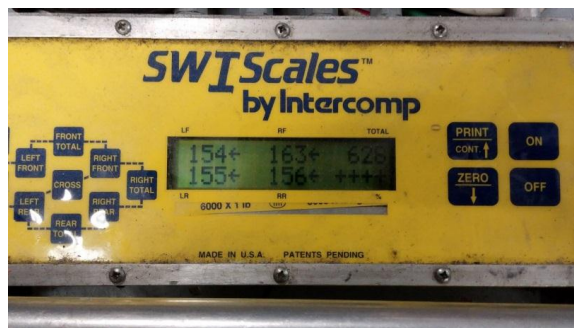


Figure 4: FSAE Car Corner Weights

Table 1: Corner Weights

| Corner Weights | Left | Right |
|----------------|--------|--------|
| Front | 154lbs | 163lbs |
| Back | 155lbs | 156lbs |
| Total | 628lbs | |

As seen in Table 1, the corner weights are very close to 50% weight distribution front to rear. This is optimal since it allows for more natural handling and better responsiveness. For the analysis, the weight will be rounded to a perfect 50/50 weight distribution since driver weight can vary. This allowed the CoG to be found on the car's centerline. The overall CoG is centered between the front and rear wheels. Since the wheelbase of the 2014 FSAE car is 66", this placed the CoG at 33" behind the front wheels. These measurements were confirmed with Suspension Calculator by Cristobal Lowery. This software package is able to perform a wide variety of load-based suspension calculations including 3D loads on double wishbone suspensions. In Figure 5, the longitudinal CoG was calculated. It was found to be 0.838m from the front wheels which is exactly 32.990".

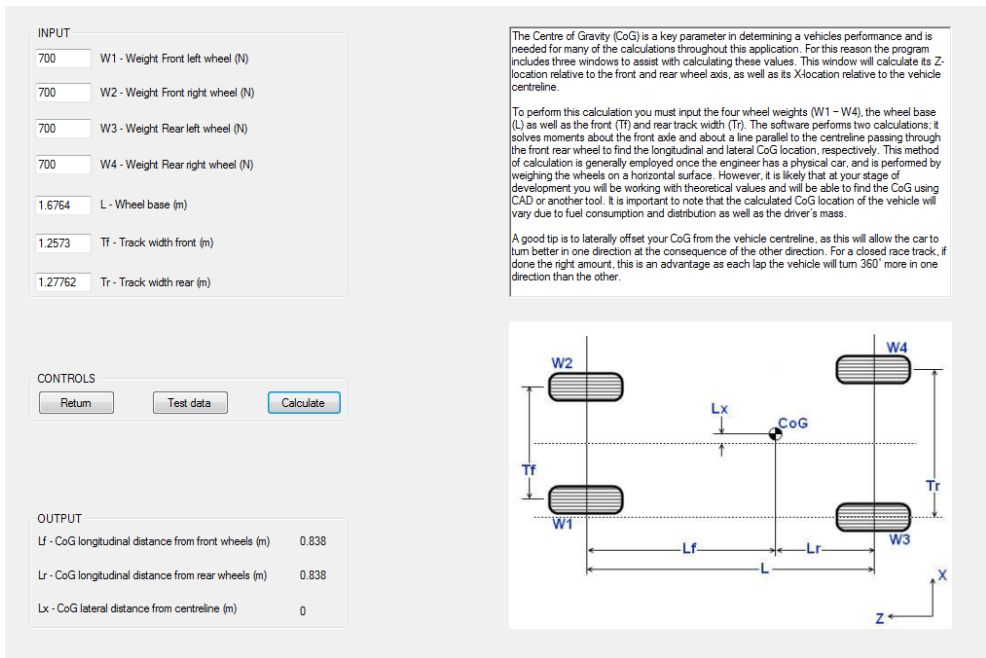


Figure 5: Static CoG Location

However, the height of the CoG was still not known. To find the height of CoG, the car needed to be raised at the rear wheels while the load of the front wheels was measured. Then, by using the angle between the car and the ground, the height of the CoG can be determined. To do this, the corner weight scales were placed under the front wheels and the car was jacked up to 5.27° from horizontal. Once again, by using Suspension Calculator, the CoG height was determined to be 0.242m or 9.528” from ground.

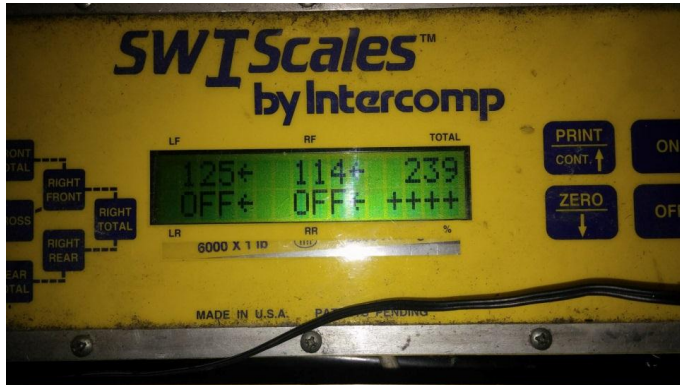


Figure 6: Front Weight at 5.27°

INPUT

1063 Wf - Weight measured when elevated (N)

84.73 θ - Angle when elevated (degrees)

2800 W - Vehicle weight (N)

0.8382 Lr - CoG longitudinal distance from rear wheels (m)

1.6764 L - Wheelbase (m)

0.26035 Rf - Loaded radius of front wheels (m)

0.26035 Rr - Loaded radius of rear wheels (m)

CONTROLS

OUTPUT

h - CoG height (m): 0.242

This window calculates the height of the CoG relative to the ground, based on physically measured data.

To perform this calculation you will need to enter the loaded radius of both the front and rear wheels, if this value is unknown a good estimate is the actual (unloaded) wheel radius. Another required variable is the "CoG longitudinal distance from rear wheels", if this is unknown this can be found using the horizontal CoG location window.

To obtain the physically measured variables, it is necessary to lock the suspension, fasten loose objects and to then jack up the rear axle as seen in the figure below. The front wheels should be chocked onto scales, to prevent them moving. Using this methodology the elevated weight of the vehicle (addition of two front wheel weights recorded by scales) and the angle at which it occurs is recorded. The program then uses this data alongside geometry and moment analysis to calculate the CoG height.

The procedure used in jacking up the rear axle, is a procedure that requires great care and much more attention to detail than set out here. Please, refer to other texts before performing such a procedure.

Figure 7: Height of CoG

Calculating Roll Center

With both the longitudinal position and height of the CoG known, the next step was to determine the roll center of the rear suspension geometry. The roll center of a vehicle is the notional point at which the cornering forces of the suspension are reacted to the frame. The roll center is very important to the loading of the rear suspension while cornering. During the 2012 FSAE MQP, the front suspension roll center and instant roll centers were calculated; however, during the 2013 FSAE MQP, the roll center was not calculated. As such, it needed to be found using frame and control arm dimensions. For this, Racing Aspirations Suspension Geometry Calculator was used. This tool allows for the suspension geometry data to be input and the software creates a virtual model of the rear suspension. Using measurements from SolidWorks, the rear suspension was replicated into this tool. The final roll center was found to be at 107mm above the ground or 4.213" at estimated ride height. While the ride height of the vehicle may be lowered to decrease this roll center, the given calculation will provide a good worst case scenario for suspension loads. The front roll center is 40mm or 1.5748" as outlined in the 2012 FSAE MQP report.

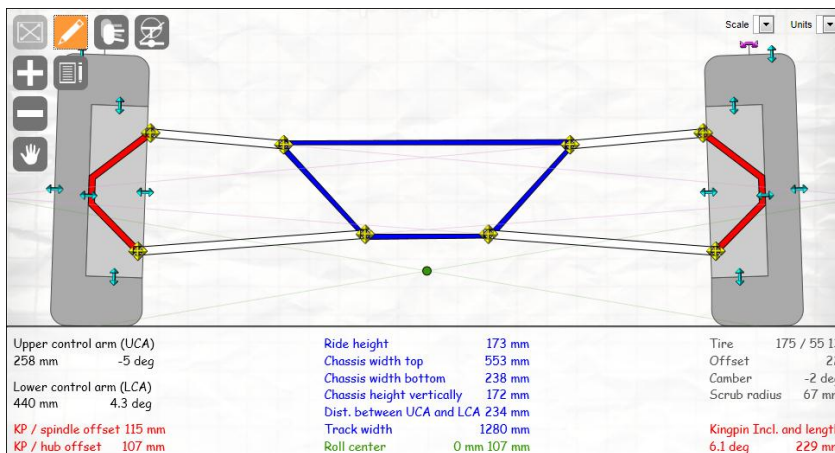


Figure 8: Suspension Roll Center Calculation

Dynamic Event Forces

To fully test the design of the new rear suspension, the forces applied to the car during different dynamic events needed to be calculated. For the purpose of these simulations, four different dynamic event situations were calculated. These were during 1.5g braking, 1.5g acceleration, 1.5g lateral load, and 3.5g of suspension bump. These values were taken from *Race Car Vehicle Dynamics*, as recommended dynamic testing situations. By calculating these four different events, the highest possible loads on each component can be found and can be used for FEA simulations. All dynamic suspension calculations were completed using Suspension Calculator.

Dynamic 1.5g Braking

The first step to determining the loads placed on the rear suspension during 1.5g of braking is to find the load transfer caused by the deceleration of the car. This is where the CoG values were used.

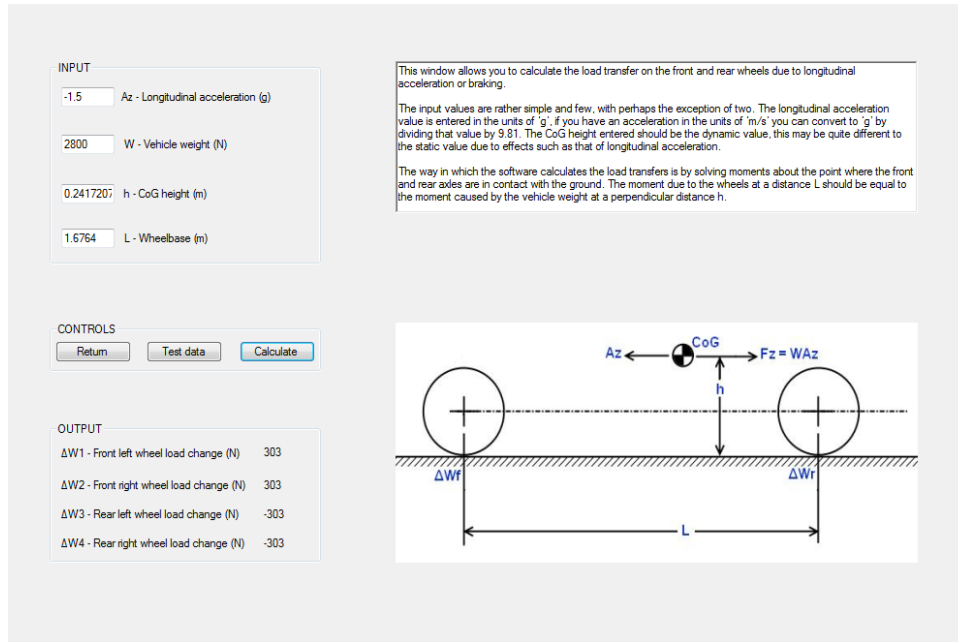


Figure 9: Load Transfer during 1.5g Braking

During a hard braking situation, the front wheels will see an increased load of 303N while the rear wheels will be unloaded by 303N. To find the total wheel load, the static load must be added to this load transfer. Under a 1.5g braking event, the final rear wheel load is 397N.

Equation 1

$$\text{Wheel Load} = \text{Load Transfer} + (\text{Static Weight}/4)$$

$$397N = -303N + (2800N/4)$$

After the wheel load had been determined, the next step was to calculate the suspension loads. Suspension Calculator has a built in tool that calculates the forces on each suspension joint in X, Y, and Z coordinates. To use this tool, first the suspension joints' coordinates needed to be determined. These values were obtained from the SolidWorks model.

INPUT

0 Ax - Lateral Acceleration (g) 0 Wheel Force x-direction (N)

-1.5 Az - Longitudinal Acceleration (g) 397 Wheel Force y-direction (N)

1.2 Coefficient of Friction -476.4 Wheel Force z-direction (N)

397 Wheel Load (N)

Use left column Use right column

| | x | y | z |
|---|-------|--------|--------|
| 1 | 0.276 | 0.109 | -0.134 |
| 2 | 0.276 | 0.109 | 0.167 |
| 3 | 0.533 | 0.132 | 0.017 |
| 4 | 0.119 | -0.063 | 0.177 |
| 5 | 0.119 | -0.063 | -0.144 |
| 6 | 0.558 | -0.096 | 0.017 |
| 7 | 0.241 | 0.141 | -0.03 |

This window is used to calculate the forces acting at the pushrod and wishbones. These values can then be used alongside FEA software to test the integrity of components such as wishbones and uprights. The software assumes a double wishbone system, with a pushrod attached at point '6' in the diagram. It also assumes that the full vertical force on the wheel is taken by the pushrod, and as such this analysis will be inaccurate if the wishbones are not horizontally attached to the chassis.

There are several important points worth noting when it comes to interpreting the data. One of these is that the wheel forces entered are the forces applied by the ground onto the wheel. If these values are unknown the software allows you to enter 4 values in the left column and it will calculate these for you using the most common way. The software also asks you to enter the coordinates of the 7 points shown in the diagram, as it uses many geometrical properties in the calculations. The outputted values (will be displayed in a new window) are the values applied by the wishbones and pushrod onto the upright. As such, the force value obtained at point 7, should not be used to perform other calculations such as on the pushrod without further manipulation. The value outputted at point 6 is the force applied by the lower wishbone onto the upright, thus to find the overall force applied to the upright at point 6 this force should be added to the pushrod force. Finally, the value outputted at point 7 is the force applied by the pushrod onto the upright or its attachment.

The analysis is carried out by assuming that the forces found at points 3 and 6 in the figure would counteract the tyre reaction forces and that the pushrod would take the full vertical load, then resolving the dynamic forces into three force components at each point and solving by equating these in the x-, y-, and z- planes respectively. The accuracy of the solution is therefore limited to the accuracy of the tyre reaction forces.

COORDINATES

| | x | y | z |
|---|-------|--------|--------|
| 1 | 0.276 | 0.109 | -0.134 |
| 2 | 0.276 | 0.109 | 0.167 |
| 3 | 0.533 | 0.132 | 0.017 |
| 4 | 0.119 | -0.063 | 0.177 |
| 5 | 0.119 | -0.063 | -0.144 |
| 6 | 0.558 | -0.096 | 0.017 |
| 7 | 0.241 | 0.141 | -0.03 |

CONTROLS

The diagram illustrates a double wishbone suspension system. A coordinate system is defined with X pointing right, Y pointing up, and Z pointing forward. Seven points are marked: 1 and 2 are the upper wishbone attachment points; 3 and 6 are the lower wishbone attachment points; 4 and 5 are the lower wishbone ends; and 7 is the pushrod attachment point. Lines connect the points to show the wishbones and pushrod.

Figure 10: Suspension Coordinates

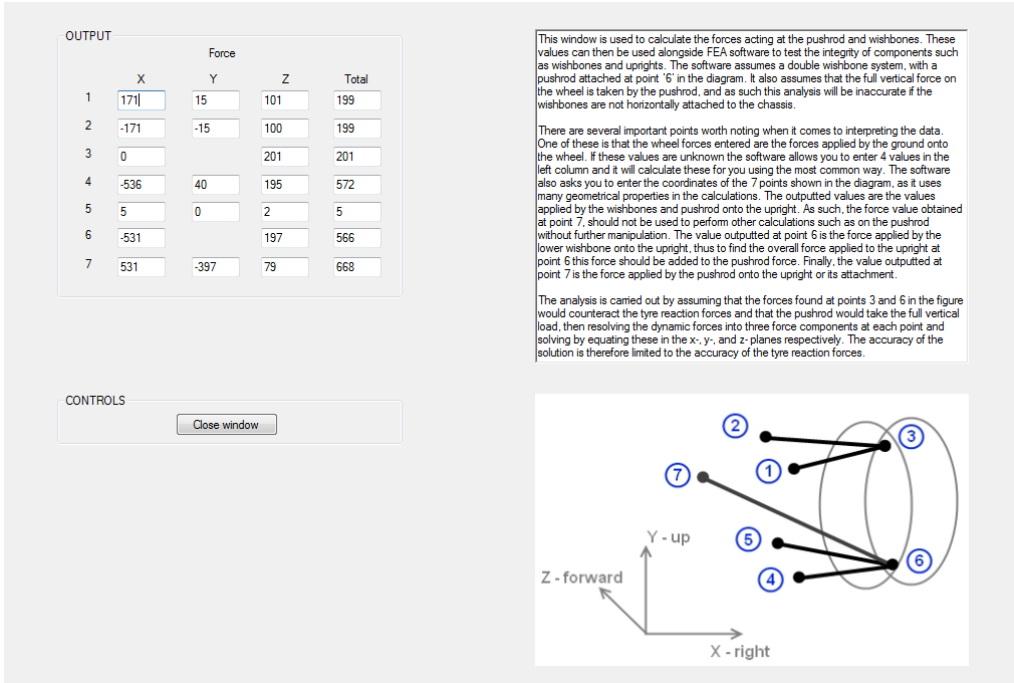


Figure 11: Suspension Arm and Pushrod Forces Under 1.5g Deceleration

The 1.5g braking rear wheel suspension forces are seen in Figure 11. These loads are small since the rear wheels are unloaded during a hard braking event. As such, a braking event was not be used during FEA modeling.

Dynamic 1.5g Acceleration

The first step to determining the loads placed on the rear suspension during 1.5g of acceleration is to find the load transfer caused by the acceleration of the car. Once again, the previously calculated CoG values were used.

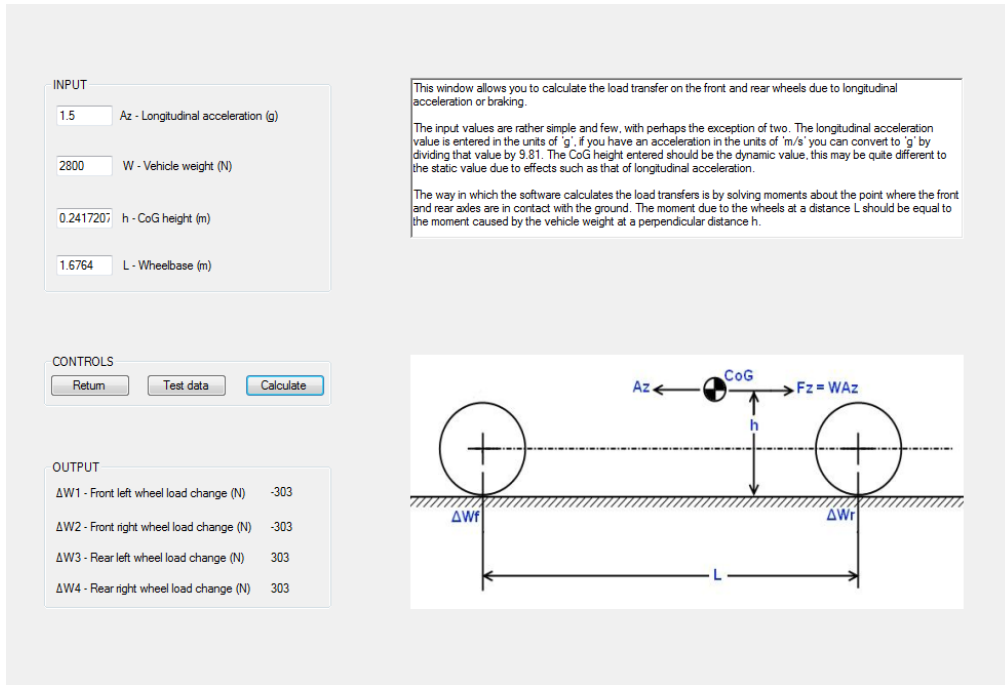


Figure 12: Load Transfer during 1.5g Acceleration

During a hard acceleration situation, the front wheels will see a decreased load of 303N while the rear wheels' load increased 303N. To find the total wheel load, the static load must be added to this load transfer. Under a 1.5g acceleration event, the final rear wheel load is 1003N.

$$\text{Wheel Load} = \text{Load Transfer} + (\text{Static Weight}/4)$$

$$1003N = 303N + (2800N/4)$$

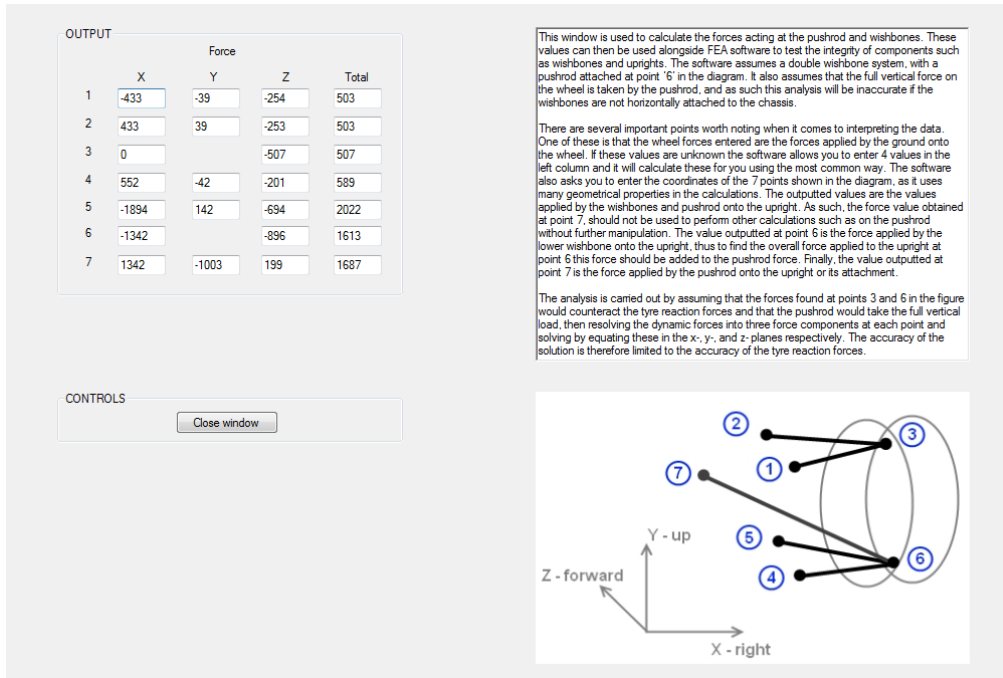


Figure 13: Suspension Arm and Pushrod Forces under 1.5g Acceleration

The 1.5g acceleration rear wheel suspension forces are seen in Figure 13. These loads are much larger since the rear wheels are loaded during acceleration. As such, a hard acceleration event was used during FEA modeling of rear subframe.

Dynamic 1.5g Lateral Load

The first step to determining the loads placed on the rear suspension during 1.5g of lateral load is to find the load transfer caused by the lateral acceleration of the car. Once again, the previously calculated CoG values were used.

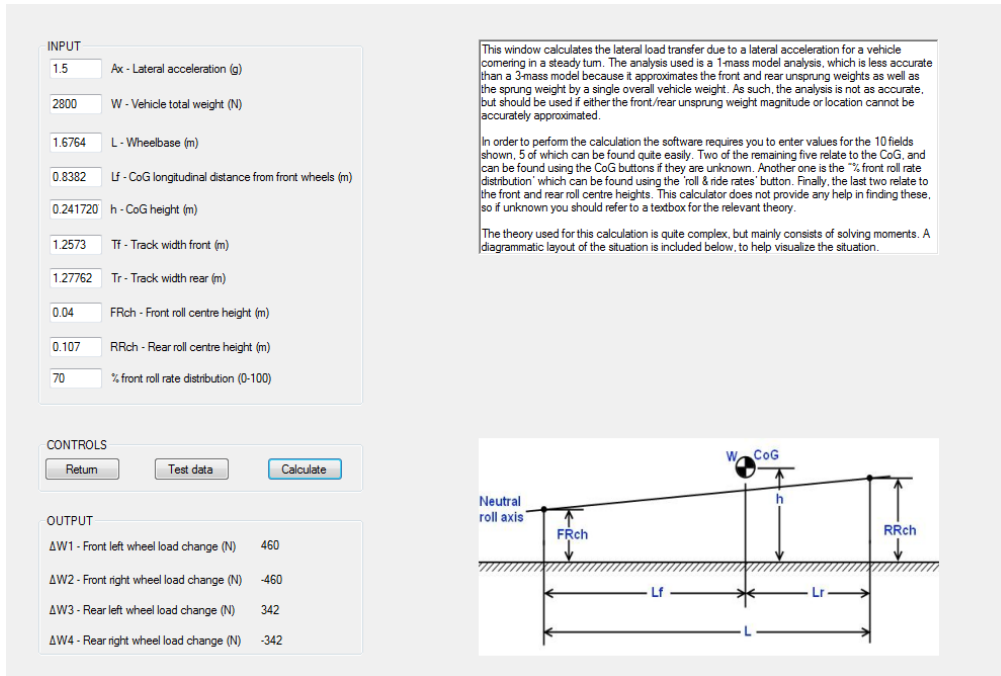


Figure 14: Load Transfer during 1.5g Lateral Load

The calculator requires several more inputs for this calculation. All variables have been determined except for front roll rate distribution. This is calculated by using the front and rear spring rates along with total suspension travel front and rear. During a hard cornering event, the inside wheels experience decreased loading while the outside wheel loads are increased. The rear wheels see a load transfer of 342N from right to left. To find the total wheel load, the static load must be added to this load transfer. Under a 1.5g lateral event, the final rear wheel load is 1042N.

$$\text{Wheel Load} = \text{Load Transfer} + (\text{Static Weight}/4)$$

$$1003N = 342N + (2800N/4)$$

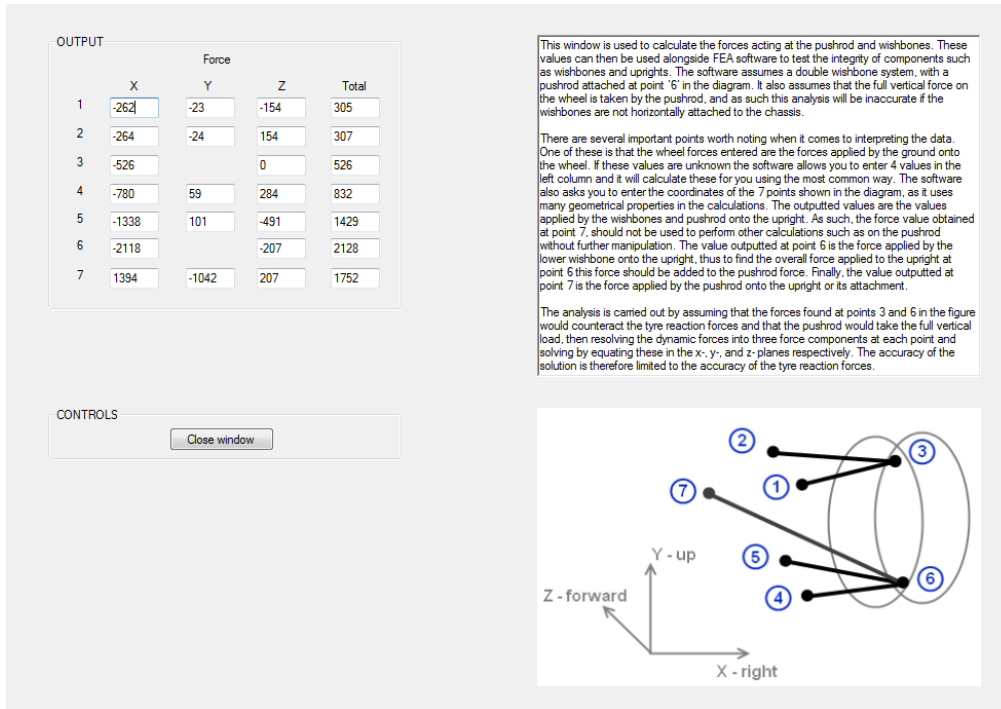


Figure 15: Suspension Arm and Pushrod Forces under 1.5g Lateral Acceleration

The 1.5g lateral acceleration forces on the rear wheel suspension are seen in Figure 15. These loads are somewhat larger than the 1.5g acceleration forces; however, the forces seen on the right side wheel are much lower. As such, a hard cornering event was not used during FEA modeling of rear subframe.

Dynamic 3.5g Bump

The first step to determining the loads placed on the rear suspension during 3.5g of suspension bump is to find the wheel load caused by this upward wheel acceleration. The only needed value for this calculation is the unsprung wheel weights. These were found by weighing suspension components of the car.

INPUT

134 Wu1 - Unsprung Weight front left wheel (N)

134 Wu2 - Unsprung Weight front right wheel (N)

180 Wu3 - Unsprung Weight rear left wheel (N)

180 Wu4 - Unsprung Weight rear right wheel (N)

0 Magnitude of kerb hit front left wheel (g)

0 Magnitude of kerb hit front right wheel (g)

3.5 Magnitude of kerb hit rear left wheel (g)

0 Magnitude of kerb hit rear right wheel (g)

CONTROLS

Return Test data Calculate

OUTPUT

ΔW1 - Load transfer front left wheel (N) 0

ΔW2 - Load transfer front right wheel (N) 0

ΔW3 - Load transfer rear left wheel (N) 630

ΔW4 - Load transfer rear right wheel (N) 0

This window calculates the load transfer on all of the wheels due to a kerb strike. The way in which it performs this calculation is by multiplying the unsprung weight of the wheel by the magnitude of the kerb strike (measured in 'g') on that wheel.

A useful point is that if you have an acceleration in the units of 'm/s²' you can convert to 'g' by dividing the value by 9.81. It is also important to note that generally these load transfers are predominantly absorbed by the dampers as opposed to the spring due to their high velocity.

Figure 16: Load Transfer during 1.5g Lateral Load

During a bump event, the affected wheels experience a greatly increased load. To find the total wheel load, the static load must be added to this load transfer. Under a 3.5g bump event, the affected rear wheel experiences a 1330N load.

$$\text{Wheel Load} = \text{Load Transfer} + (\text{Static Weight}/4)$$

$$1330N = 630N + (2800N/4)$$

INPUT

0 Ax - Lateral Acceleration (g) NaN Wheel Force x-direction (N)

0 Az - Longitudinal Acceleration (g) 1330 Wheel Force y-direction (N)

1.2 Coefficient of Friction NaN Wheel Force z-direction (N)

1330 Wheel Load (N)

Use left column Use right column

| Coordinates | | | |
|-------------|-------|--------|--------|
| | x | y | z |
| 1 | 0.276 | 0.109 | -0.134 |
| 2 | 0.276 | 0.109 | 0.167 |
| 3 | 0.533 | 0.132 | 0.017 |
| 4 | 0.119 | -0.063 | 0.177 |
| 5 | 0.119 | -0.063 | -0.144 |
| 6 | 0.558 | -0.096 | 0.017 |
| 7 | 0.241 | 0.141 | -0.03 |

This window is used to calculate the forces acting at the pushrod and wishbones. These values can then be used alongside FEA software to test the integrity of components such as wishbones and uprights. The software assumes a double wishbone system, with a pushrod attached at point '6' in the diagram. It also assumes that the full vertical force on the wheel is taken by the pushrod, and as such this analysis will be inaccurate if the wishbones are not horizontally attached to the chassis.

There are several important points worth noting when it comes to interpreting the data. One of these is that the wheel forces entered are the forces applied by the ground onto the wheel. If these values are unknown the software allows you to enter 4 values in the left column and it will calculate these for you using the most common way. The software also asks you to enter the coordinates of the 7 points shown in the diagram, as it uses many geometrical properties in the calculations. The outputted values (will be displayed in a new window) are the values applied by the wishbones and pushrod onto the upright. As such, the force value obtained at point 7, should not be used to perform other calculations such as on the pushrod without further manipulation. The value outputted at point 6 is the force applied by the lower wishbone onto the upright, thus to find the overall force applied to the upright at point 6 this force should be added to the pushrod force. Finally, the value outputted at point 7 is the force applied by the pushrod onto the upright or its attachment.

The analysis is carried out by assuming that the forces found at points 3 and 6 in the figure would counteract the tyre reaction forces and that the pushrod would take the full vertical load, then resolving the dynamic forces into three force components at each point and solving by equating these in the x-, y-, and z-planes respectively. The accuracy of the solution is therefore limited to the accuracy of the tyre reaction forces.

CONTROLS

Figure 17: Suspension Arm and Pushrod Forces under 1.5g Lateral Acceleration

The 1.5g lateral acceleration forces on the rear wheel suspension are seen in Figure 17. These loads are somewhat larger than the 1.5g acceleration forces; however, the forces seen on the right side wheel are much lower. As such, a hard cornering event was not used during FEA modeling of rear subframe.

SolidWorks Validation

To make sure all simulated results from SolidWorks Simulations were correct, testing was performed using SolidWorks' built in validation tools. These tests were run and compared to actual recorded values in SolidWorks' test files. All simulation results passed without any issues. In addition NAFEMS Benchmarks were also run to further confirm the accuracy of simulations.

Subframe

Overview

With the design of the 2012 WPI FSAE car, the goal was to keep weight down and build the simplest, most robust car possible. As such, the decision was made to go with a solid rear axle. With the start of the 2013 WPI FSAE MQP, the decision was made to convert the existing car over to an independent rear suspension setup. This was done to improve the cars dynamic handling abilities. In order to do this, a subframe was developed to bolt into the place of the solid rear axle and allow for the mounting of control arms, shock absorbers, and other driveline components without major modifications of the main front frame.

Initial State

The design of the 2013 MQP team's suspension design was well thought out in theory; however, there were several issues that kept the car from ever being completed and run in practice. The two main issues that kept the car from being driven were the material choice for the rear subframe and the pushrod/shock design.

While in concept the 2013 frame design seemed like a viable solution to provide suspension mounting points and retain low weight, the overall end product was less than acceptable. The main issue with the subframe was the 6061-T6 aluminum material chosen in its construction. While aluminum is easy to machine and lightweight, it is hard to weld correctly. Even though TIG was used during the welding process, the welds used too much heat which caused the material to lose its temper in key areas, causing the welded frame to become very brittle in welded areas. Since many of the mounting points used on the car can be subjected to high shock loads, this was less than acceptable. A disadvantage to the use of aluminum is its lack of structural rigidity when compared to other materials. This is of key importance due to the high loading conditions of the rear suspension during dynamic events such as acceleration and cornering. The use of box tubing was another area of concern. While this material is easy to work with, it does not provide the same structural properties as round tubing construction. Another issue with the subframe was that it did not completely clear the engine or main drive sprocket. These clearance problems caused major issues during the final assembly process.

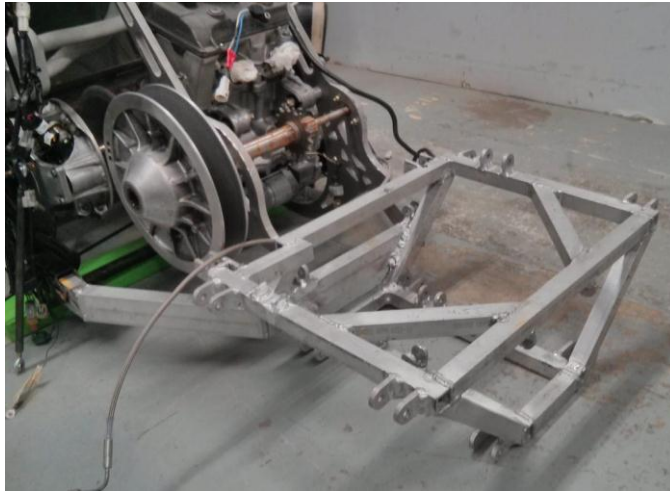


Figure 18: Welded Aluminum Rear Subframe on Car

Upon first inspection of the subframe, several issues were noted that made the reuse of the old subframe impossible. First, due to the poor welds, several frame tabs had broken off. Next, due to incorrect sizing, several suspension components had clearance issues. A new subframe needed to be manufactured.

Objective

After analyzing the 2013 suspension design, several areas of improvement were identified for the redesign of the subframe. A design goal was identified for each of these aspects. In addition to minimizing costs during the manufacturing and assembly of the 2014 subframe, components from the 2013 suspension would be used when possible after they had been inspected.

The new subframe must integrate with the existing chassis mounting points, differential, and suspension A-arms. The material used in its manufacture must be able to withstand forces seen in a typical FSAE car and must be made of material that will not be compromised during welding. Finally, the overall weight and cost of the subframe must be kept within acceptable bounds. It also must be able to clear the drive sprocket and driveline components.

Research

During the redesign of the rear subframe, the first decision that needed to be made was the choice of material to use for the construction of the new frame. As stated previously, the 2013 subframe was made out of 6061-T6 aluminum box tubing. Aluminum has several advantages, including light weight and ease of machining. However, it is difficult to weld correctly and has lower strength than steel.

After the development of this first concept, the decision was made to look into alternative materials to construct the subframe from. Chromoly steel is a high strength material that is used

in many aerospace and motorsport applications, including many FSAE cars. It is very strong, providing better structural stiffness than aluminum. It is not as affected by welding when compared to aluminum and it is easier to achieve a high strength weld. While it is entirely possible to weld an aluminum frame, the strength of these welds to fatigue and shock loads are lower than Chromoly since welding aluminum weakens the material in the heat affected zone. There are many benefits of using Chromoly steel as opposed to aluminum, including:

- Steel and aluminum have a very similar strength-to-weight ratio. Steel is heavier than aluminum but less of it is required to yield the same strength as aluminum.
- Chromoly steel's modulus of elasticity is roughly 30,000ksi, while aluminum's is only about 10,000ksi. Therefore, the final steel frame would be stiffer than an aluminum frame.
- Steel is easier to weld than aluminum and the final welds are more resistant to fatigue.
- Chromoly frame that uses 1/16" thick steel would be nearly three times as strong as a 1/8" thick aluminum frame.
- Most automotive and FSAE applications use Chromoly steel tubing for their frames.
- Chromoly tubing can be bent to form complex tube geometry.

Another decision was the choice between box and round tubing. Both Chromoly and 6061-T6 aluminum are available in either profile. Round tubing has a few advantages over box tubing. Round tubing is stronger and lighter than box for the same given length and corner joints are higher strength than box tubing. Round tubing can be bent which allows greater freedom during frame design. One concern with round tubing is the ability to weld mounting tabs for suspension arms and other components. However, this issue can be resolved by using correctly notched mounting tabs which can be welded around the tubular frame. Due to the reasons above, round tubing was selected for the next concept subframe.

Design

The first new frame concept that was developed used aluminum box tubing similar to the 2013 design; however, it used larger lower frame rails and the overall frame was extended by 1.5" to allow for easier removal and installation of the rear differential. It was also designed to use a different shock mounting setup that placed the shock absorbers horizontally to allow them to be mounted in-line with the lower control arm.

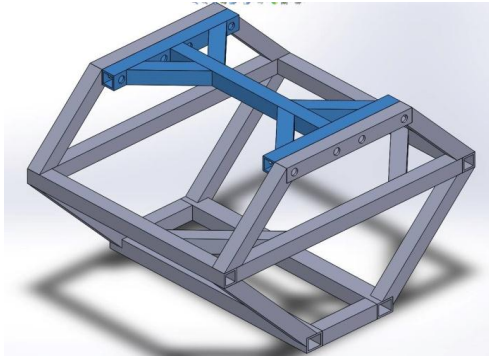


Figure 19: Subframe Aluminum Box Design Concept

Besides this updated aluminum box subframe, a second concept was developed that used round steel tubing. With the use of the 2013 CAD models reference, a Chromoly tube frame was created in SolidWorks using a 3D sketch to locate all mounting points. The 3D sketch was constructed so it could be easily modified in the future as the design of the frame was changed. Next, using the weldment tools, profiles of 1.000" x 0.095" wall thickness and 0.750" x 0.095" thick round tubing were applied to this 3D sketch. Mounting tabs were placed on suspension and frame pickup points. The material wall thickness was chosen for several reasons. First, a thicker wall tube is easier to bend than thin wall tubing. Second, thicker wall tubing is easier to weld than thin wall tubing. There is a small weight disadvantage to using a thicker wall tubing but this was marginal (only adding around 1lb of weight over .063 wall tubing).

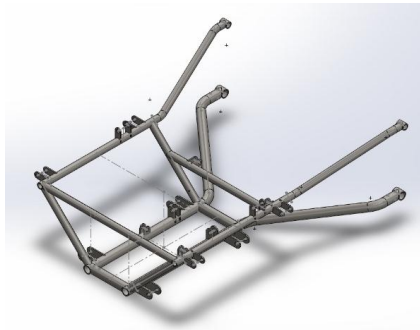


Figure 20: Round Tube Concept Subframe

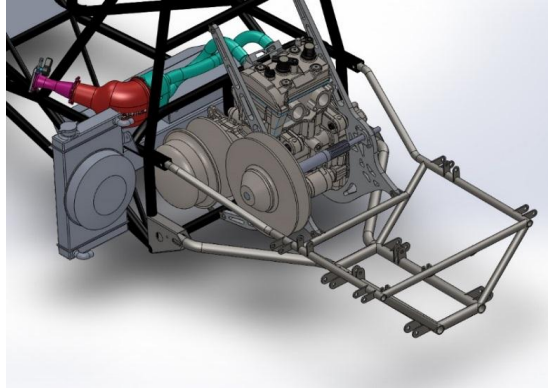


Figure 21: Tube Subframe Concept Mounted Onto Chassis

One advantage of using steel tubing is the ability to bend it. One problem with the 2013 aluminum subframe was clearance issues with the CVT and engine. By bending the tube sections around these areas, a cleaner design approach could be used. The final frame design uses less material than the old design and is similar in total weight, even though it is made out of steel instead of aluminum. As a comparison, the aluminum frame design would weigh 12lbs and the steel frame design would weigh 16lbs.

Preliminary Design Concepts

After the research phase of development was completed, the next step was to use the design process to select the design that best met the design goals. Since there were two separate frame designs and two separate rocker designs, this produced four different concept designs.

Concept 1: Aluminum Frame and Vertical Shocks

The first concept design used an aluminum box frame design. The new aluminum frame was designed to allow for better clearance of suspension and driveline components (not pictured below). It also integrated the vertical shock orientation with the rocker design and new pushrod design. A visual concept of this design is in Figure 22.

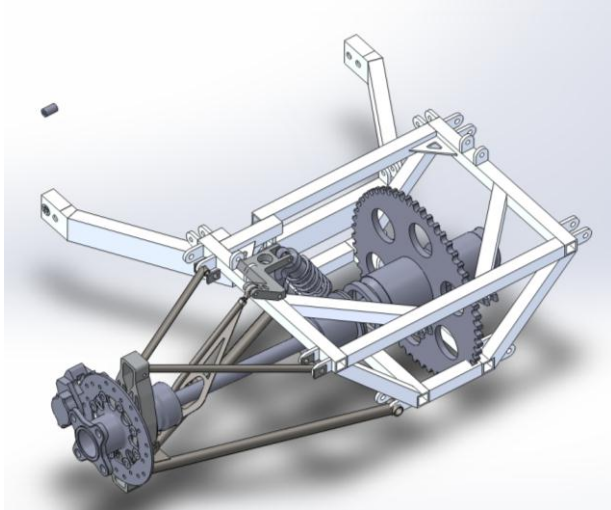


Figure 22: Visual Representation of Concept One

Concept 2: Aluminum Frame and Horizontal Shocks

The second conceptual design used the same aluminum box frame as concept one. The new aluminum frame was designed to allow for better clearance of suspension and driveline components. It also integrated the horizontal shock orientation with flat plate rockers and new pushrod designs. Since this design used a horizontal shock placement, the aluminum box frame needed to have a support structure added for shock mounts. To allow for better access to the differential and other driveline components, this section was designed to be removable. A visual concept of this design is in Figure 23.

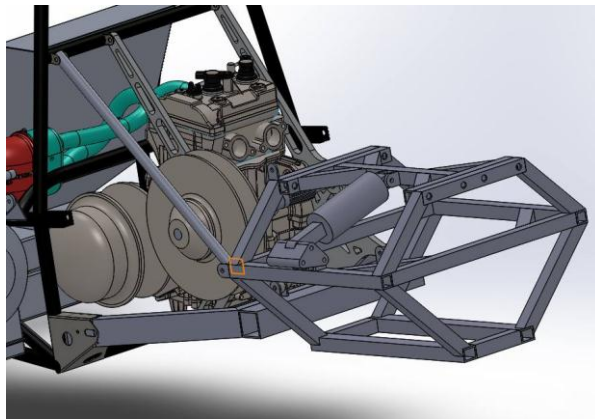


Figure 23: Visual Representation of Concept Two

Concept 3: Steel Frame and Vertical Shocks

The third conceptual design used the Chromoly steel frame. This frame design allowed for plenty of clearance around suspension and driveline components. In addition, support bars were added to pick up mounting points near the top of the roll hoop in order to add extra stiffness. This design also used the vertical shock orientation with transfer rocker design and new pushrod design. A visual concept of this design is in Figure 24.

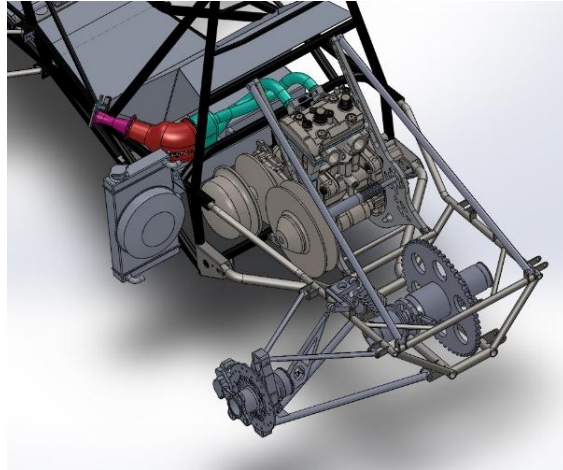


Figure 24: Visual Representation of Concept Three

Concept 4: Steel Frame and Horizontal Shocks

The fourth conceptual design used the round Chromoly steel tubing. Due to the placement of shocks, the addition of support bars was not able to be included in this design. Due to the welded nature of this design, the top section of frame is not removable. This design used the horizontal shock orientation with flat plate rocker design and a new pushrod design. A visual concept of this design is in Figure 25.

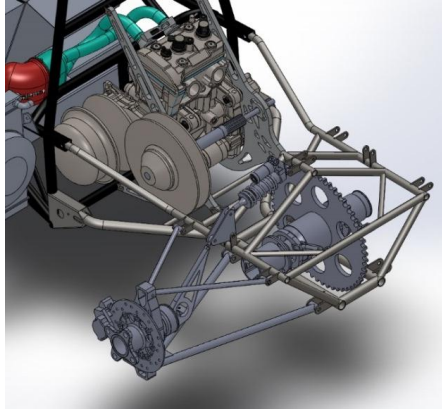


Figure 25: Visual Representation of Concept Four

Concept Selection

To select a final design, a design matrix was created. The first step in creating the design matrix was to break down each aspect that made the designs valuable (the decision factor). These factors were then weighted based on importance. Next, the four conceptual designs were listed. These covered both steel and aluminum versions of each design. This equaled a total of four different conceptual designs. Next, each design was scored from 1-10 based on its ranking. The end design with the highest score would be the best overall balance of design aspects. Below is a list of the ranking weight criteria.

Ease of Access: Ease of access refers to the ability to remove and replace suspension and driveline components. This is most important during assembly, tuning, and repair of the car. Due to the target consumer for this vehicle, this was weighted as 8 since the ability to repair and tune the car without removing additional assemblies or having special tools was a goal for the final design. The vertical shock design has a key advantage in this area since the top of the subframe is open.

Durability: Due to the high stress environment this car is placed in, durability was ranked very high at 9. Since this car is used in a competition environment, any mechanical or electrical issues would be unfavorable. Therefore, all components were analyzed for potential weak points. With proper design, durability should be close to equal across all concepts.

Strength of Design: Strength of design was ranked low at 6 for several reasons. First, this criterion refers to the strength of the pushrod and suspension assemblies. There is a main distinction between the strength of the horizontal design compared to the vertical shock design. With correct engineering and analysis, these differences are negligible; however, the horizontal shock design has advantages due to its load path.

Simplicity: To ensure the final design would meet budget and timeline requirements, the design needed to be made as simple as possible. This was weighed high since, due to the limited time frame and budget provided to this project, it was imperative that the design was kept as simple as possible. The vertical shock designs use fewer components, therefore they ranked higher.

Ease of Welding: Since welding was a major area of concern for last year's design, it was decided to include welding ease in the design matrix. This was weighed as 6 due to its importance during manufacturing. Steel is a more easily welded material, therefore it ranked higher.

Cost: As stated previously, cost is a major area of concern. Since the overall budget of this project was low, the final design needed to be relatively low-cost in order to allow for other subsystems to be manufactured. Therefore, material and manufacturing costs were considered.

Frame Strength: Also, due to the lessons learned during the 2013 MQP, the decision was made to include final frame strength in the analysis. This was ranked very high due to the importance of strength and rigidity in this area. Steel ranked highly in this category since it provides a much more rigid assembly.

Compatibility: Since the final design needed to be integrated into the existing front frame from the 2012 MQP, it was decided that compatibility with existing components was important. The vertical shock design maintained a similar layout and design to the 2013 MQP, while the horizontal shock design would have clearance issues with the existing exhaust and sprocket.

Serviceability: Similar to ease of access, serviceability is the ability to easily tune the car without advanced knowledge of its design. For example, the ability to adjust suspension settings. This was weighted 6 due to the target consumer.

Manufacturability: To be able to manufacture all components within the allotted time period, manufacturability was of great importance. Manufacturability took into account the amount of components that needed to be machined and made. It also takes into account the complexity of said components.

Table 2: Rear Subframe Design Matrix

| Decision Factor | Weight | Concept 1 | | Concept 2 | | Concept 3 | | Concept 4 | |
|--------------------|--------|-------------------------------------|------------|---------------------------------------|------------|----------------------------------|------------|------------------------------------|------------|
| | | Aluminum Frame with Vertical Shocks | | Aluminum Frame with Horizontal Shocks | | Steel Frame with Vertical Shocks | | Steel Frame with Horizontal Shocks | |
| | | Score | Value | Score | Value | Score | Value | Score | Value |
| Ease of Access | 8 | 9 | 72 | 6 | 48 | 9 | 72 | 6 | 48 |
| Durability | 9 | 4 | 36 | 4 | 36 | 8 | 72 | 8 | 72 |
| Strength of Design | 6 | 6 | 36 | 8 | 48 | 6 | 36 | 8 | 48 |
| Simplicity | 8 | 5 | 40 | 6 | 48 | 7 | 56 | 8 | 64 |
| Ease of Welding | 6 | 4 | 24 | 4 | 24 | 8 | 48 | 8 | 48 |
| Cost | 4 | 4 | 16 | 4 | 16 | 8 | 32 | 8 | 32 |
| Frame Strength | 9 | 5 | 45 | 6 | 54 | 8 | 72 | 9 | 81 |
| Compatibility | 8 | 8 | 64 | 5 | 40 | 8 | 64 | 5 | 40 |
| Serviceability | 6 | 7 | 42 | 5 | 30 | 7 | 42 | 5 | 30 |
| Manufacturability | 7 | 4 | 28 | 6 | 42 | 7 | 49 | 8 | 56 |
| Totals | | | 403 | | 386 | | 543 | | 519 |

As seen in Table 2, Concept 3 (Chromoly steel tube frame with vertically-mounted shocks using transfer rocker and new pushrods) scored the highest.

Final Design

The design chosen uses a Chromoly steel frame with vertically mounted shocks. Due to the placement of the shock, a new rocker and pushrod design had to be developed. This design provides over 1" more clearance for important driveline components. Because of this, the overall length of the base is increased by 4". The improved structural rigidity of this frame also allows for the use of solid frame mounts for attachment to front frame. For added rigidity, support bars were installed from the top engine mounts to rear tabs.

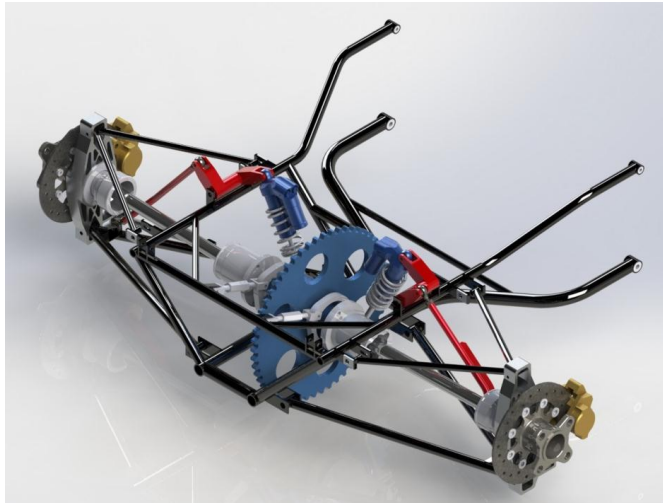


Figure 26: Final Subframe Design

Analysis of Final Design

With a solid understanding of the dynamics of the suspension, the next step was to simulate actual loads on the final subframe to prove its ability to complete its designed task. The first step was to mesh the frame. To do this, the subframe was simplified as much as possible. Next, due to the use of mixed bodies, a solid mesh type was used. For the part to mesh correctly, a curvature mesh was used. The resulting mesh contained 104,886 nodes and 51,405 elements.

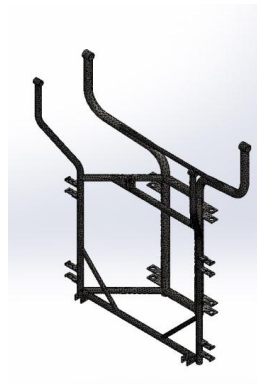


Figure 27: Subframe Mesh

Next, fixtures were applied to the frame. The subframe mounting points were affixed using fixed geometry. This included the pickup points for the front frame, “banana” engine mounts, and roll hoop supports. With the frame held in place, loads were applied to the suspension pickup points, as seen in Table 3. Using the already known suspension loads during

1.5g acceleration, loads were applied to the upper and lower mounting tabs on both sides of the frame. This proved the most accurate simulation of the maximum stresses under hard acceleration.

Table 3: Subframe Loads under 1.5g Acceleration (force in Newton)

| | Force | | | Total |
|---|-------|-------|------|-------|
| | X | Y | Z | |
| 1 | -433 | -39 | -254 | 503 |
| 2 | 433 | 39 | -253 | 503 |
| 3 | 0 | | -507 | 507 |
| 4 | 552 | -42 | -201 | 589 |
| 5 | -1894 | 142 | -694 | 2022 |
| 6 | -1342 | | -896 | 1613 |
| 7 | 1342 | -1003 | 199 | 1687 |

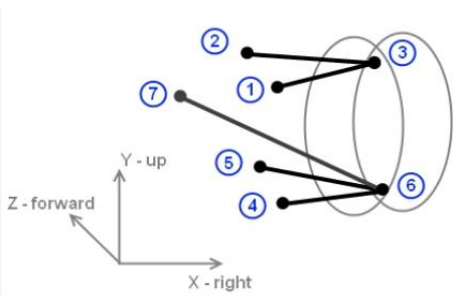
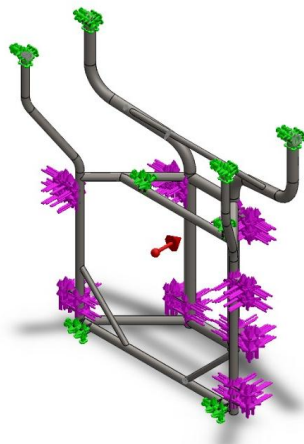



Figure 28: Applied Loads and Fixtures

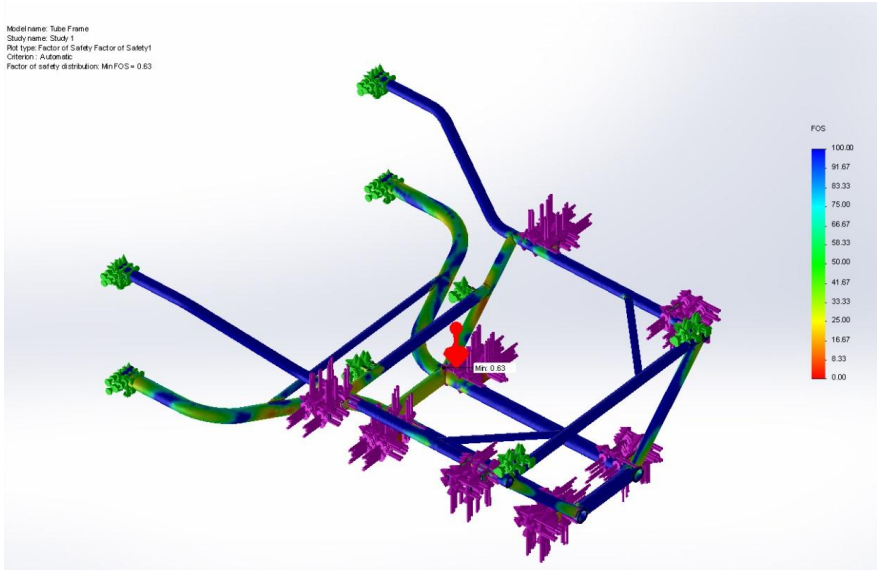


Figure 29: Factor of Safety for Subframe

Figure 29 displays the results from the factor of safety (FOS) plot. A very low 0.63 FOS was recorded, however this value was measured in a sharp corner which caused a stress riser that does not exist on the actual subframe, therefore this value was ignored. The average lowest FOS was around 3.52; this is well above the recommend minimum 2.0 FOS which is used as an industry standard in motorsport (*Race Car Vehicle Dynamic*).

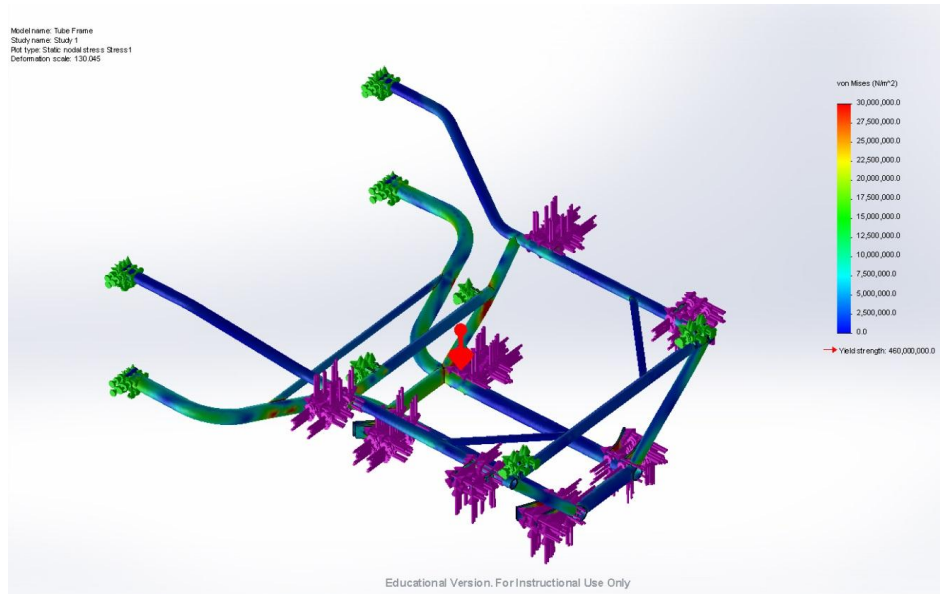


Figure 30: Stresses on Subframe

The stress plot is shown in Figure 30. The maximum stress seen in the frame was around 388,292,000 N/m² while the yield strength of 4130 Chromoly is 460,000,000 N/m².

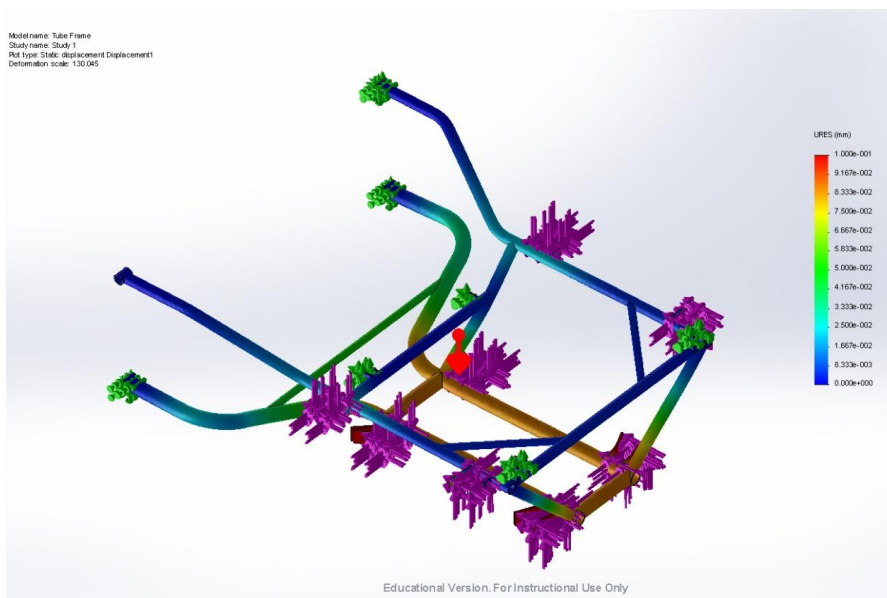


Figure 31: Displacement Subframe

Seen in Figure 31 is the displacement plot for the subframe. Overall frame displacement under these loads was small at 0.582mm. This is due to the rigidity of 4130 Chromoly tubing and frame design.

Refinement of Design

Due to the poor dimensional accuracy of the previous control arms, the ability to adjust the rear camber 2° was desired to ensure the car could keep optimal tire contact patch at all times. The system needed to be simple to integrate into the rear subframe design. To do this, the upper mounting tabs were redesigned. The camber is adjusted by inserting different camber adjustment plates into slots cut into the upper mounting tabs. A set of inserts with different offset holes allows the camber to be adjusted independently on both sides. This setup is very similar to the system on the front of the car. The final system is able to adjust camber from +0.5 to -2.9°. The mounting tabs were welded onto the tube similar to the other mounting tabs.

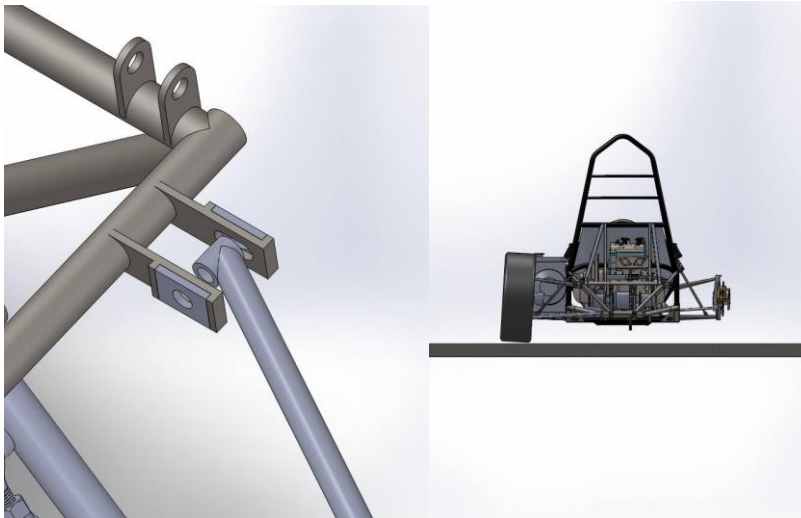


Figure 32: View of Camber Adjustment Tabs and Max Negative Camber

Manufacturing

After the subframe design was finalized, the CAD models were placed into a drawing package and sent to Cartesian Tubing for manufacturing. Each sub component was CNC bent and notched to allow for accurate fitment during the welding process.

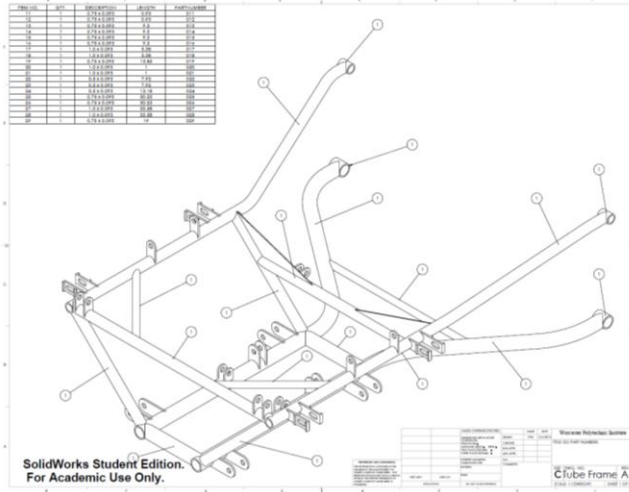


Figure 33: Subframe Drawing

While the tubes were being manufactured, progress began on machining the frame tabs to allow for attachment of key suspension components. All tabs were CNC machined from 4140 Chromoly steel to allow for the best weldability to the 4130 Chromoly tubing. Each tab was notched to fit over the tubes so no gap would be present during welding. This provided the best quality weld.



Figure 34: Frame Tabs during Manufacturing

Once the tubes were received from Cartesian Tubing, they were sent to City Welding & Fabrication for final welding. Drawings were provided to City Welding & Fabrication to make sure the frame was fixture correctly. The final welded frame as received from City Welding & Fabrication is shown in Figure 35.



Figure 35: Welded Frame

After the frame was received back from City Welding & Fabrication, progress began on welding on all frame tabs and suspension pickup tabs. The goal of this step was to have proper fitment of all components. This was done by bolting all suspension arms into place during welding. The setup of the frame for welding can be seen in Figure 36. A similar setup was used when welding on suspension arm pickup tabs.



Figure 36: Welding of Subframe

The final welded subframe is shown in Figure 37. The final product bolts up to existing suspension arms and frame mounting points.



Figure 37: Final Subframe with Tabs

To protect the frame from rusting and to improve aesthetics, the subframe and other suspension components were painted. Since powder coating would add a long delay to the assembly timeline, automotive enamel spray paint was used. The frame, suspension arms, supports, and pushrods were sanded and cleaned. Next, etching primer was used to get an optimal surface for the paint to adhere to. Next, a semi-gloss black enamel was applied, which matched the front frame's pre-existing powder coat finish.



Figure 38: Painted Suspension Parts

Integration

With the subframe completed, it was bolted onto the rear frame. Assembly began by installing control arms, differential, support bars, shock absorbers, and rockers. There was no noticeable play or flex in the frame once it was installed on the car. There was also plenty of clearance for such items as the CVT, chain, and exhaust.



Figure 39: Subframe Installed

Conclusion

The final subframe assembly meets all objectives. It provides a rigid platform to bolt suspension components onto. The frame is lightweight and only adds 2lbs onto the 2013 FSAE subframe design. The adjustable upper suspension tabs allow for adjustment and tuning of suspension geometry. SolidWorks Simulation confirmed that the frame meets stress requirements under typical operation of vehicle. Larger dimensions allow for easier access to suspension components.

Future Recommendations

Several areas of improvement exist for the rear subframe. They are listed below:

- Manufacture frame with rear subframe welded to the front frame. Modular design is not as rigid as a fully welded design.
- Suspension tabs should be made from sections of box tubing to allow for easier welding and stronger engagement.
- Rear jack bar should be integrated into subframe and not as a removable piece.
- Additional bracing could be used in some areas to decrease wall thickness.

Pushrod

Overview

During the 2013 FSAE MQP, the decision was made to integrate a pushrod system to transfer the motion of the wheels to the shock absorbers. This system works by having a rod that is connected to the lower control arm and the rocker assembly. When the wheel moves, the pushrod transfers this motion through the rocker and then actuates the shock. This system has several advantages. First, it decreases the unsprung weight of each wheel and second, it is easier to integrate from a packaging standpoint. It also allows for more adjustability of the suspension dynamics.

Initial State

On the 2013 suspension design, the suspension pushrods were able to clear the half shaft axles by angling the pushrod upwards towards the front of the car. This angle allowed the motion of the lower control arm to be transferred to the rocker assembly while not hitting the half shaft axles. While this design worked in concept, it caused unwanted torsional forces in the rocker assembly and its mounting points. Due to the poor welding on the subframe, this caused the mounting tabs to shear off. This setup also caused the end link on the pushrod to bend. Any of these failures occurring during operation of the running car could result in serious injury. As such, a complete redesign of the rear subframe and pushrods was needed.

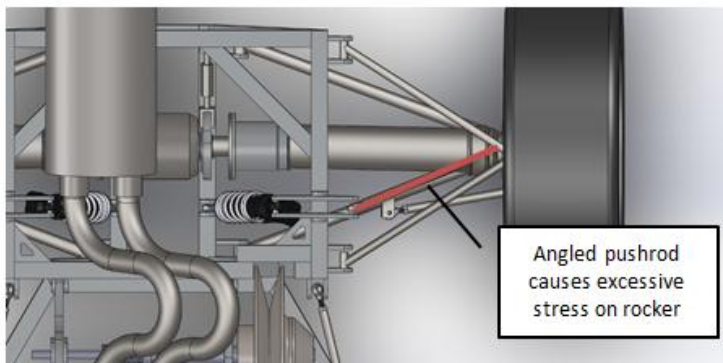


Figure 40: Top View of Angled Push Rod

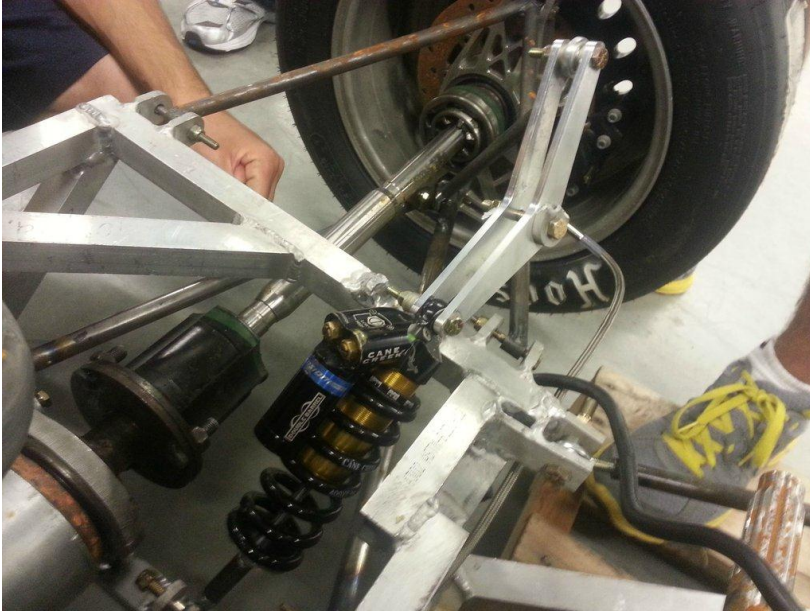


Figure 41: Sheared Off Mounting Tabs

Objective

After analyzing the 2013 suspension design, several areas of improvement were identified for the pushrod design. A design goal was identified for the pushrods. In addition to minimizing costs during the manufacturing and assembly of the 2014 suspension, components from the 2013 suspension would be used when possible after they had been inspected. In the case of the pushrod, rod ends were reusable along with the shock absorbers.

The design of the pushrod must maintain all forces on the same plane with the rocker and shock absorber. This is to keep the rocker from exerting any unwanted forces on the subframe mounting tabs, rocker, and rod ends. It must clear existing suspension and drivetrain components. It must be simple to manufacture and also be easy to install. It must have the ability to adjust ride height.

Research

There are many different ways of transferring the vertical motion of the wheels to the shock absorbers on a car. Most vehicles use a direct acting system where the shock is directly connected to the lower control arm. However, this setup requires additional frame mounting points and also adds unsprung weight. The 2013 FSAE MQP car used a pushrod system to transfer this suspension motion to the shock absorber and spring. There are, however, several different systems that could be used. The main one of these is a pullrod system. On most F1 cars, pullrods have been used due to their lower center of gravity and improved strength since the rod is in tension. The system works by flipping the pushrod system upside down and

mounting the rod to the upper control arm. This places the rod in tension and moves the shocks, springs, and rockers lower to the ground.



Figure 42: Example of Pushrod Suspension

In Figure 43 a typical pushrod and pull rod system can be seen.

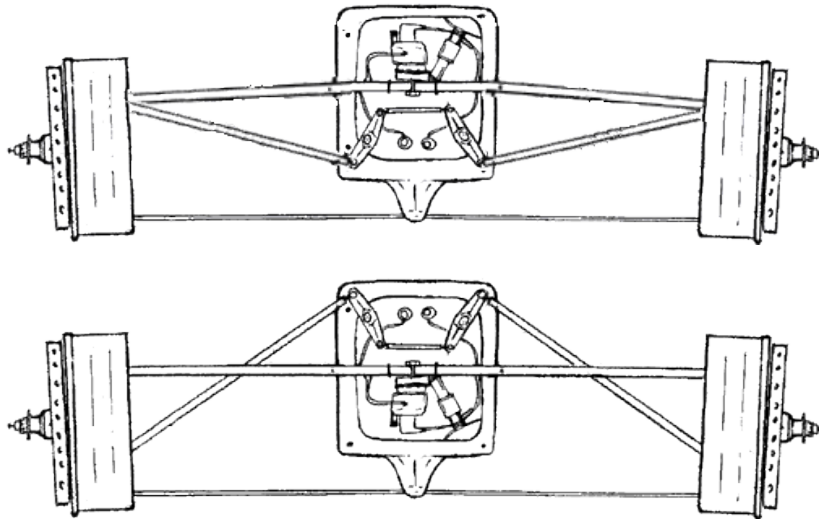


Figure 43: Pullrod vs Pushrod

Due to the complex nature of integrating a pullrod system into the current FSAE car, the decision was made to maintain the pushrod setup of the 2013 rear suspension design.

Design

The next step in achieving the defined design goals was to fix the issues in the 2013 pushrod and rocker designs. To accomplish this, a design had to be developed to keep all forces on the same plane. Since it was determined that the 2013 control arms were going to be used, the same pickup points needed to be used. The pushrod designs used a bent tubular rod

that curved around the half shaft axles to achieve this goal. A reinforcing rib was added to the second design.

Preliminary Design/Concepts

The new pushrod designs used a bent tube that curved around the half shaft axle. The pushrod was made from 0.500" outer diameter, 0.120" wall thickness 4130 Chromoly steel. The rod was made out of tube to both allow the ends to be threaded for rod end inserts and also to make the part lighter.



Figure 44: Pushrod Design

After the primary concept was developed, a second design modification was made. To maintain structural strength of the pushrod under compression, a steel plate made from 1/16" 4140 Chromoly steel was welded onto the rod as a rib to maintain the structural rigidity of the pushrod. The steel rib, however, needs to be able to clear the half shaft during suspension travel. Therefore, a clearance hole was made in the center of the rib to allow the half shaft to pass through. The pushrod bent design keeps all forces in a vertical plane and eliminates the torsional forces seen on the rocker in the 2013 design.

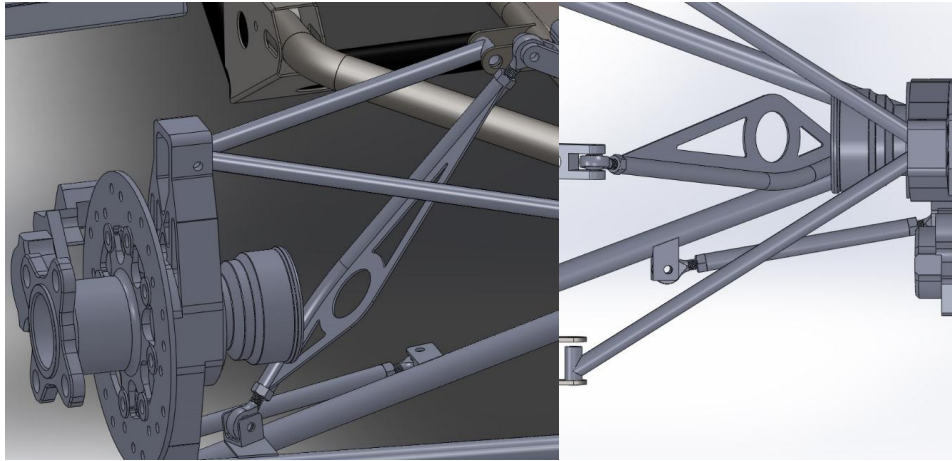


Figure 45: Pushrod

The round hole in the center of the rib allows the half shaft to clear the arm. This rib is essential in making sure the bent tube section does not collapse under the loads of the car.

Concept Selection

After research and concept designs were developed, the decision was made to move forward with the bent pushrod design with the strengthening rib. This was decided upon for several reasons. First, this design was stronger than a purely tubular design and second, other concept pushrods did not fit the packaging and size requirements.

Final Design

The final pushrod design was updated from the concept design. First, the rib design was changed from having a clearance hole for the half shaft to go through. Instead, the rib was made .500" wide. This completely avoids the half shaft axles. This is a small loss in strength, but this is negligible. Seen in Figure 46 is the final pushrod design.

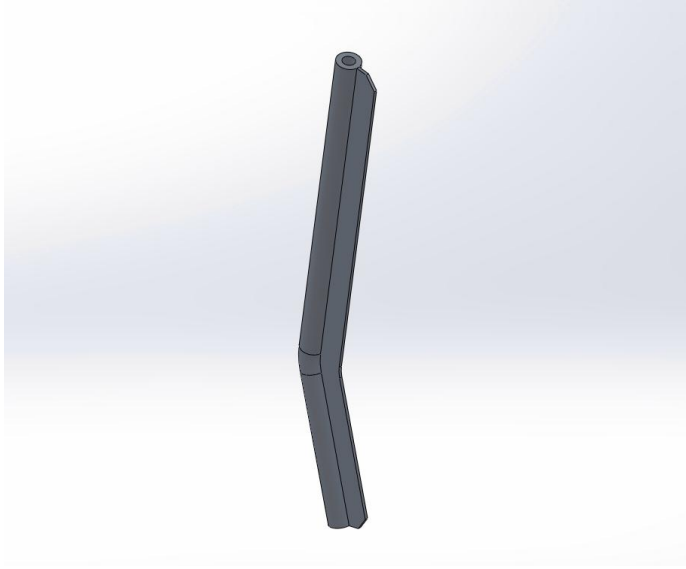


Figure 46: Final Pushrod with Thin Rib

Refinement of Design

During the assembly of the rear suspension, a design refinement was made to the final pushrod design. One of the main issues with the first concept design was the installation difficulty due to the half shaft axle clearance hole. To avoid this problem, the reinforcement rib was made smaller such that it no longer interfered with the half shaft axles. However, this rib was still positioned on the inside of the pushrod. Since the dust boots for the CV axles interfere with this, the rib was moved to the outside of the pushrod in order to provide additional clearance to the CV boots. Also, for the ease of manufacturing, the rib was made shorter so it could fit into a standard 6" mill vise. As with the previous designs, the ends of the pushrod are tapped to accept spherical rod ends.



Figure 47: Refined Pushrod Design

Analysis of Final Design

With a solid understanding of the dynamics of the suspension, the next step was to simulate actual loads on the final pushrod to prove its ability to complete its designed task. In addition, the pushrod was simulated with and without the reinforcing rib to understand how this design change affected the overall strength of the rod. The first step was to mesh the pushrod without a rib. For the part to mesh correctly, a curvature mesh was used. The resulting mesh contained 18,311 nodes and 10,308 elements.

Model name: Pushrod
Study name: Study.1
Mesh type: Solid mesh



Figure 48: Pushrod without Rib Mesh

Next, fixtures were applied to the pushrod. The pushrod upper face was affixed using fixed geometry. With the pushrod held in place, loads were applied to the suspension pickup points as seen in Table 4. Using the already known suspension loads during a 3.5g bump, a load of 1330N was applied to the lower face of the pushrod. This proved to be the most accurate simulation of the maximum stresses under hard bump.

Table 4: Pushrod Loads under 3.5g Bump (force in Newton)

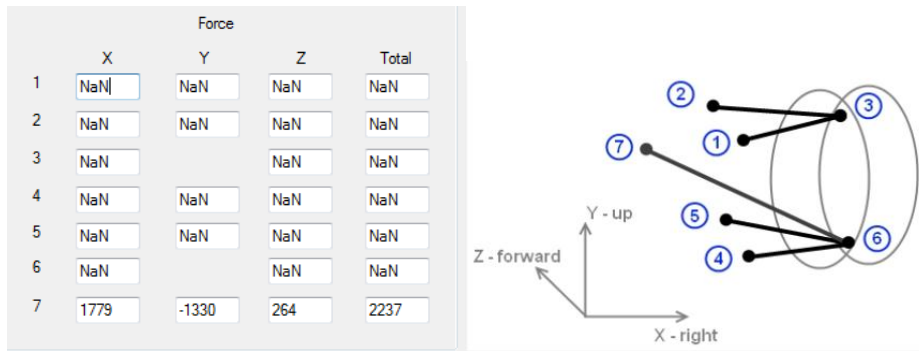


Figure 49: Applied Loads and Fixtures

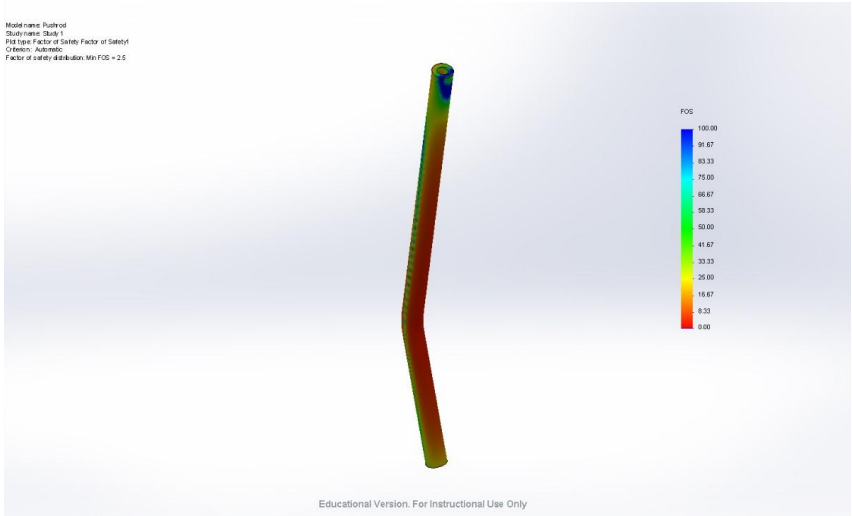


Figure 50: Factor of Safety for Pushrod without Rib

In Figure 50 are the results from the factor of safety plot. The lowest FOS recorded was 2.5. The average lowest FOS measure was around 4.6. This is well above the recommended minimum 2.0 factor of safety which is used as an industry standard in motorsport (*Race Car Vehicle Dynamic*).

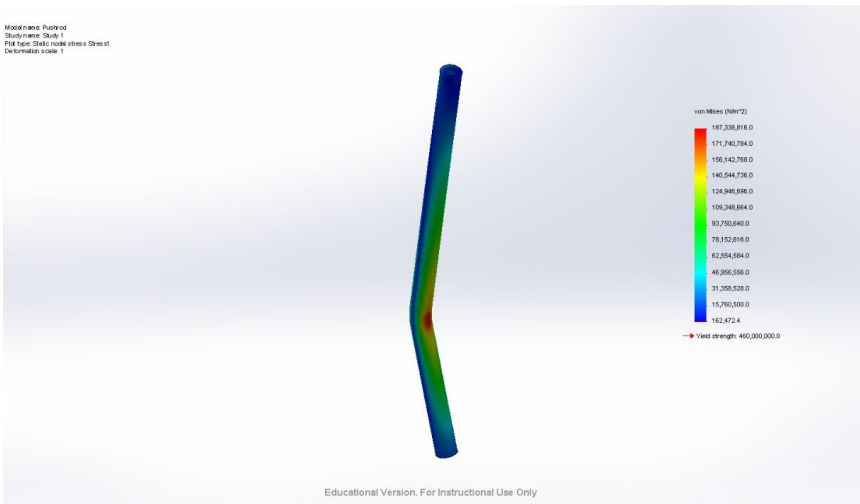


Figure 51: Stresses on Pushrod without Rib

The stress plot is shown in Figure 51. The maximum stress seen in the pushrod was around 187,339,000 N/m² while the yield strength of 4130 Chromoly is 460,000,000 N/m².

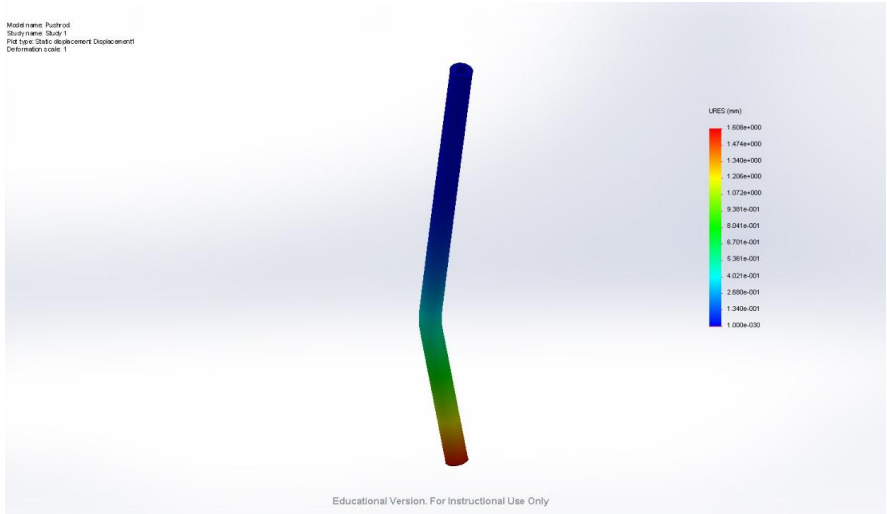


Figure 52: Displacement Pushrod without Rib

Seen in Figure 52 is the displacement plot for the subframe. Overall displacement under these loads was small at 1.608mm. This is due to the rigidity of 4130 tubing.

Next, the pushrod with the rib was tested. The first step was to mesh the pushrod with the rib. For the part to mesh correctly, a curvature mesh was used. The resulting mesh contained 23,721 nodes and 13,721 elements.



Figure 53: Pushrod with Rib Mesh



Figure 54: Applied Loads and Fixtures

Model name: Pushrod
 Study name: Study 1
 Plot type: Factor of Safety Factor of Safety1
 Criterion: Submerged
 Factor of safety distribution: Min FOS = 4.8

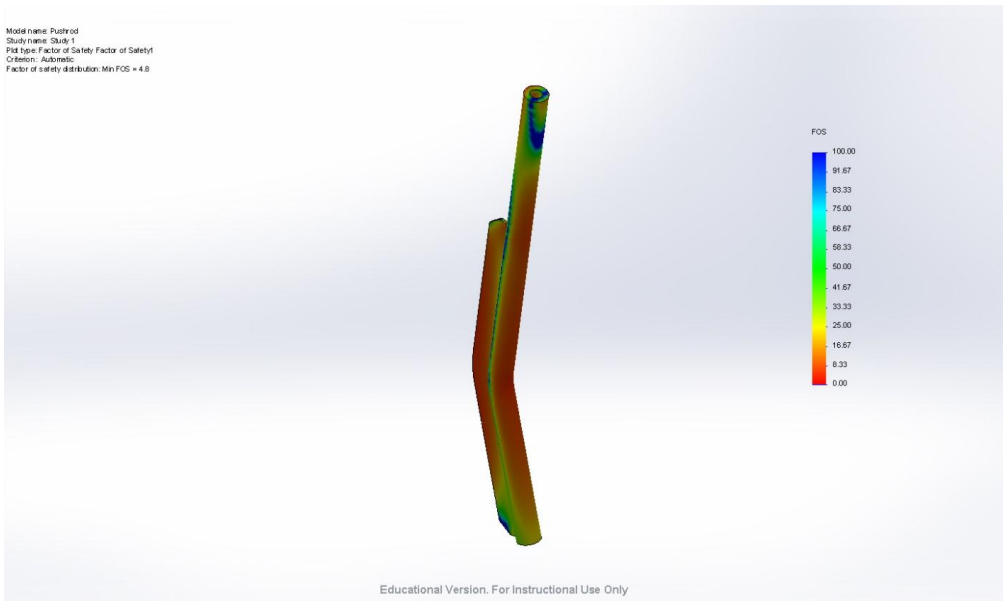


Figure 55: Factor of Safety for Pushrod with Rib

In Figure 55 are the results from the factor of safety plot. The lowest FOS recorded was 4.78, an increase of 2.28 from the pushrod without the rib. The average lowest FOS was around

7.6. This is well above the recommended minimum 2.0 factor of safety which is used as an industry standard in motorsport (*Race Car Vehicle Dynamic*).

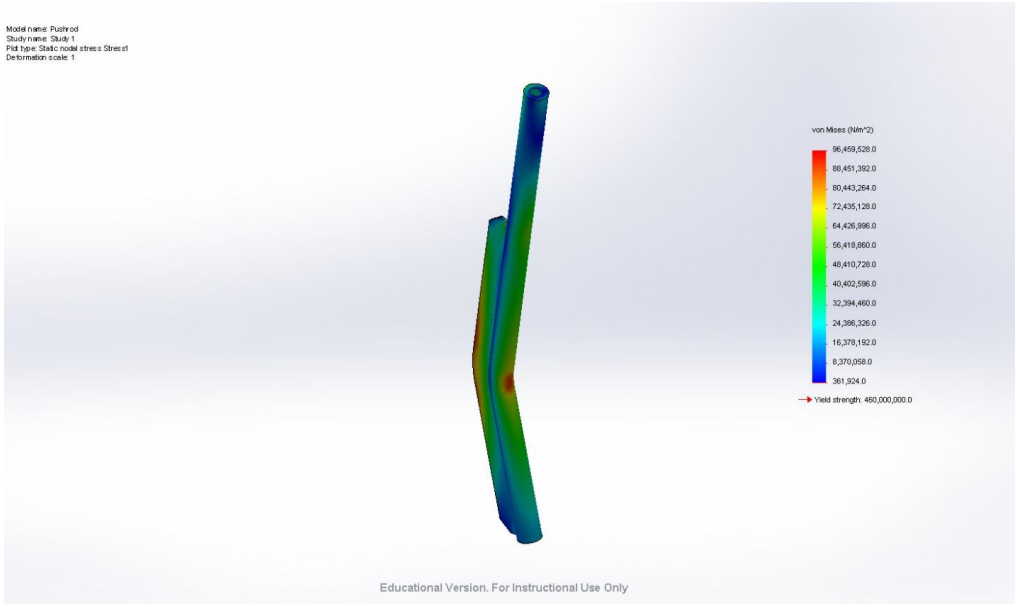


Figure 56: Stresses on Pushrod with Rib

The stress plot is shown in Figure 56 for the pushrod with the rib. The maximum stress seen in the pushrod was around 96,459,500 N/m², a decrease of 90,879,500 N/m².

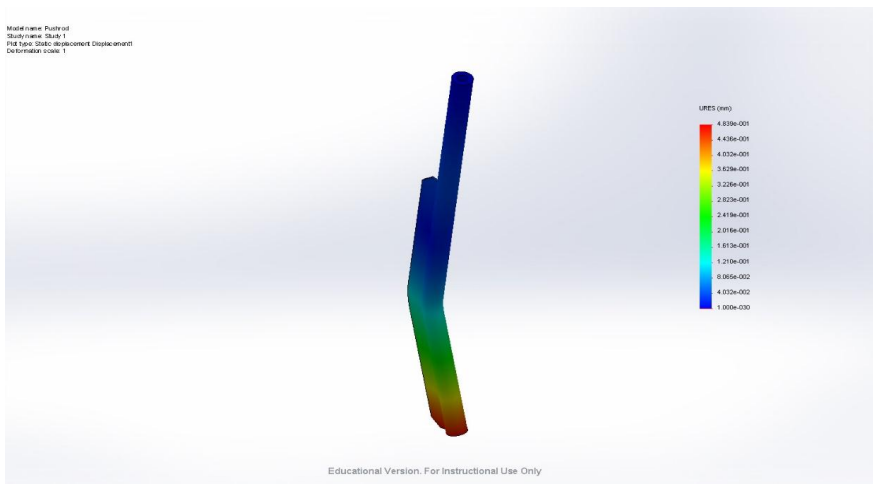


Figure 57: Displacement Pushrod with Rib

Seen in Figure 57 is the displacement plot for the pushrod. Overall displacement under these loads was 0.484mm compared to 1.608mm without the rib. This is a 232% decrease in deflection. This is due to the rigidity added by the rib.

Manufacturing

Due to the precision bending needed to manufacture the pushrod, Cartesian Tubing was chosen to manufacture the bent section of tubing which makes up the main body of the rod. The rib for the pushrods was machined using a Haas VM2 and a fixture plate. The rib was then TIG welded onto the pushrod. Next, the ends of the rod were tapped to 5/16-24 to accept rod ends.



Figure 58: Machined Pushrod and Rib

Integration

In Figure 59, the pushrod can be seen in the rocker and pushrod assembly. The bent design allows it to easily clear the haft shaft axle. The inverted rib design also gives more clearance to the CV boots. The rod ends allow for adjustment of the total length of the rod which allows for adjustment of ride height.



Figure 59: Pushrod Assembly

After all suspension components were completed, the pushrods, shocks, rocker, and arms were bolted up and test fitted. Several adjustments were made. First, due to an inaccuracy in the subframe welding, the shock extensions had to be trimmed on one side so the rocker angles would match. Second, the pushrods had to be trimmed to allow for a lower ride height so the car would have less rake. Next, the CVT boots had to be trimmed in order to clear the push rods.



Figure 60: Pushrod System

After these modifications were completed, the final ride height and rocker angles matched with the CAD model. The suspension was statically tested by loading 250lbs of weight onto the back of the frame. The suspension moved freely and the pushrods easily handled this force.



Figure 61: Suspension at Ride Height

Conclusion

The final pushrods allow for the rear suspension to operate properly. The improved strength of the pushrod, due to the addition of a rib, ensures the design will be able to withstand suspension impacts that exceed forces seen during normal operation. The bend pushrod design allows for all forces to be maintained on a single plane of action while still allowing the pushrod to clear all driveline components.

Future Recommendations

Several areas of improvement exist for the pushrod. They are listed below:

- Future designs should look into angled pushrod setups to avoid the use of bent links.
- More adjustment should be built into the pushrods.
- New suspension arms should have offset pushrod pickup points to allow for more clearance with half shafts.

Rocker

Overview

The rockers main job is to translate the motion of the suspension to the shock absorber. It does this by pivoting around a central point. The distance between both of the rocker arms defines the rocker ratio. The angle between these arms also defines the transmission angle of the shock absorber and pushrod.

Initial State

The main issue with the rocker was the rocker geometry at suspension ride height. While the suspension is sitting in a neutral position, the pushrod and shock should sit at near 90° angles with the rocker. This is because the rocker needs to be kept as far away from its trigger angle as possible. Also, by keeping these angles around 90° , the angle of transmission is kept as efficient as possible. However, the current shock/rocker setup has a much larger angle at normal ride height. As seen in Figure 62, the pushrod has a 103° angle with the rocker, and the shock has a 116° angle with the pushrod. These large angles mean that the arm motion will not be transferred as efficiently as possible during suspension travel. It is also possible the suspension could lock up if these angles approach near 180° .

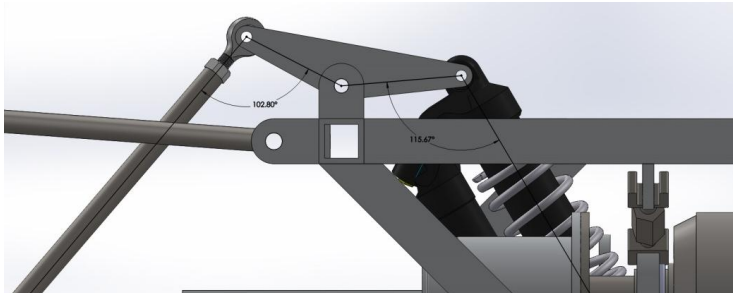


Figure 62: Rocker Angles

Objective

After analyzing the 2013 suspension design, several areas of improvement were identified in the rocker design. A design goal was identified for each of these aspects. In addition to minimizing costs during the manufacturing and assembly of the 2014 suspension, components from the 2013 suspension would be used when possible after they had been inspected.

The new rocker design must be able to withstand forces exerted on it during suspension operation. It must be able to transmit motion from the suspension to the shock absorber. It must also limit motion of the suspension to be within the FSAE rule of no more than 2" of total suspension travel.

Research

Several different rocker designs were studied while developing the final concept designs. These included a simple plane flat plate rocker, angled rockers, and two plane rocker designs. Two different concepts were looked at. With the horizontal shock concept, a flat plate rocker was used. For the horizontal shock concepts, a two plane rocker was used.

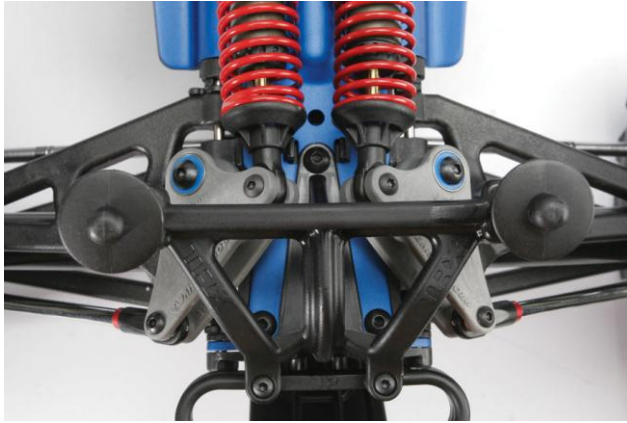


Figure 63: Example of Single Plane Flat Rockers

Design

The first concept design used a unique rocker layout. Since one of the main design goals was to eliminate any torsional loads in the rocker mounting tabs, a way of transferring the load of the pushrod to the shock was needed. Since the differential and half shaft axles were in the way of mounting the shocks in-line with the pushrod, the 2013 flat plate rocker would not work. Since the packaging advantages of keeping the shock mounted inside was a desirable aspect of the 2013 design, a method of keeping the shock in this vertical orientation required a change in rocker design.

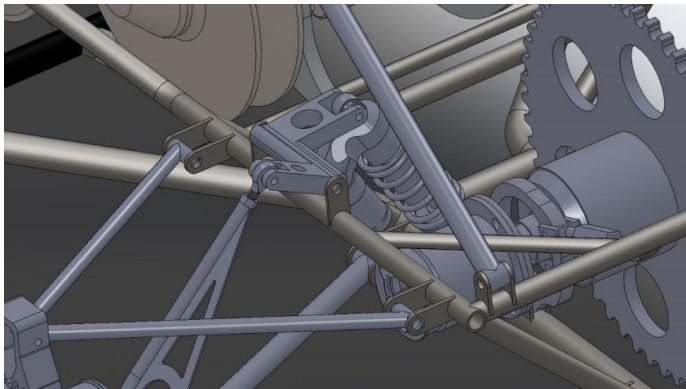


Figure 64: Rocker Design Concept One

In Figure 64, a SolidWorks model of two plane rocker design is illustrated. By using the rocker arm to translate the linear motion of the suspension travel into rotational motion, the forces could be transferred to a different plane without putting extra forces on the pushrod, rocker mounts, or shocks. The main load seen inside of the rocker arm is as a torsional force. However, this force should not be an issue with a properly designed rocker. To optimize this design, SolidWorks Simulation will be used.

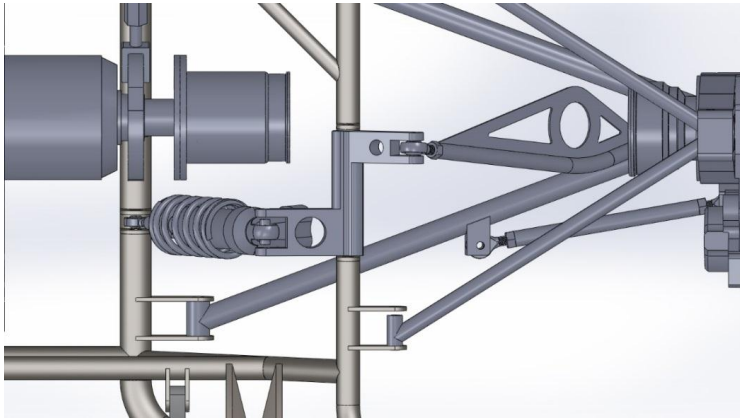


Figure 65: Top View of the New Pushrod Design

The next rocker concept design mounts the shocks horizontally above the differential. This design was based on similar pushrod concepts utilized in other suspension setups as seen in road cars and Formula 1 cars. The main advantage to this concept is it simplifies the rocker design by ensuring all moving components are on the same plane. To hold the shocks above the differential, an extra support structure would have to be made that would hold the shock mounting tabs above the differential. This triangular frame was designed to be as small as possible to reduce weight and to allow for easier access to the differential and chain tensioning system.

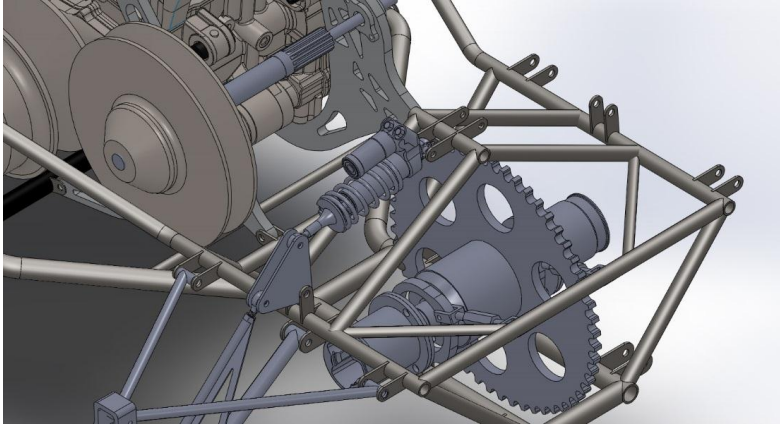


Figure 66: Second Rocker Design Concept

The main advantage to this system can be seen in Figure 66. By mounting the shock in-line with the pushrod, the rocker arms can be made of simple flat plates. This also eliminates the forces found in the other rocker design since the rocker does not transfer any forces onto a different plane.

This design does have several disadvantages. First, the construction of the upper triangular frame will add extra weight and complexity during welding. It also blocks access to removing the differential and the main sprocket. Another issue is the frame does not clear the existing 2013 exhaust system and is also in the way of the roll hoop support bars.

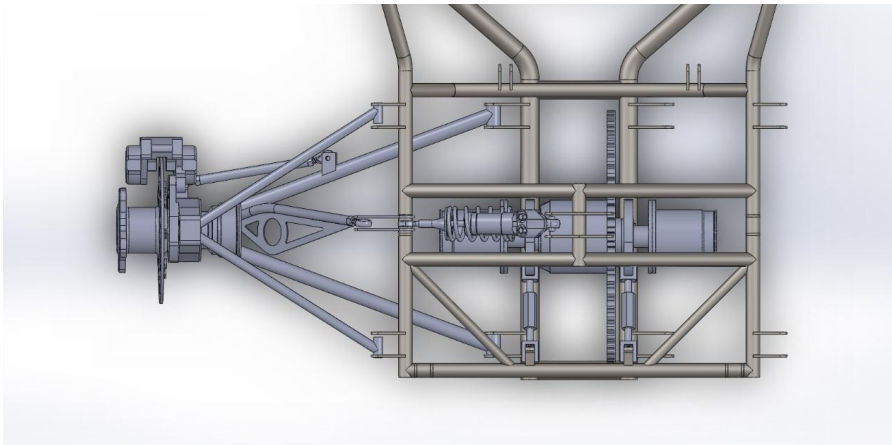


Figure 67: Top View of the Second Design

Preliminary Design/Concepts

Seen in Figure 68, Figure 69, and Figure 70 are the three concept designs. The final rocker design needed to be both manufacturable and have high strength to survive the rigors of an FSAE car.



Figure 68: Rocker Design One

Design One was developed off of the first concept. It was machined out of a solid block of 6061-T6 aluminum to form an angled piece. This formed a very strong, single part. However, due to the size of the material stock, the cost of material would be higher. Machining time for this component would also be somewhat high due to the more complex machining operations. Another issue with this rocker was that it did not allow for future adjustments.



Figure 69: Rocker Design Two

Design Two used a Chromoly tube with tabs welded to it. Inserted into the ends of the tube were bronze bushings, which provide a surface for the rocker to rotate on. The advantage of such a design is its lower cost due to the use of cheaper materials. However, the design would require accurate welding of the tabs. Therefore, the setup of this part was somewhat complex. Also, since it used welds, there is a possibility it could break if the welds are less than perfect.

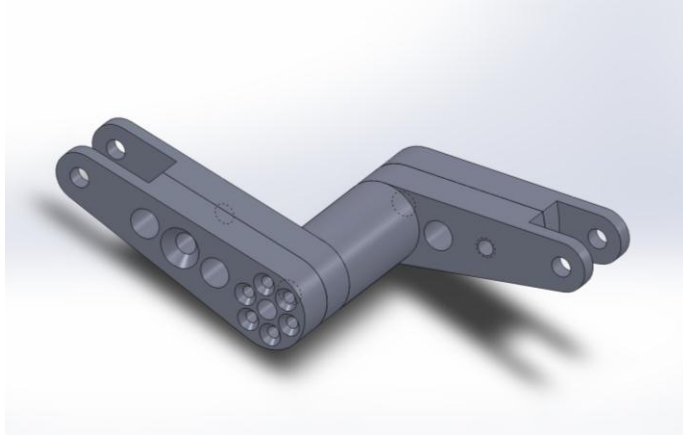


Figure 70: Rocker Design Three

Design Three was made up of three simple parts. This included the large rocker, small rocker, and rocker center. The small and large outer rocker arms were bolted onto the center rocker by six 6-32 flat head screws. This allowed for the simple machining of the rocker out of already available stock material. This design has several advantages over the first two designs. First, the rocker angle can be adjusted by only re-machining a single, simple part (the rocker center) since the angle is controlled by the offset of each bolt circle between sides. Second, the outer arms can be changed without re-machining the whole rocker assembly. This was the design that was chosen for the final car.

Concept Selection

Several different aspects were looked at before a final decision was made regarding the three concept designs. The first concept involves machining the rocker from a solid block of material. This is both expensive and time consuming. Therefore, this concept was discarded. The second rocker design is cheap, but the use of welding on a high stress component such as the rocker was less than desirable. In addition, fixturing this design for welding would be challenging. The final design used three separate components. As such, the rocker ratio and rocker angle could be adjusted without remanufacturing the whole rocker assembly. This design was chosen for this reason.

Final Design

Several changes were made between the third concept design and the final design. First, the rocker arms were changed from being manufactured from four separate 0.500" aluminum plates to being machined from a single piece of 1" x 1" 6061-T6 aluminum bar stock. Next, the shock absorber rocker arm was machined to allow for more clearance for the shock absorber at full suspension droop.

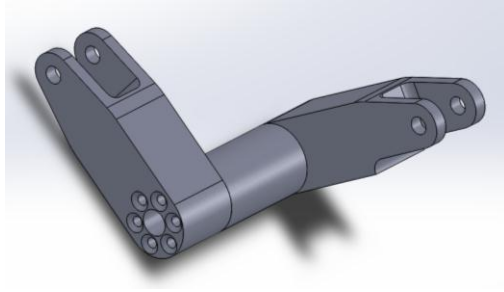


Figure 71: Final Rocker Design

Analysis of Final Design

With a solid understanding of the dynamics of the suspension, the next step was to simulate actual loads on the final rocker design to prove its ability to complete its designed task. The first step was to mesh the rocker. Next, due to the use of mixed materials, a solid mesh type was used. In order for the part to mesh correctly, a curvature mesh was used. The resulting mesh contained 95,724 nodes and 62,278 elements.

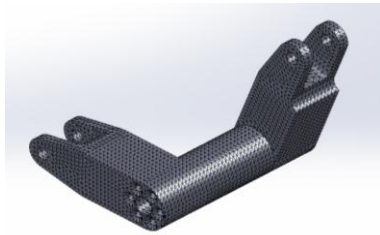


Figure 72: Rocker Mesh

Next, fixtures were applied to the rocker. One side of the rocker mounting holes was affixed using fixed geometry. A hinge joint was applied to the center of the rocker to allow the rocker to pivot. Bolt connections were added to all twelve screw holes with a no contact rule between the face of the center rocker and rocker arms. With the rocker held in place, a force was applied to the other rocker mounting holes as seen in Table 5 using the already known suspension loads during a 3.5g bump. This proved the most accurate simulation of the maximum stresses under hard suspension movement.

Table 5: Rocker Loads under 3.5g Bump (Force in Newton)

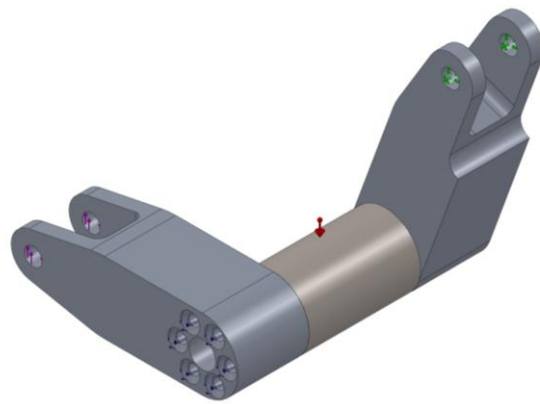
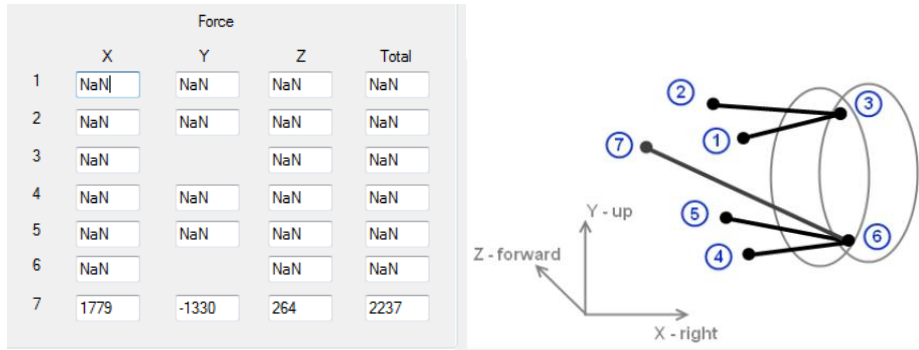


Figure 73: Applied Loads and Fixtures

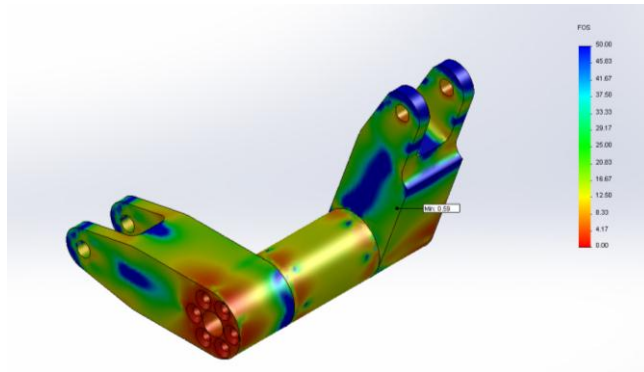


Figure 74: Factor of Safety for Rocker

In Figure 74 are the results from the factor of safety plot. A 0.59 FOS was recorded; however, this value was measured in a sharp corner which caused a stress riser that does not exist on the actual rocker, therefore this value was ignored. The average lowest FOS was around 2.1. This is very close to the recommended minimum 2.0 factor of safety which is used as an industry standard in motorsport (*Race Car Vehicle Dynamic*).

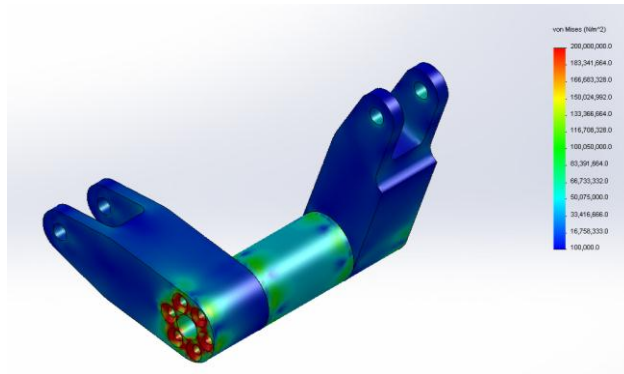


Figure 75: Stresses on Rocker

The stress plot is shown in Figure 75. The maximum stress seen in the frame was around 722,501,000 N/m².

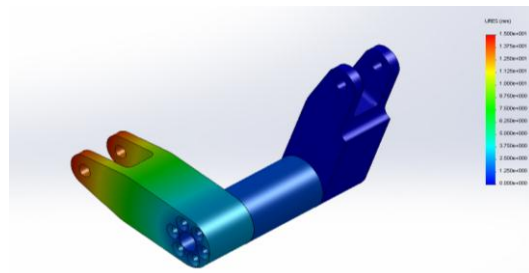


Figure 76: Displacement Rocker

Seen in Figure 76 is the displacement plot for the rocker. Overall rocker displacement under these loads was 14.801mm. This large displacement is due to the spring nature of the center steel section.

Refinement of Design

The next step in the rocker design was to determine the final rocker offset angle given suspension geometry and actual ride height of the car. Using SolidWorks, the suspension ride height was determined and the suspension was moved to a maximum of 2" of total travel. Once completed, the middle point was chosen for the ride height at 0.500" total shock travel. Next, the angle of the rocker was set such that the pushrod and shock made 90° degree transmission

angles with the rocker. This gave the optimal possible trigger angles during the full range of motion of the suspension.

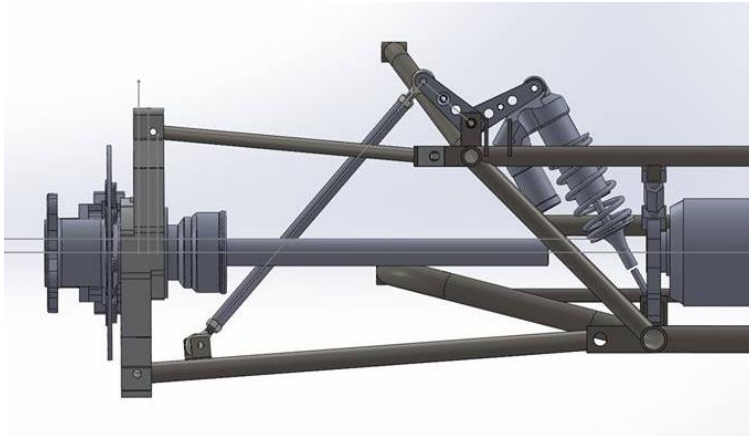


Figure 77: Ride Height

At ride height, the half shaft axles sit parallel to the ground, giving them the most efficient operation possible. This also gives the bottom arm a slight downwards angle of 5°.

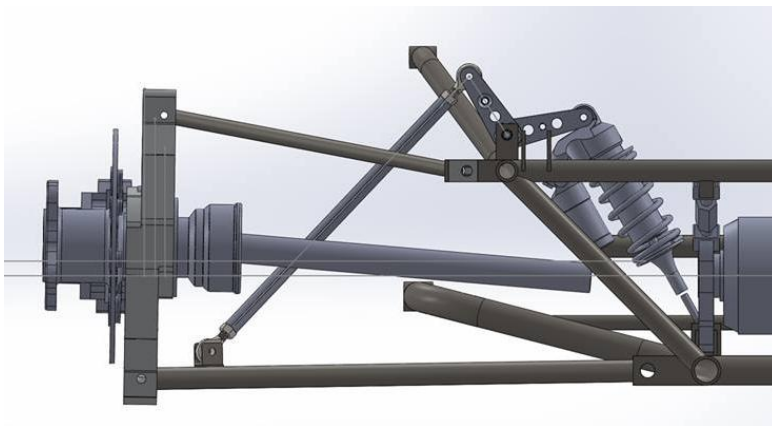


Figure 78: Full Bump

During bump, the total upwards travel is 1". This is before the shock absorber runs out of travel. The overall rocker geometry operates well at this position.

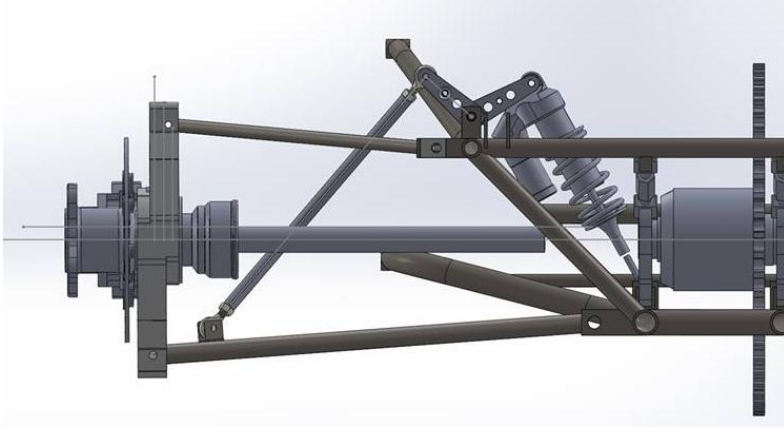


Figure 79: Full Droop

An issue was noticed during full suspension droop. At this angle, the bottom of the rocker contacts the top of the shock. To fix this issue, a rounded cutout was created to provide around 1/32" of extra clearance.

Manufacturing

The rocker components were designed for ease of manufacturability. This enabled the components to be manufactured with the machining resources available at WPI and also improved the vehicle's performance in the FSAE Competition's static events as manufacturability is a judged criterion for the design and cost events. The rocker arms were designed and manufactured from 6061-T6 aluminum on a Haas CNC Mini-mill. The rocker center pieces were designed and manufactured from 1144 alloy steel on a manual lathe and Haas CNC Mini-mill. Once the components were manufactured, they were assembled using twelve 6-32 screws and a shoulder bolt. Lastly, they were installed on the car as seen in Figure 80.



Figure 80: Rocker Assembled on Car

Integration

In Figure 81, the rocker can be seen in the rocker and pushrod assembly. The offset rocker design allows the pushrod and shock absorber to easily clear the half shaft axle. The rocker angles were optimized for suspension ride height. The extra clearance on the bottom of the rocker arm allows the shock absorber to clear the rocker under full suspension droop.



Figure 81: Rocker Assembly

After all suspension components were completed, the pushrods, shocks, rocker, and arms were bolted up and test fit. A picture is shown in Figure 82 of the final assembly.



Figure 82: Pushrod System

Testing

The car was tested by running the suspension through several suspension travel cycles. This was done by bouncing the rear of the vehicle. All tests passed, however after several suspension cycles under heavier loads, play of several degrees was noticed in the rocker assemblies. This was found to be caused by the bolt circle beginning to round out the aluminum material. This fatigue failure was not accounted for in the SolidWorks simulation models. If this problem was left uncorrected, the suspension could collapse during operation. Therefore, a design change was needed to make sure a failure would not occur.

Final Design Revision

Due to the rocker's failing during testing, a design revision was needed. Since all tuning had been completed using the adjustable rockers, it was decided to weld the assembly together with an aluminum center section.

To make sure this design change would not affect the strength of the rocker, a SolidWorks simulation was run. The same conditions were used during this test as the final design simulation. The results are seen in Figure 83: Factor of Safety for Rocker Revision.

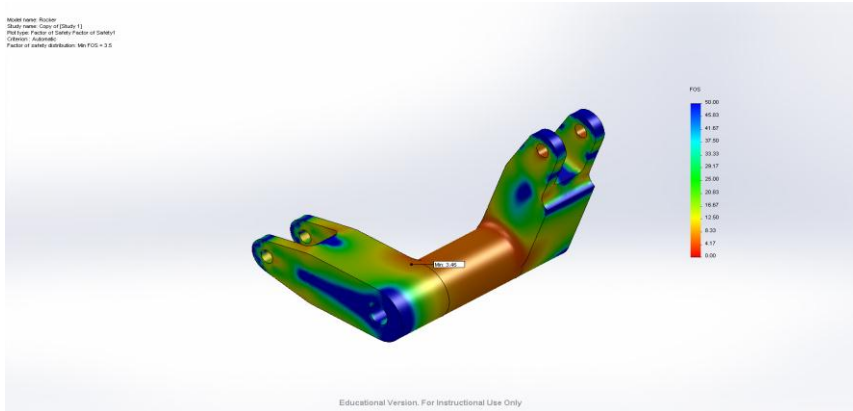


Figure 83: Factor of Safety for Rocker Revision

The removal of screws resulted in a final factor of safety of 3.5. This proves that the welded assembly is much stronger than the bolted assembly. The rocker was TIG welded in Washburn shops and is pictured in Figure 84: Welded Rocker.

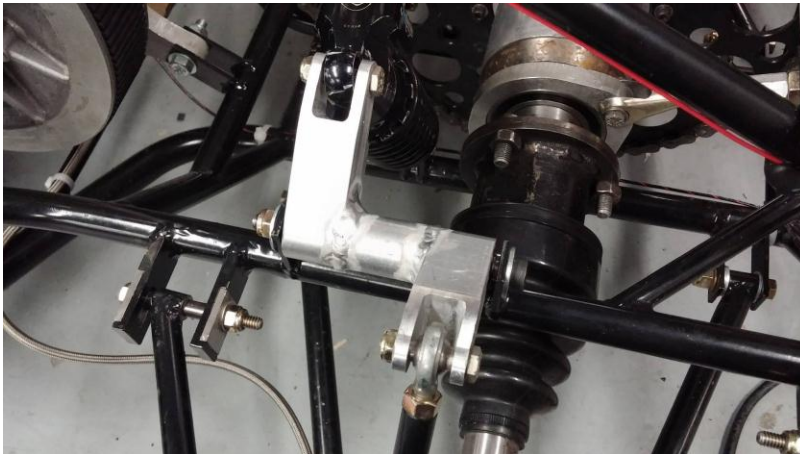


Figure 84: Welded Rocker

Conclusion

The final rocker design meets all design specifications. The offset design allows for forces to be maintained on a single plane of action. The three-piece design allowed for built in tuning of transmission angles. The design was improved upon after tuning to provide a more rigid assembly with the welding of the three separate sections. This final design exceeds the design requirements for minimum factor of safety.

Future Recommendations

Several areas of improvement exist for the rocker. They are listed below:

- Future designs should look into angled pushrod setups to avoid the use of an offset rocker.
- Use of different clamping methods to allow for more fine adjustment of rocker angles.
- Install bushings into center pivot to allow for smoother operation.

Differential

Overview

The purpose of a differential is to allow the outer wheel to spin more quickly than the inner wheel in a corner, which prevents the car from hopping and increases handling stability. Torsen limited-slip differentials, like the one on the WPI FSAE car, also ensure that torque is being transmitted to the wheel with the most traction. A differential is a vital part of a vehicle's drivetrain and must be built to withstand the rigors of auto racing in an FSAE car.

Initial Condition

The differential and corresponding equipment on the FSAE car were taken apart and an inspection was conducted, which revealed a few problems. The two sealed bearings that were pressed into the differential mounts were pressed out and examined. While they were not completely seized, the bearings were difficult to rotate and made a scraping noise when turned, indicating that they could not be used upon reinstallation of the differential. The old bearings are shown in Figure 85.



Figure 85: Old Differential Bearing

The differential internals needed to be greased but were otherwise in operating condition. However, there was an issue with the output shaft housings on each side of the differential. One side was too small for the bearing to press onto; its outer diameter measured 1.881" while the inner diameter of the bearing measured 1.965". This difference of 0.084" was too great to allow for a proper press fit. The other output shaft housing was mushroomed out on the end from a previous FSAE team hitting it with a hammer. This side was the correct diameter but would need some resurfacing. The gap between the housing and the bearing's inner race is shown in Figure 86.

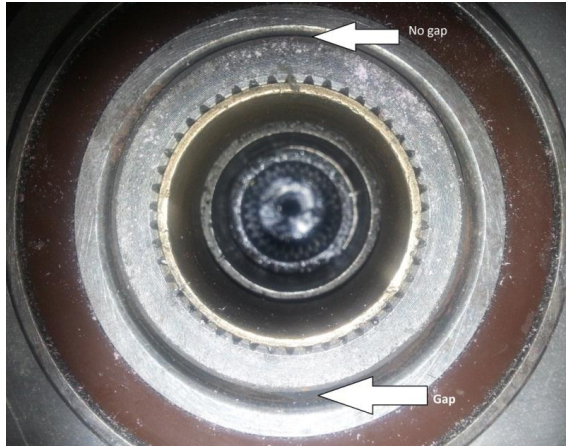


Figure 86: Gap between Housing and Bearing

The sprocket is held to the differential by a custom-machined mounting plate, which has three bolts connecting it to the differential. This plate had an issue where the bolts were pulling themselves through the counterbored holes that they ran through. The 0.500" diameter heads of the bolts sat on 0.030" thick aluminum, which was too thin and was bending. Failure of this part would result in the sprocket becoming disconnected from the differential. The sprocket mount in its original state is shown in Figure 87.



Figure 87: Sprocket Mount before Machining

Research

The worn bearings needed replacement and research begun on the type of bearing that should be used. The FSAE forums were consulted and other FSAE teams suggested the use of sealed ball bearings, which were the same as the worn bearings that were already on the car.

The old bearings were measured to have an inner diameter of 50mm (1.965”), an outer diameter of 80mm (3.150”), and a thickness of 16mm (0.630”); therefore bearings of this size were searched for. Boca Bearings, an online bearing distributor, has sealed ball bearings of various capabilities that met the size requirements. The bearings were characterized by their allowed revolutions per minute (RPM), so a calculation needed to be done on the expected RPM of the rear wheels on the FSAE car.

The velocity used for calculations was 100mph (8800 ft/min), which is a higher velocity than the FSAE will travel on a racetrack. The diameter of the tire is 16” (1.333 ft.)

Equation 2

$$RPM = \frac{v}{\pi d}$$
$$RPM = \frac{8800ft/min}{4.187ft/rev} = 2102rpm$$

As seen in Equation 2, the calculated RPM at 100mph is about 2100rpm. The MR6010-2RS bearing, from the Boca Bearings website, has a rating of 6300rpm, which provides a safety factor of three. These bearings were under \$40.00 each and two of them were purchased for use in the FSAE car.

Design

Preliminary Design

A design for a shaft bushing on the sprocket-side differential output shaft housing needed to be created. A shaft bushing is a thin piece of tubing that can be made to fill a gap, which in this case is the gap between the output shaft housing and the surface of the bearing's inner race. The shaft bushing's design would allow its inner surface to press fit onto the differential output shaft housing while the bearing would press fit onto the outer surface of the shaft bushing. A drawing of the preliminary design is shown in Figure 88.

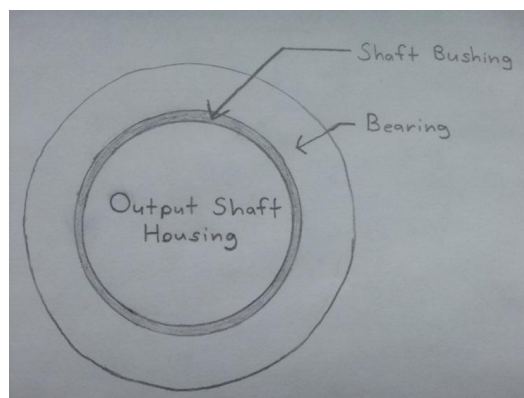


Figure 88: Preliminary Design of Output Shaft Bushing

A design regarding the sprocket mount also needed to be created. The bolts holding the sprocket mount to the differential had too small of a head diameter in comparison to the thread diameter; therefore there was an insufficient surface area for the bolt to seat onto. Additionally, the area onto which the bolts sat was only 0.030" in thickness. The material, being aluminum, bent inward and was at risk of failure.

There were three bolts holding the sprocket mount to the differential, but there were six holes drilled in the bolt circle. The three holes that did not have bolts in them were not counterbored or modified in any way, allowing them to be machined easily. The preliminary design, shown in Figure 89, incorporates a counter bored hole of a wider diameter and a washer between the head of the bolt and the surface area to which it seats. This allows the force of the bolt to be spread over a larger area. Additionally, the thickness of the seating area is increased to prevent the aluminum from yielding as it did originally.

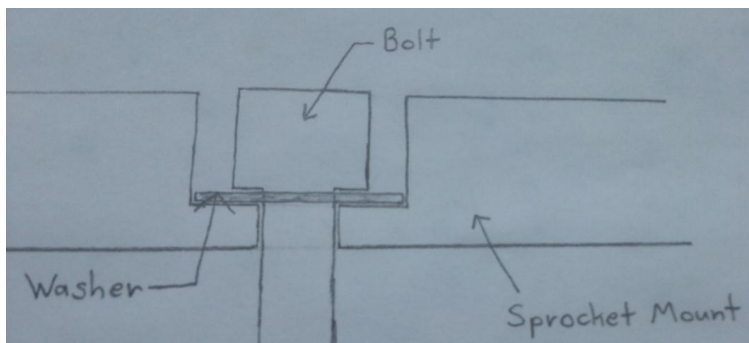


Figure 89: Preliminary Design of Sprocket Mount Hole

Final Design

The final design of the shaft bushing began by selecting a material. 6061-T6 aluminum was chosen due to its machinability, malleability, and the wide range of tube thicknesses available. The outer diameter of the differential output shaft housing is 1.881" and the diameter of the inner race of the bearing is 1.965". A search on OnlineMetals.com showed that a foot-long tube of 6061-T6 aluminum could be purchased with an inner diameter of 1.884" and an outer diameter of 2.000". The inner diameter of the tube was just 0.003" larger than the outer diameter of the housing, which not only ensured an excellent press fit, but also eliminated a step in the machining process (boring out the inner diameter of the tube). The tube's outer diameter would be machined to 1.960" to allow for the bearing to be pressed onto it. The tube would be cut to a length of 1.000" in order to cover nearly the entire length of the differential output shaft housing.

The goal of the final design of the counterbored holes in the sprocket mount was to make the holes three times more resistant to yielding, at a minimum. The bore diameter was 0.500". The bore diameter in the final design was changed to 0.750" to incorporate washers of the same diameter, which would rest between the bolt and the bottom surface of the hole. After taking measurements, it was found that the thickness of the seating surface could be increased

to as much as 0.060" (from the previous 0.030") without the head of the bolt protruding too far past the face of the sprocket mount, which would result in it contacting the bearing. Equation 3 and Equation 4 display the increase in yielding resistance as a result of the increased surface area (A) and increased thickness (t).

Equation 3

$$A = \pi \left(\frac{d_{outer}}{2} \right)^2 - \pi \left(\frac{d_{inner}}{2} \right)^2$$

$$A_1 = \pi \left(\frac{0.500in}{2} \right)^2 - \pi \left(\frac{0.375in}{2} \right)^2 = 0.086in^2$$

$$A_2 = \pi \left(\frac{0.750in}{2} \right)^2 - \pi \left(\frac{0.375in}{2} \right)^2 = 0.332in^2$$

Equation 4

$$ratio\ of\ yielding\ resistance = \frac{A_2 t_2}{A_1 t_1}$$

$$ratio\ of\ yielding\ resistance = \frac{0.332in^2 * 0.060in}{0.086in^2 * 0.030in} = 7.72$$

The combined increase in surface area and thickness increased the resistance to yielding by a ratio of 7.72. The surface area over which the force of each bolt is applied was increased by a ratio of nearly 4.0. This increase combined with doubling the thickness of the bottom of the bore provides a significantly more robust surface for the bolts to seat on.

Manufacturing

The manufacturing of the shaft bushing began by cutting it to a length of 1.000" on a band saw. It was then faced on a lathe and the outer diameter was trimmed to 1.960" after measuring runout to be less than 0.002". Sharp edges were eliminated on a belt sander. While the lathe was in use, the other differential output shaft housing was attached and the mushroomed end of it was resurfaced. The final product pressed onto the differential is shown in Figure 90.



Figure 90: Shaft Bushing Pressed into Place

The manufacturing of the counterbored holes began by setting up a manual mill with a flat 0.750" endmill attached. Once the depth was set to achieve a thickness of 0.060" at the bottom of the hole, the three holes were milled. The washers were then installed in the holes. While the sprocket mount was already on the mill, the old, bowed-out holes were drilled out to improve the aesthetics of the piece and eliminate the protruding ends of the holes. The final product is shown in Figure 91.



Figure 91: Sprocket Mount with New Counterbored Holes

Integration

Once complete, the shaft bushing and the sprocket mount were attached to the differential after the differential was opened up and greased. All parts fit without an issue. The complete differential assembly is shown in Figure 92 prior to the bearings being pressed on.



Figure 92: Differential Assembly

Conclusion

Summary

The differential on the FSAE car started out with some major issues that needed to be resolved in order to have a running car. Not only was it unable to be assembled, but it also was at risk of a dangerous failure if it were assembled in its current state. Research on the problems was conducted, leading to preliminary designs that would solve these problems. Final designs were created that allowed for a smooth manufacturing process and an effective final product. Once integrated into the FSAE car, the shaft bushing and the sprocket mount worked flawlessly in completing their design goals.

Future Recommendations

The only recommendation to future FSAE teams would be to closely monitor the differential and its components for wear or any unusual play in the bearings.

Continuously Variable Transmission (CVT)

Overview

Using a Continuously Variable Transmission (CVT) in a vehicle eliminates many of the limitations that are caused by more commonly used fixed gear ratio transmissions. Additionally, using a CVT eliminates the use of a clutch pedal and a shifter. This allows for a wider range of drivers to be able to operate the vehicle that may not be able to use a manual transmission. For these reasons, WPI's Formula SAE Cars have used CVT's since 2009.

A CVT is made up of two pulleys that adjust based on the centripetal force produced by the engine's rotation. These pulleys are known as the primary and secondary sheaves. The primary sheave is affixed directly to the crankshaft of the engine. It engages the CVT belt at a predetermined engagement speed which then accelerates the car from idle. The primary sheave also controls the engine speed as to correlate with the wheel speed. When the primary sheave is tuned properly it maintains the engine at a constant speed producing optimum power. The secondary sheave's main function is to backshift the CVT belt when the driver releases the throttle to maintain the engine's speed. Table 6 identifies some of the most relevant advantages of CVT over manual transmissions.

Table 6: Advantages of CVTs over a Manual Transmission

| Advantages of CVT over a Manual Transmission | |
|--|---|
| Feature | Benefit |
| Constant, stepless acceleration from a complete stop to a cruising speed | Eliminates "Shift Shock" and delivers a smoother ride. |
| Works to keep the car in its optimum power range regardless of how fast the car is traveling | Improved fuel efficiency |
| Responds better to changing conditions, such as changes in the throttle and speed | Eliminates the need to know in what gear the car will perform better under certain velocities and slopes. |
| Less power loss than in a typical automatic transmission | Better Acceleration |
| Better control of gasoline engine's speed range | Better Controls over emissions |

Initial Condition and Past Work

In the past several MQP teams have done some significant adjustments to the current CVT setup. The 2012 FSAE MQP team had diagnosed two problems in the previous car (2011 MQP team) CVT setup and focused their efforts in addressing and resolving these issues.

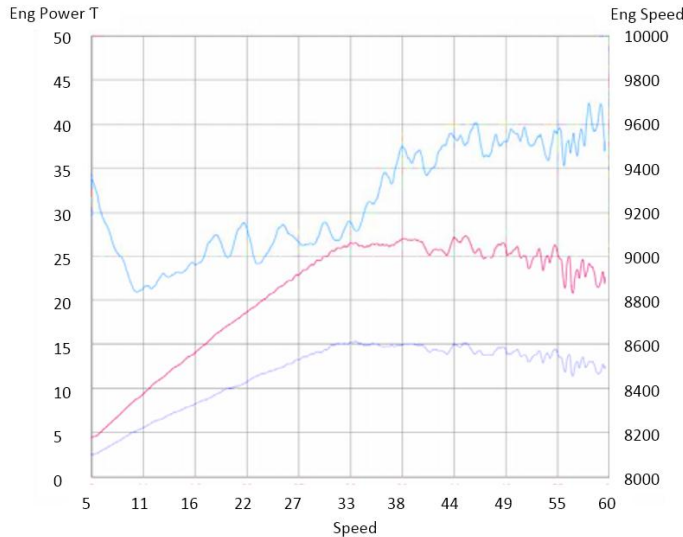


Figure 93: FSAE Speed Diagram CVT Graph (2011 MQP)

In order to properly address these issues, the 2012 FSAE MQP team measured the power, torque and the rotational speed of the engine by placing the vehicle in a dynamometer. The dynamometer was used to provide a simulated road load on the engine and through a data acquisition system provided the 2012 FSAE team with the speed diagram shown in Figure 93. This diagram provides an understanding of the overall performance of the transmission in the 2011 vehicle. One of the problems identified from this graph was how the primary clutch engages just above 8500rpm and then starts increasing until 9600rpm at which the CVT is completely shifted out and in overdrive. This analysis suggested that the 2011 car was severely underpowered because it was choking airflow from engagement to overdrive.

The second problem that was diagnosed was the wide power band that reached 9500rpm. Unlike traditional transmissions, which reach peak torque output as they increase speed, the CVT holds the engine at its peak torque output regardless of the vehicle speed. Because of this the engine operates at a constant speed when shifting from engagement to overdrive.

To address these issues, the 2012 FSAE MQP team determined that the desired shift of the CVT would be 7500rpm. Due to the CVT engaging and shifting out higher than the desired speed, an adjustable flyweight 18% heavier than the stock weight was installed. These flyweights also had the ability to weigh between 68g to 82g. The heavier flyweights lowered the engagement and shift speed meaning that the engine needed more power for the centrifugal force to push the primary sheaves apart. Neither the primary compression spring nor the secondary clutch was modified or tuned properly therefore there is still room for improvement in the areas of back shifting and efficiency of the system.

Objectives & Criteria

The objective of the 2014 FSAE MQP team with respect to the continuous variable transmission is to achieve a desired shift speed, engagement speed and top speed. These objectives will serve as benchmarks and indicators when evaluating the efficiency of the transmission. When comparing different test results these parameters will be a determining factor in deciding which configuration of components work best with the current engine.

Table 7: CVT Tuning Objectives

| Objectives | |
|------------------|-------------------|
| Shift Speed | 7500rpm |
| Engagement Speed | 3500rpm – 4000rpm |
| Top Speed | 60mph |

These tuning objectives were derived from extensive research on continuous variable transmissions for SAE applications. Interviews were carried out with past WPI FSAE MQP groups as well as with FSAE teams from other schools who had past experience using this type of transmission. Once the tuning objectives were determined, free body diagrams were drawn out for each component. This exercise helped determine the different forces acting on the transmission while it is in motion. These free body diagrams were later used to identify how to improve the performance of the CVT. Different equations were derived from the free body diagram analysis and were used to select the different CVT components to achieve the performance objectives in Table 7 above.

Background Research

Olav Aaen's Clutch Tuning Handbook

The main source of information used by the 2014 MQP team to gain knowledge in continuous variable transmission systems was the *Clutch Tuning Handbook* written by Olav Aaen, owner and founder of AAEN Performance a professional snowmobile parts manufacturer. This technical handbook provides a sufficient amount of research done on tuning continuous variable transmissions (CVT) and also provides the background information required for any user to tune a CVT without necessarily having detailed knowledge of how the design works.

In his book the author offers a particular tuning strategy, an empirical approach is recommended when working with CVTs where educated guessing and a trial and error methodology are needed. To follow the handbook's methods, the user must go to a facility with consistent track conditions and prepare for an extensive testing session. The user must change the available combinations of the transmission components to see which setup produces the best performance.

After acquiring comparable data and a set of valuable parameters on each individual test drive, the user must analyze and decide what combination of CVT components that will produce the closest results to the desired tuning goals. In addition to describing the tuning method, Aaen's CVT handbook provides knowledge on how the common primary and secondary pulleys function and describes the cause and effect relation between the different components in CVTs.

Tuning the Primary/Driver Clutch

Adjustments done on the driven clutch determine the efficiency and back shifting of the transmission while the driving clutch determines the engine speed (engagement speed and shift speed). When tuned properly, both systems will function correctly and provide a combination of maximum horsepower and high efficiency.

The first step in tuning the primary clutch is to verify that the current flyweights place the CVT in a desired operating range with regards to the desired engagement and shift speed. The heavier the flyweights, the less engine power is required for the CVT to engage and physically shift out the primary.

After verifying the flyweights, the primary spring will be analyzed to confirm that it properly resists the centrifugal force of the flyweights as the primary is shifting out. If while shifting out the operating speed rises, then a different spring with a lesser spring rate will be considered to help flatten the power band throughout wheel speed.

Figure 94 is a spring chart showing the spring tensions at idle and full shift. The chart shows how the spring rate (lbf) increases as the spring height increases. Different springs with the same rating at one point will not have the same rate at engagement if one spring is much stiffer than the other while it is being compressed or stretched.

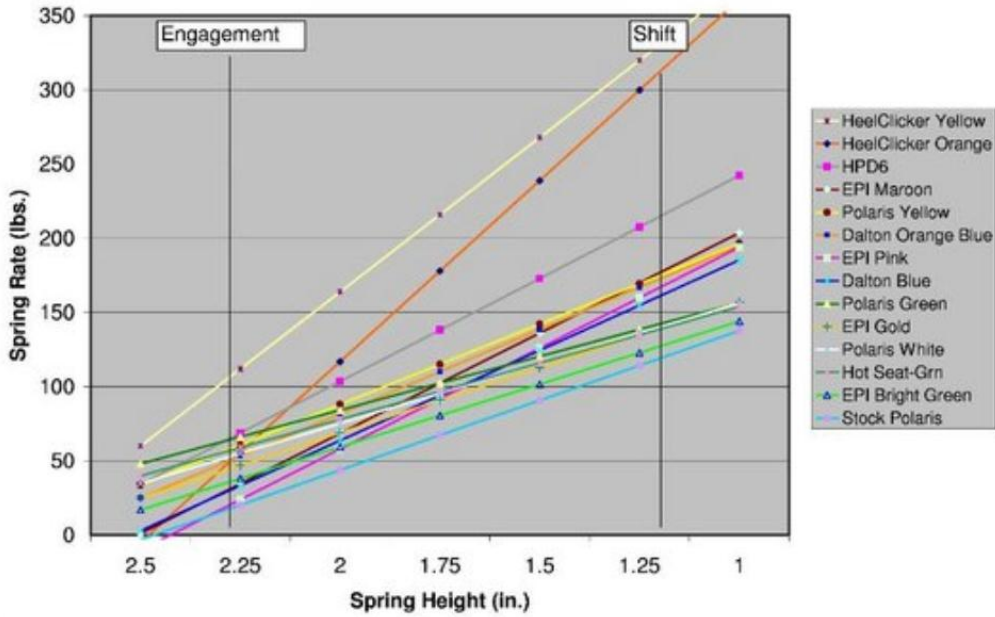


Figure 94: Spring Height vs. Spring Rate

Figure 95 plots the speed in mph vs the engine speed in rpm and demonstrates the ideal performance the user targets when tuning the CVT. The two diagonal lines represent the low range and high range of the system. The low range is the initial state of the CVT (has not started to shift yet) and the max speed the car would get if it did not shift. The high ratio is when the system is completely shifted out.

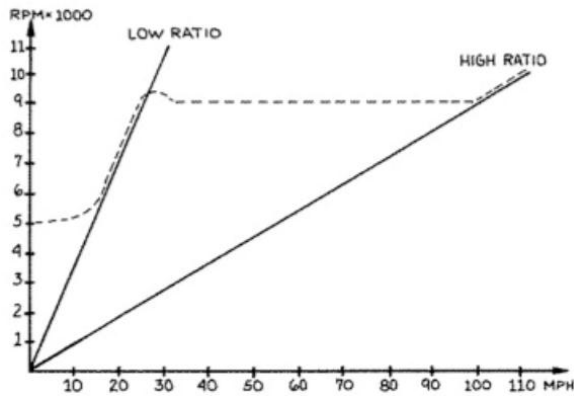


Figure 95: Ideal CVT Performance Curve

The dotted line is the ideal CVT curve for any engine using this type of transmission. The plot simulates the revolutions per minute increasing at a constant but faster rate than the miles per hour. It also shows how the engine revs but does not engage the clutch until around 5k-5.5k rpm. After this, the engine continues to accelerate and the CVT starts upshifting the ratio until the final ratio of the CVT is reached. As you can see below the entire shift out from low ratio to high ratio is done while constantly maintaining the engine speed at 9000rpm. When the final ratio is reached then the engine speed will start climbing up again.

In order to understand the flyweight system and how these forces act against each other (flyweight force against the spring force) it is important to understand the fundamentals of the centrifugal force. It can be assumed that the basic mathematical formula for centrifugal force is the following:

Equation 5

$$F_c = mr\omega^2$$

Knowing the relationships between these forces will help in testing and making choices between different flyweights and springs. Centrifugal Force increases proportionally with the weight, radius and speed.

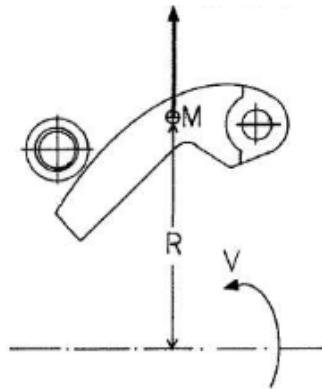


Figure 96: Free Body Diagram of Flyweight

Another adjustment that needs to be considered when tuning the primary clutch is applying pretension to the primary spring. Increasing the pretension of the primary spring means more force will be required for the sheaves to come in contact with the CVT and therefore the engagement speed will be higher. A spring with a pretension of 100lbs and a rate of 50lbs will have a total of 150lbs after one inch of sheave travel. The higher the load, the more engine speed (rpm) is needed to overcome its force.

In order to keep track of the different test results the exact preloads and rates of the springs must be recorded. This information can be extracted from a clutch model index. After

some use, the total length of the spring shortens by as much as half of an inch. This situation may alter any testing results as performance parameters may lower.

To better illustrate the mechanism of a continuous variable transmission, Figure 97 demonstrates the different phases of the CVT while being operated. Phase A is the free running stage (disengaged) where the driving clutch is disengaged below the engagement speed. At engine speeds below engagement, the pretension load of the spring is larger than the flyweight force. At point B the belt is engaged, at this stage the engine velocity has to be high enough to produce useful torque that can accelerate the car. At point C, the clutching action takes place where the sheaves come in contact with the belt. During the area labeled as D, the engine accelerates at low ratio where the belt remains at the bottom of the sheaves. At point E, the belt starts shifting out into a higher ratio. At point F the CVT is shifting out maintaining a constant engine speed. At this point the belt crawls up the primary sheaves and sinks into the secondary sheaves reaching overdrive. At point G the engine is over-revving in high ratio.

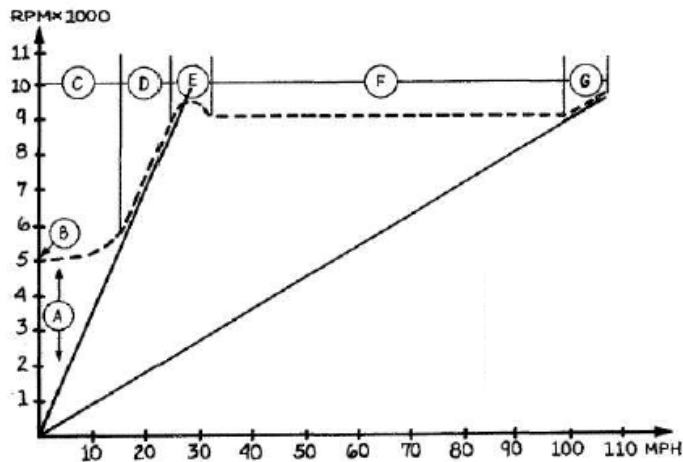


Figure 97: CVT Curve Plot - RPM vs Speed

In Figure 98 the same graph as Figure 97 is plotted but now showing the different phases of a manual transmission. The ratio of each gear is represented in a diagonal line on the graph. By analyzing the figure below we can see how in a normal transmission if the user driving the vehicle would keep the transmission in in 2nd gear, his or her car would only reach 50mph. The CVT keeps the engine at its peak power band more often than a manual transmission. When shifting a manual transmission from one velocity to another, the engine speed drops and then the engine needs to climb back up again. With a properly tuned CVT the engine can continuously operate at the speed where it generates the most power. This is also known as the peak power band.

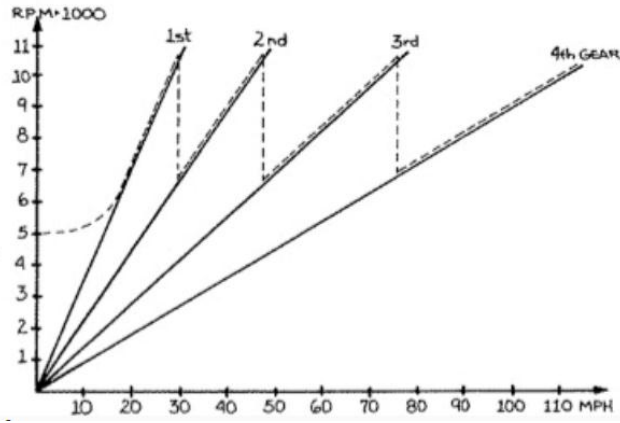


Figure 98: Manual Transmission

Tuning the Secondary/Driven Clutch:

The secondary clutch consists of a stationary sheave and a movable sheave that work against the forces of the feedback cam and torsion spring. The secondary can be tuned by changing the torsion spring, adjusting the pretension on the torsion spring, and changing the helix cam angle. As mentioned before, the driven (secondary) clutch determines the efficiency and back shifting of the entire system.

Comment [FE1]: How will it be considered he wants tables

The back shifting of the CVT is regulated by the friction between the helical cam and the rollers, and by the spring rate of the torsion spring. Also, the efficiency of this system is primarily governed by how well the CVT backshifts and by the belt pressure.

Efficiency: Drive Ratio and Belt Tension

Drive efficiency (η) is defined as the power output (P_{out}) from the driven clutch divided by the power input (P_{in}) of the driving clutch (see Equation 6 below).

Equation 6

$$\eta = \frac{P_{out}}{P_{in}}$$

The efficiency varies with respect to the drive ratio, the belt pressure and the clutch design. A basic efficiency curve starts out lowest in low ratio due to high belt loads. Between 2:1 and 1:1 the efficiency reaches its maximum value (see Figure 99).

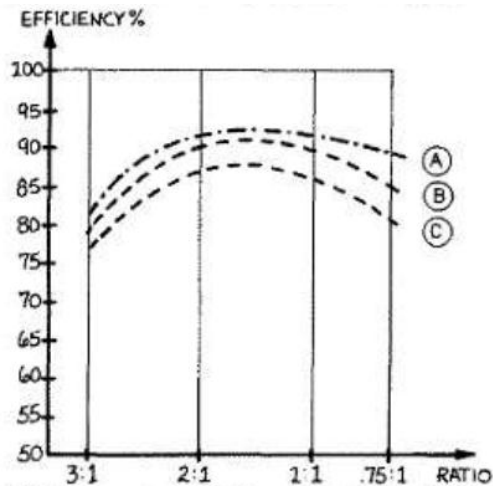


Figure 99: Efficiency Curve

Drive Ratio

The drive ratio of the transmission is determined by the radii of the belt on the driver and driven clutch (See Equation 7). This radius is measured at the pitch radius of the belt. In which we divide the driven pitch radius by the pitch radius of the driving clutch. The overall ratio of the transmission is measured by dividing the low ratio by the overdrive ratio (final stage of the CVT). Both of these equations provide critical parameters for maximizing efficiency.

Equation 7

$$R_{drive} = \frac{p_{driven}}{p_{driving}}$$

Equation 8

$$R_{overall} = \frac{R_{low}}{R_{overdrive}}$$

Figure 100, Figure 101, and Figure 102 are representations of how the belt would be positioned when the CVT is at low ratio, when both clutches spin at the same speed and when the CVT is at its final stage in high ratio.

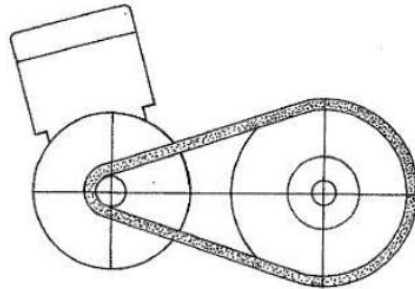


Figure 100: Low Ratio 3:1

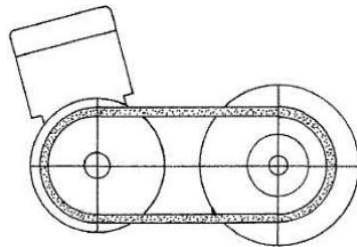


Figure 101: Secondary and Primary at Equal Speed - 1:1 Ratio

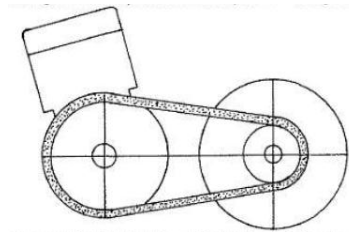


Figure 102: High Ratio Overdrive

Table 8 shows the radius and ratios of a typical CVT setup of a FSAE team.

Table 8: CVT Ratios

| | (A) Secondary Driven Radius | (B) Primary Driving Radius | (A/B) Ratio |
|-------------------|-----------------------------|----------------------------|-------------|
| <i>Low Ratio</i> | 4.5" | 1.5" | 3:1 |
| <i>High Ratio</i> | 3" | 4" | .75:1 |

CVT Belt Pressure

Other elements in the CVT configuration have an effect on the overall ratio such as the belt tension. If we were to use a belt that is too loose then the belt would ride out to far in the

driver reducing the overall ratio. On the other hand if the belt is too tight then the belt would run further in the driven clutch and reducing once more the overall ratio.

Efficiency is mainly dependent on the belt tension of the system as well as the ability for the secondary to backshift. While back shifting is dictated by the friction in the helix cam and the rollers, the belt tension is dependent on the side pressure between the belt and the metal sheaves.

Figure 103 is a MATLAB plot that simulates how the tight and slack side belt tensions over time. Tight and slack refers to the side of the belt that has high and low tension respectively. This plot was generated through a MATLAB code done by the Iowa State FSAE Team in 2010. The code MATLAB plots the shift ratio vs the max belt tension. The plot demonstrates how the slack and tight tensions vary, particularly at low end shift ratios, on both the secondary and primary sheaves. The belt tension varies around the contact arc of each pulley.

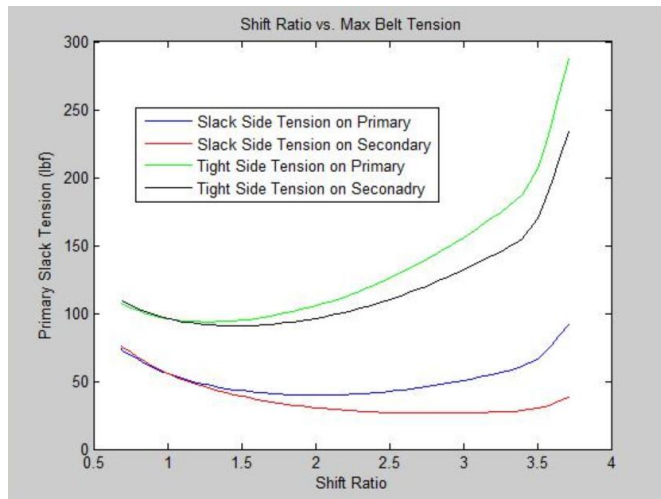


Figure 103: Shift Ratio vs. Max Belt Tension

The tension is highest where the belt enters the smaller pulley and the second highest point is where the belt leaves the larger pulley. During under drive, the smaller pulley will be the primary and the larger will be the secondary and in overdrive the larger pulley will be the secondary and the smaller will be the primary.

The main purpose of the driven clutch is to provide enough side pressure on the belt to allow the power to be transmitted, if there isn't enough pressure between the belt and the sheaves, it is possible for the belt to slip or making the transmission backshift when the car is on a steep slope.

Belt losses are influenced by the turning radius of the car, belt speed, belt tension and friction loss. The tighter the belt has to turn, the higher the loss of power. The higher the belt

speed, the more often it has to be bent around the sheaves and the higher the belt tension becomes due to centrifugal force.

Design

In both the 2012 and 2013 FSAE MQP's testing results; each team identified the CVTs back shifting to be an area of improvement. Both teams distinguished that the CVT was extremely slow to backshift when the driver released the throttle pedal. This prevented the engine from being able to maintain a constant speed. It also caused the car to have unpredictable handling characteristics under braking. Additionally, the unpredictable handling forced the drivers to utilize more brakes going into the corners. The slow back shifting, also made the car slower on corner exits. This was mainly because the engine needed to accelerate back up to the CVTs shift speed rather than remaining at the shift speed throughout the corner.

To improve the back shifting of the CVT, extensive research was carried out and CVT tuning professionals were reached out in search for support and advice. Various FSAE teams from different schools were contacted in order to identify additional ways to improve back shifting for FSAE applications. A roller secondary clutch with a Yamaha spline pattern was recommended by these different sources. The roller secondary offers a 90% reduction in helical cam friction over the OEM secondary having a radical improvement in back shifting. After careful consideration an Aaen Roller Secondary Clutch was selected that had its spline modified to have the Yamaha secondary spline. This feature made the secondary able to integrate with the car's current jackshaft.

Current CVT Components

After extensive research in the basic mechanisms of the transmission, different CVT components were purchased for later use in testing the transmission. Testing allows the combination of CVT parts to be verified and improved upon to meet the team's performance objectives. In Table 9 is a list of WPI's current CVT component inventory.

Table 9: Current CVT Inventory

| | Stock | Custom Made |
|---|----------------------------|----------------------------|
| Helix CAM Angle | 39° | 48° |
| Primary Clutch Spring Constant | 3kg.mm | 3kg.mm |
| Secondary Clutch Torsion Spring Constant | 0.74kgf/mm/rad | 0.63kgf/mm/rad |
| Flyweights | 76g | 76g |
| Secondary Sheave Angle | 15° | 15° |
| Preload adjustability | 4 available configurations | 6 available configurations |
| Engagement Speed | 3500rpm | 3300rpm |
| Shift out Speed | 7500rpm | 7700rpm |

Calculations

The 2012 FSAE MQP previously performed CVT tuning with the intent of reducing the engagement speed to 3500rpm as well as reducing the shift speed to 7500rpm. This previous project team installed heavier flyweights on the primary clutch. The heavier flyweights weighted 76g each, a 9g increase over the 67g stock flyweights. Following this change, there was no testing or calculations completed to verify that the 9g increase will help reach their tuning goal. Because of this, the calculations in this section were carried out to determine the effectiveness of the 2012 CVT modifications. Table 10 contains the variables used to perform these calculations along with their descriptions.

Table 10: Definition of Variables

| Variables in CVT Equations | |
|----------------------------|--------------------------------|
| Variable | Description |
| ω | Rotational Velocity (rpm) |
| F_p | Pretension Force on Spring (N) |
| k_p | Primary Spring Constant (N/m) |
| r_f | Flyweight Radius (mm) |
| x | Sheave Displacement (mm) |
| F_c | Centrifugal Force (N) |
| F_{cam} | Side Force of Helical Cam (N) |
| η | Efficiency |
| m_f | Flyweight Mass (kg) |
| F_{cam} | Side Force of Cam (N) |
| P_{in} | Power Input |
| P_{out} | Power Output |
| v_{car} | Velocity of Car (mph) |
| R_{shift} | Shift Ratio |
| R_{gear} | Gear Ratio |
| R_{drive} | Drive Ratio |
| $R_{overall}$ | Overall Shift Ratio |
| R_{low} | Low Ratio |
| $R_{overdrive}$ | Overdrive Ratio |
| p_{driven} | Driven Pitch Radius |
| $p_{driving}$ | Driving Pitch Radius |
| $d_{sprocket}$ | Sprocket Pitch Diameter |
| α_{cam} | Helix Cam Angle (Degrees) |
| r_{ramp} | Ramp Radius (mm) |
| $\tau_{secondary}$ | Secondary Torque (N*m) |

In order to start performing calculations, a free body diagram was created (Figure 104) of the CVT Primary to understand the forces acting on the moveable sheave of the primary which engages and shifts the CVT belt.

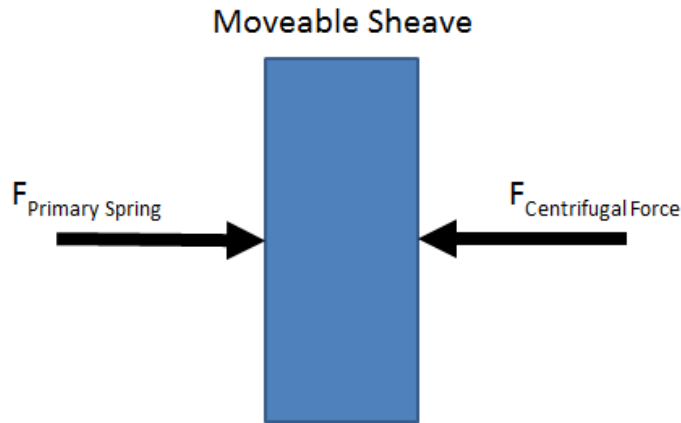


Figure 104: Moveable Sheave Free Body Diagram

Once the free body diagram was created, the forces acting on the moveable sheave were identified as F_p , the force of the primary spring, and F_c , the centrifugal force created by the rotation flyweights. An equation was then derived in order to calculate sheave displacement. Equation 9 calculates the sheave displacement (x) when given the mass of the flyweights (m) the flyweight's radius (r_f), the spring constant (k) the engine's speed (ω) and the spring's pretension (F_p).

Equation 9

$$\frac{F_c - F_p}{k_p} = x$$

Equation 10

$$\frac{3 \cdot m_f \cdot r_f \cdot \omega^2 - F_p}{k} = x$$

Once the equations were determined, the known and unknown variables were identified. After reviewing the current CVT configuration the only variable that was identified as an unknown variable was the radius of the flyweight. Because of this, the center of mass of the flyweight was then determined. This was accomplished by initially creating a 3D CAD model of the flyweight in SolidWorks and then using the mass properties function to determine the center of mass. The completed model is shown in Figure 105.

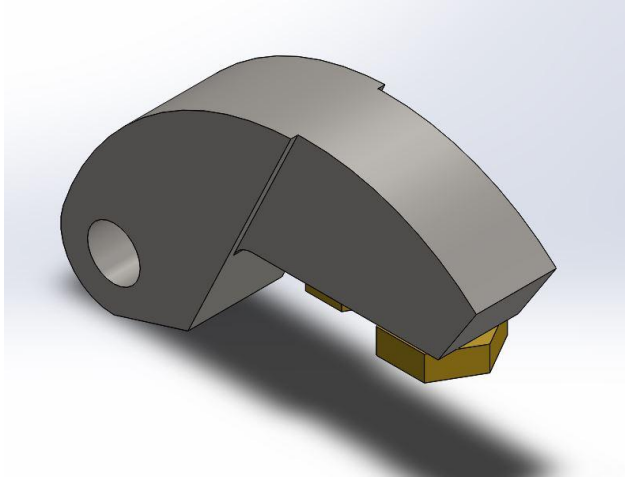


Figure 105: SolidWorks Model of Flyweight

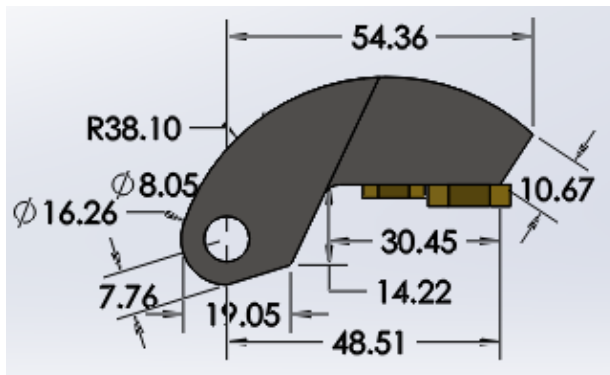


Figure 106: Dimensioned Flyweight in mm

Once the radius of the flyweight was found, the equation was then solved to find out how far the primary sheave will displace itself when the engine is running at 3500rpm. It was calculated that the primary sheave will displace itself 12.7mm which is approximately 0.5", the distance that the primary sheave needs to displace itself in order to engage the CVT belt.

$$\frac{F_c - F_p}{k} = x$$

$$\frac{3 \cdot m_f \cdot r_f \cdot \omega^2 - F_p x}{k} = x$$

$$m_f = 0.075 \text{ kg}$$

$$r_f = 19.3 \text{ mm}$$

$$\omega = 366 \frac{rad}{s} = 3500rpm$$

$$F_p = 20 kg \cdot 9.8 \frac{m}{s^2} = 196.13N$$

$$k = 29410 \frac{N}{m}$$

$$x = 0.0127m = 12.7mm = 0.5"$$

Furthermore, it was verified that the CVT primary will shift from engagement to overdrive at 7500rpm. This was done by calculating the sheave displacement at 7500rpm. The displacement was found to be 0.084 m. which is greater than the free length of the primary spring which is 0.072m in length. As a result the CVT will shift into its overdrive position at 7500rpm.

$$\frac{3 \cdot m_f \cdot r_f \cdot \omega^2 - F_p x}{k} = x$$

$$m_f = 0.075kg$$

$$r_f = 0.0193m$$

$$\omega = 785 rad/s = 7500rpm$$

$$F_p = 20 kg \cdot 9.8 \frac{m}{s^2} = 196.13N$$

$$k = 29410 \frac{N}{m}$$

$$x = 0.084m$$

Other CVT Equations

The equations below were used as a reference when analyzing and researching how the CVT behaves under different loads. Although the equations below were not used for any of the necessary calculations, they provided a broader understanding of the CVT mechanism by demonstrating the relations between the different variables there for making the CVT behavior more predictable when carrying out performance tests.

Equation 11

$$v_{car} = \frac{\omega * d_{sprocket}}{R_{shift} * R_{gear} * 336}$$

Equation 12

$$R_{shift} = \frac{\omega * d_{sprocket}}{v_{car} * R_{gear} * 336}$$

Equation 13

$$R_{gear} = \frac{\omega * d_{sprocket}}{R_{shift} * v_{car} * 336}$$

Equation 14

$$F_{cam} = \frac{\tau_{secondary} * R_{shift} * 12}{2 * r_{ramp} * Tan(\alpha_{cam})}$$

New Secondary Clutch vs Old Secondary Clutch

The new secondary clutch has a helix cam with slope of 48° vs the 39° slope in the Yamaha helix Cam Stock. Larger surface angles will open the sheaves at a higher velocity and there for it would ultimately lower the shift speed of the transmission. On the other hand Helix cams with smaller slope angles will open the sheaves at a lower velocity there for the shift speed would be higher. The type of helix cam and the angle of its surface have a significant influence on the side pressure that's applied on the belt by the sheaves. The angle of the sheaves has an indirect relation with the pressure applied on the belt, meaning that as the angle increases the side pressure decreases.

Currently, the old secondary clutch is assembled with a stock pretension of 16 ft-lbs. The stock CVT clutch will aid the team when tuning the CVT by comparing the difference in performance with the newly purchased clutch. In regards with the secondary/torsion springs, four springs with a rate increase of 18% between each one from the softest to the stiffest were set out to be purchased. On the other hand the custom made secondary roller was designed to meet racing standards and has multiple pretension configurations available that allow the user to adjust the tension of the spring without having to manually replace it.

The new secondary clutch has the ability to adjust the pre-tension from 6lbf to 25lbf by using a different locating hole in the CAM. By tightening up the spring, more force will be required to open the sheaves and a higher rotational velocity is needed to overcome the extra tension. In conclusion, the spring stiffness has a direct relationship with the side force. In other words, the stiffer the spring the higher the side force.

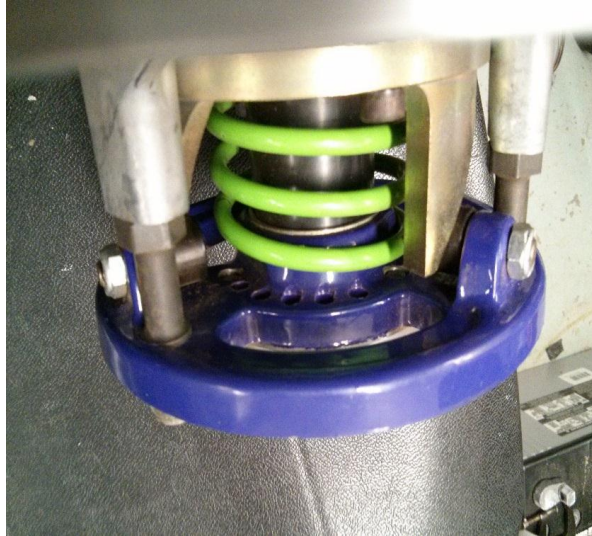


Figure 107: Custom Made Secondary Pretension Capabilities

CVT Primary Verification

The calculations of the CVT's engagement speed and shift speed were verified by running the engine on a test stand with the CVT primary and secondary installed. The engine was started and run to 3500rpm to verify that the CVT engaged the belt at the intended speed. The engine was run to 7500rpm to verify that it shifted properly. It was run at full throttle to confirm that it did not exceed 7500rpm while the belt was in the overdrive position. These tests were successful and confirmed the calculations were correct. These tests also proved that the CVT keeps the engine running at its optimum speed of 7500rpm, where it is tuned to make the most power.

Testing

The future goal for this project is to successfully carry out our CVT testing with the current working engine and have it properly tuned to meet each one of our tuning objectives. Different testing sessions will be scheduled to test new components and compare transmission performance with the use of a tachometer. In order to understand what happens to the transmission while it's in motion, speed diagrams that fulfill the primary objectives must be designed and analyzed. By knowing the engine power curve, the user can design an ideal shift curve diagram for the engine that is being used. With the use of a tachometer the user may determine how far off performance results are from the ideal shift curve. With this comparison, intelligent decisions can be made regarding what components may be switched in order to achieve certain objectives.

Integration

The Aaen Secondary was procured once it was determined that it would be used to replace the stock secondary to improve the CVT's back shifting. Once it arrived, the team

attempted to install it. During the installations it was discovered that the secondary did not have the same spline pattern as the car's jackshaft. The secondary had a Yamaha Nytro spline pattern instead of a Yamaha Phazer spline pattern. Additionally, it was found that the newly designed rear subframe interfered with the secondary's operation. As a result of these issues, the newly purchased Aaen secondary was not used. Instead, the stock secondary was tuned to improve the drivetrain's back shifting.

Comment [FEI2]: Show me a figure

Comment [GEJ3]:

The stock secondary was tuned by changing the helix cam and the torsion spring to improve back shifting. The helix cam was changed from the stock 39° cam to an aftermarket 37° cam. The torsion spring was changed from the stock spring, which has a spring constant of 7147 N*mm/rad, to an aftermarket torsion spring that has a spring constant of 6003 N*mm/rad. The shallower angle and reduced spring constant will require less force to backshift the CVT belt under braking. These changes were recommended by students on other FSAE teams with CVT tuning experience and CVT tuning professionals.

Summary/Conclusion

At the conclusion of the CVT tuning aspect of the project the team has a few recommendations for future FSAE MQP teams. The first recommendation is to have a custom jackshaft manufactured that has the correct spline pattern for the Aaen aftermarket secondary. Secondly, future teams should ensure that the chassis does not interfere with the CVT secondary when designing a new frame. These recommendations will allow future teams to be able to test and optimize the purchased Aaen secondary. It is also recommended that future FSAE teams continue to use CVTs for the performance benefits mentioned in Table 6.

Electrical

The goal of the Electrical and Computer Engineering team was to design and integrate a heads up display (HUD) for the FSAE vehicle. Changing performance in response to feedback is a fundamental response of humans. Without a system that provides feedback, the driver is required to rely on those around them. With this display the driver can adjust his driving based on the provided feedback. Practice driving can be done before events to determine to what is most effective for the various events of the competition. A specific speed or RPM range may be known from test runs to be the most effective for particular events at competition. Having this information readily available in both testing and competition will help improve driver performance.

Heads up Display (HUD)

Introduction

In order to create a heads up display for the driver to retrieve information from, the display must be integrated with the existing sensor system in the vehicle. The sensor system is controlled by the electronic control unit (ECU) of the vehicle. The ECU being used is the Haltech Platinum Sport Series 2000. The Haltech ECU provides a lot of useful features for testing and tuning the vehicle. It has data logging and a generic heads up display that both can be viewed by a PC via a USB cable. Their tuning and data logging interfaces are very useful when a computer is available but their heads up display is sloppy and not as driver friendly as it could be. On this conclusion, the heads up display needed to be improved rather than just integrated into the vehicle system. The choice to go with a custom dash HUD has many reasons. The benefit of a custom dash is to have the ability to change what's displayed when relevant to the application. The dash will display real-time information that will aid the driver.

Previous Design

The previous design used an off the shelf display for monitoring the sensors. This display was the Drew Technologies DashDAQ XL unit. The device was chosen because of its compatibility with the ECU and its ability to log data. The DashDAQ XL also provided a real time display and as well as an SD card slot to export the logged data. The touch screen allowed the driver to navigate the display without having to remove safety equipment or even stop the vehicle. The dash was mounted in acrylic and angled towards the driver to provide better visibility.

Hardware Research and Design

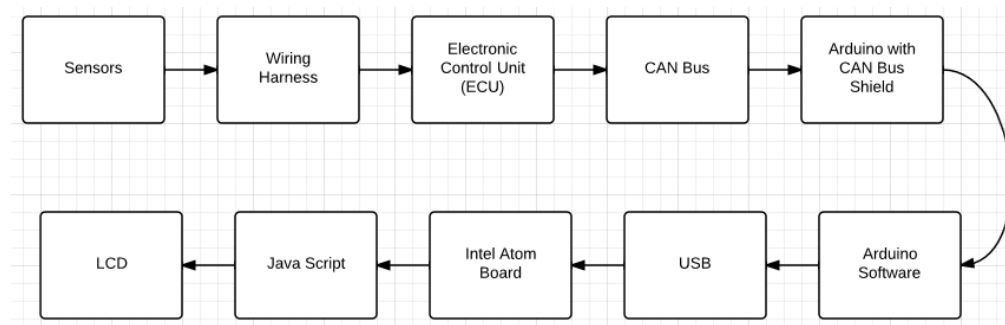


Figure 108: System Flow Chart

Figure 108 shows the flow of data from the primitive stage of the sensor data to the presentation of the data on the LCD screen mounted for the driver to view. The sensors provide electrical signals interpreted from the environment within the engine. These electrical signals are transmitted over the wiring harness to the ECU. The ECU interprets the various signals from the sensors into manageable numbers. These numbers are then broadcast over the CAN bus in the ECU using the differential voltage scheme shown in Figure 109. The Arduino acts as a CAN bus sniffer, reading in all of the messages from the CAN bus and filtering out the messages that are not needed by the system. The Arduino receives the data in two bits. The bits are then converted into a single integer representing the value of the parameter being received from the sensor. This integer value is sent using a standard message format over the USB cable to the Intel board. This board is running Windows XP with the dash display Java script. The Java script program reads the message being sent by the Arduino in via the COM port. The resolution of the data is then determined and the appropriate gauge is displayed on the LCD screen for the driver to view.

One of the objectives for integrating the system was to integrate the ECU with a PC unit. The ECU does most of the data processing for the sensor outputs. The ECU performs analog to digital conversion as well as uses an internal CAN bus to transmit the data to an external source. The USB port on the ECU also transmits the data to an external source but the protocol for this transmission could not be disclosed by Haltech. Their CAN bus protocol however, was readily available.

The CAN Bus

The CAN bus data is broadcasted over pins 23 and 24. A CAN bus uses a differential voltage to transmit data. Pin 23 is CAN High and Pin 24 is CAN Low. These two pins, when idle, will be around 2.5V each. This leaves the differential at approximately 0. When the differential is 0, this represents a logic output of 1. When a 0 is to be broadcasted, CAN low drops to 1.25V and CAN high rises to 3.75V. This provides a differential of 2.5V. This CAN protocol can be seen in Figure 109. With some software coding, this signal can be interpreted to extract engine parameters.

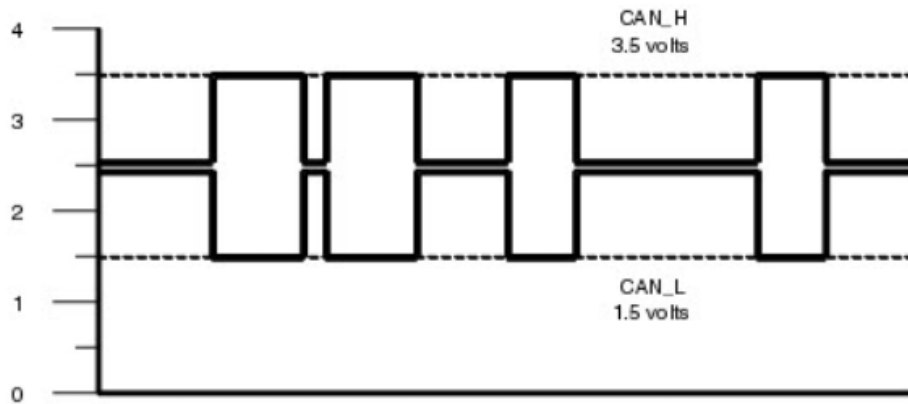


Figure 109: CAN Bus Output Protocol

The Haltech ECU broadcasts a number of engine parameters and sensor readings on the CAN bus. Any third party device can read these CAN packets and use the values if correctly configured. The CAN bus operates at 1MBit, uses 11-bit identifiers expressed in hexadecimal, and is encoded in Big Endian. The information is encoded as shown in Figure 110.

| ID | Byte | Channel | Units | Resolution |
|-------|---------|----------------------------|---|------------|
| 0x010 | 0 - 1 | RPM | RPM | 1 RPM |
| | 2 - 3 | Road Speed | Km/h | 0.1 km/h |
| | 4 - 5 | Oil Pressure | Bar | 0.1 Bar |
| | 6 - 7 | Oil Temperature | Deg C | 0.1 Deg C |
| | 8 - 9 | Coolant Temperature | Deg C | 0.1 Deg C |
| 0x011 | 10 - 11 | Fuel Pressure | Bar | 0.1 Bar |
| | 12 - 13 | Battery Voltage | Volts | 0.01 Volts |
| | 14 - 15 | Throttle Position | % | 0.1 % |
| | 16 - 17 | Manifold Pressure | mBar | 1 mBar |
| 0x012 | 18 - 19 | Air Temperature | Deg C | 0.1 Deg C |
| | 20 - 21 | Exhaust Gas Temperature | Deg C | 1 Deg C |
| | 22 - 23 | Lambda | Lambda | 0.001 λ |
| 0x013 | 24 - 25 | Ignition Advance | Degrees | 0.1 Deg |
| | 26 - 27 | Gear | 0 = neutral, 1 = first, 2 = second, etc | |
| | 28 - 29 | Injector Duty Cycle | % | 1 % |
| | 30 | Data Bytes Sent | 30 | |
| | 31 | Marker Byte 1 [^] | FC | |
| 0x014 | 32 | Marker Byte 2 [^] | FB | |
| | 33 | Marker Byte 3 [^] | FA | |
| | 34 | Checksum [*] | | |

[^]. Marker Bytes are from the original AIM CAN protocol and are in to maintain compatibility.

^{*}. Checksum is the sum of all bytes of the structure up to and including marker byte.

Figure 110: Haltech CAN Protocol Bit Breakdown

The calculations that will need to be done to the raw data are very simple. The data is passed through the CAN bus as a two's complement signed integer. This integer needs to simply be multiplied by the resolution column of Figure 110.

Equation 15

$$\text{Channel} = \text{Byte} \times \text{Resolution (Units)}$$

The calculations done on the data is not the difficult process of the display. The interface between the PC and the CAN bus was difficult because the CAN bus cable that was standard to the ECU was not compatible with the PC. The ECU provides two outputs for the CAN bus. One is the standard plug that is provided by Haltech but the output pins on the opposite side of the ECU provide a CAN Hi, CAN Low, and CAN Ground outputs. With these outputs, we could monitor and transmit the outputs of the CAN bus to external sources such as the PC unit. One issue that was found with this exchange of data was the software application needed to read the CAN bus on the PC unit. The PC would need to be constantly checking for new data from the CAN bus and processing it. To solve this problem, a CAN bus sniffer was implemented using an Arduino Uno board along with a CAN Bus Shield.

Arduino CAN Bus Interface

Arduino is a single-board microcontroller. The hardware is an open source hardware board designed around an 8-bit Atmel AVR microcontroller. The current Uno model features a USB interface, 6 analog input pins, as well as 14 digital I/O pins to allow attachment of various extensions. The CAN Bus shield was the attachment of choice for the vehicle.

Arduino boards make use of shields which are printed circuit expansion boards that plug into the supplied Arduino pin-headers. The CAN Bus shield provides two extra microcontrollers that can be used to send and receive messages across a CAN bus interface. The Arduino Uno board, with the CAN Bus shield soldered to the pin-headers, is shown Figure 111.

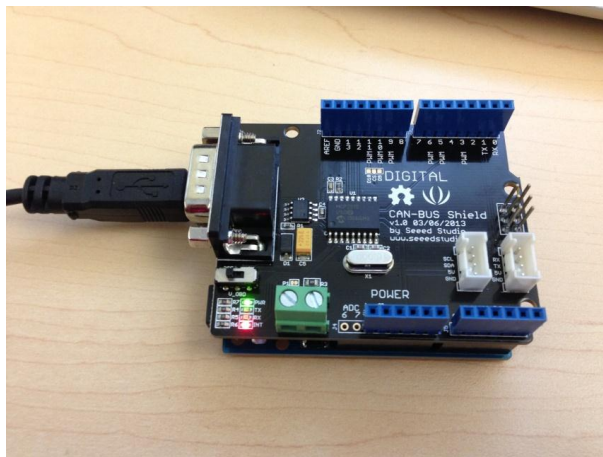


Figure 111: Arduino Uno with CAN Bus Shield

An open source code for reading in data from a CAN bus using the CAN shield is provided by the Arduino playground. This code simply reads in all of the messages and relays them through the serial cable. The ECU processes and sends out many parameters that are not needed for the display. This means that filters must be applied to the incoming CAN messages so that only the ones that contain necessary parameters are received. The rest are ignored. In doing so, the Arduino processing is more efficient in transferring the CAN bus data to the computer.

Appendixed is the code that is running on the Arduino Uno. The code only monitors or sniffs the CAN bus that is coming from the ECU. It does not send messages back to the ECU. Sending the messages is unnecessary. It does not need to request any messages to be sent again in the case of a mangled bit because the ECU will be sending the data so frequently that a missed update will not be noticeable to the human eye.

The code for the CAN bus sniffer works in the following steps.

1. Scans or waits for a CAN message to be sent over the bus.
2. Sets a flag, Flag_Recv=1, to indicate that a message is available.
3. Loop function begins when Flag_Recv=1
4. Clears Flag_Recv to indicate that the current message has been processed.
5. CAN.readMsgBuf reads the message in and places the data into buf.
6. Sets variable ID to the identifier of the CAN message. (11-bit identifier)
7. Compares ID to known set of IDs that contain desired engine parameters.
8. Enters "if" statement of specific ID.
9. Prints a message to the serial port indicating which parameter is in the message.
10. Converts the 4 Hex bits of the desired data into decimal values with HextoDec();
11. If parameter is Air Fuel Ratios (AFRs), multiplies this decimal value by 14.7 to convert the λ value to an AFR value.
12. Print a ":" to the serial port to indicate the start of a message.
13. Print the readable ID of the data to the serial port.(RPM,MPH,TMP,FR1,FR2).
14. Print the data of the parameter calculated in step 10.
15. Print a ";" to the serial port to indicate the end of a message.
16. Repeat for next CAN message.

Engine Parameters

We will be focusing on specific data that is relevant when actually driving the formula vehicle. This data will be RPM, speed, gas level, engine temperature (coolant), fuel pressure, and air fuel ratios. These are key sensors that will need to be monitored while the vehicle is running.

RPM

The Phazer engine uses a Hall Effect Sensor to determine the RPM of the engine. This sensor is a crank position sensor. It monitors the position as well as the rotational speed of the crankshaft. This information is used by the ECU to determine the ignition system timing and other engine parameters.

A Hall Effect sensor is a transducer that varies its output voltage in response to a magnetic field. In its simplest form, the sensor operates as an analog transducer, directly returning a voltage. This voltage can be corresponded to a known magnetic field. In a vehicle, the Hall Effect sensor transmits the rotations of the crank shaft based upon the impulses caused by a magnetic piece placed on the shaft itself. These pulses are what need to be emulated by a circuit to the ECU.

The RPM can be measured in a range from 0 to 16000rpm by the ECU. The ECU does not use the sign bit when measuring the RPM because the RPM cannot be negative. The resolution of the RPM is 1rpm per unit. This means that a binary reading of 1500 means that the RPM is equal to 1500rpm.

RPM: 1500

ECU CAN Output: 0x010 00001011 1011100 <Road Speed> <Oil Pressure> <Oil Temperature>

Arduino Uno Read In: 05DC (hex)

Arduino Uno Send Out: ":RPM1500;"

The ECU CAN bus output starts with the 11-bit identifier of 010 which is 16 in decimal. This is the lowest ID number and therefore it has the highest priority on the CAN bus. The first two bytes are the RPMs in binary. Byte 0 is the most significant byte and Byte 1 holds the least significant bits of the RPM reading. The Arduino Uno CAN shield converts this message from the ECU into characters to be seen when testing and for processing by the software. The value 0x05 will go in buff[0] in the Arduino software while 0xDC will be stored in buff[1].

Road Speed

The sensor used to measure the speed of the vehicle is a variable reluctance sensor. This sensor is also called a monopole. It is used to measure position and speed of moving metal components. This sensor consists of a permanent magnet, a ferromagnetic pole piece, a magnetic pickup, and a rotating toothed wheel. As the teeth of the rotating wheel pass by the face of the magnet, the amount of magnetic flux passing through the magnet and the coil varies. When the gear tooth is close to the sensor, the flux is at a maximum and when it is further away the flux drops off. This results in a flux that varies with respect to time or speed of the teeth. This varying voltage level is then processed by the ECU to determine the speed of the vehicle.

The sensor in the engine of the Formula vehicle has a voltage output that ranges from 4.8V, when the tooth is close to the face of the magnet, to 0.6V, when the tooth is furthest away from the magnet.

The road speed is measured in kilometer per hour by the ECU. The speed can be measured up to a value of 400kph. This is the equivalent of approximately 250mph. The range is far greater than we will need. Because the ECU measures the speed in kilometers per hour, an additional step must be taken in the software to convert the reading into MPH. The road

speed has a resolution of 0.1 kph meaning that a reading of 400 from the ECU indicates a road speed of 40 kph.

Road Speed: 35 MPH / 56 KPH (1MPH = 1.60934 KPH)

ECU CAN Output: 0x010 <RPM> 00000000 00111000 <Oil Pressure> <Oil Temperature>

Arduino Uno Read In: 0230(hex)

Arduino Uno Send Out: “:MPH560;”

Road speed is on the same identifier as RPM. The third and fourth bytes of this identifier hold the data for road speed. The value 0x02 will be stored in buf[2] and 0x30 will be stored in buf[3]. The road speed can be converted from MPH to KPH by dividing the integer provided by 1.69034 after multiplying it by .1 for the resolution.

Coolant Temperature

The coolant temperature sensor is used to measure the temperature of the engine coolant or engine temperature. The readings from this sensor are then fed back to the ECU to be used for adjusting the fuel injection and ignition timing. The coolant temperature sensor works using resistance. As the temperature surrounding the sensor increases, the internal resistance changes. There are two different kinds of sensors, NTC and PTC. NTC stands for negative temperature coefficient which means that as the temperature increases, the internal resistance will decrease. PTC is positive temperature coefficient and acts in the opposite manner.

The resistance begins at a range of 5.21 kilo-ohms when at 0° Celsius and drops to a resistance range of .290 to .354 kilo-ohms when it reaches 80° Celsius. These resistance amounts vary from sensor to sensor but they can be calibrated using the Haltech software for the ECU.

The operation of the sensor by the ECU is quite simple. The ECU sends out a regulated voltage that is typically 9 volts to the coolant temperature sensor. This voltage travels through the sensor and is decreased in relation to the internal resistance that has been varied by the temperature. This voltage is then returned to the ECU through the signal wire. The ECU uses this returned voltage to calculate the temperature of the engine.

The coolant temperature can be measured within the range of -400 to 1270° Celsius. The resolution of the measurement is 0.1° Celsius.

Coolant Temperature: 195 °C

ECU CAN Output: 0x011 00000111 10011110<Fuel Pressure><Battery Voltage><Throttle Position>

Arduino Uno Read In: 079E(hex)

Arduino Uno Send Out: “:ECT1950;”

The ECU CAN bus output starts with the 11-bit identifier of 011 which is 17 in decimal. This is the second lowest ID number and therefore it has the second highest priority on the CAN bus. The first two bytes are the Coolant Temperature in binary. Byte 0 is the most significant byte and Byte 1 holds the least significant bits of the Coolant Temperature reading. The Arduino Uno CAN shield converts this message from the ECU into characters to be seen when testing and for processing by the software. The value 0x07 will go in buf[0] in the Arduino software while 0x9E will be stored in buf[1].

Fuel Pressure

The fuel pressure sensor was provided by Sensata. The sensor works as a variable resistor in series with two ECU pins. The ECU sends a voltage out of the output pin through the sensor and then reads the voltage returned on the input pin. This level is a value between 0.5 and 5.0 volts; the higher the value, the higher the pressure.

The gas pressure is used to determine the amount of gasoline that is present in the tank. The fuel pressure can be measured up to 327bar. The resolution of the measurement is 0.1bar. The fuel pressure can provide the fuel level because as the fuel level decreases, the fuel pressure will decrease accordingly. The packets for fuel pressure and coolant temp have an identifier of 0x011 which is 17 in decimal. They are within the second highest priority packet.

Fuel Pressure: 100bar

ECU CAN Output: 0x011 <Coolant Temp>0000011 11101000 <Battery Voltage><Throttle Position>

Arduino Uno Read In: 03E8(hex)

Arduino Uno Send Out: “:PRF100;”

The ECU CAN bus output starts with the 11-bit identifier of 011 which is 17 in decimal. This is the second lowest ID number and therefore it has the second highest priority on the CAN bus. The second set of two bytes is the Fuel Pressure reading in binary. Byte 2 is the most significant byte and Byte 3 holds the least significant bits of the Fuel Pressure reading. The Arduino Uno CAN shield converts this message from the ECU into characters to be seen when testing and for processing by the software. The value 0x03 will go in buf[2] in the Arduino software while 0xE8 will be stored in buf[3].

Air Fuel Ratios

Air-fuel ratio is the mass ratio of air to fuel present in the exhaust of the engine. The AFR is an important measure for anti-pollution as well as performance tuning. In theory, the engine is provided with just enough air to burn the available fuel. This is why, knowing the ratios at all times from both exhaust pathways is important for understanding if both cylinders are firing correctly on the engine.

AFR: .1 λ

ECU CAN Output: 0x012 <Manifold Pressure><Air Temp><Exhaust Temp>000000001100100

Arduino Uno Read In: 0064(hex)

Arduino Uno Send Out: “:FR1100;”

The ECU CAN bus output starts with the 11-bit identifier of 012 which is 18 in decimal. This is the third lowest ID number and therefore it has the third highest priority on the CAN bus. The last set of two bytes is the Air Fuel Ratios reading in binary. Byte 6 is the most significant byte and Byte 7 holds the least significant bits of the Air Fuel Ratio reading. The Arduino Uno CAN shield converts this message from the ECU into characters to be seen when testing and for processing by the software. The value 0x00 will go in buf[6] in the Arduino software while 0x64 will be stored in buf[7].

Synchronization

A common problem with transferring data besides corruption is synchronization. When the Arduino sends a message containing data, the Java program needs to know how to interpret the different sections of the message. The Java program also needs to know when a new message is beginning as well as when the end of the message has been delivered. The same symbol is sent at the beginning and the end of every message to keep the synchronization. Each message starts with a colon “:”, followed by a three character identity tag, and the data. The message is ended with a semicolon “;”. A sample message is shown below for an RPM value of 1600.

Arduino Message: “:RPM1600;”

The three character identifiers are shown with their respective parameters in Table 11.

Table 11: Character Identifiers

| Identity | Parameter |
|----------|----------------------------|
| RPM | Rotations Per Minute |
| MPH | Road Speed |
| ECT | Engine Coolant Temperature |
| FR1 | Air Fuel Ratio 1 |
| FR2 | Air Fuel Ratio 2 |
| PRF | Fuel Pressure |
| PRO | Oil Pressure |

Software Research and Design

The standard gauges that are usually on a dash are the speedometer, tachometer, fuel gauge, and coolant temperature. Dashes can also display warning lights and indicators, such as a check engine light, shift indicator, low battery, oil level, etc. Development of this dash would be greatly beneficial to the car, as it allows information to be accessible in real-time to the driver.

Certain information is relevant at certain times and not necessarily relevant during others. For example, the information that's displayed while testing the car is not going to be the same information that's displayed while at competition, or even between different events at competition. This means that the software needs to be modular in order to allow different information to be displayed in different ways, shapes, and sizes, but also be easily customizable to the user. People have preferences and what works for one person might not work for others. Some people might prefer numbers, where others prefer colors. For example, some drivers might be interested in knowing when to shift, but might not care exactly what RPM's the engine is at for that shift as long as an indicator is green they know that they're in the right range, but others may prefer a target number, which allows for more accuracy and consistency.

Architecture

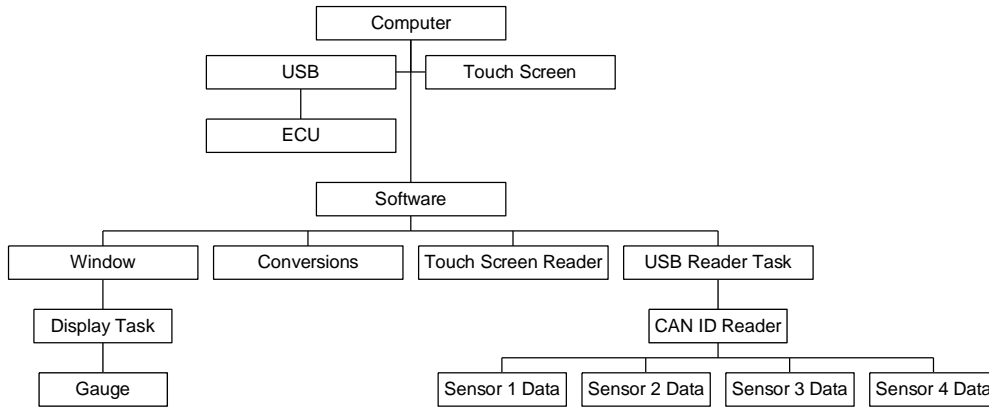


Figure 112: Preliminary Software Architecture

The software architecture is based upon the inputs of the system. These inputs are the sensor data sent by the Arduino and the touch screen inputs.

Sensor data will be read in through the USB COM port. This data is transmitted as shown in Figure 109. The function or task that is reading in the USB information will need to identify which identifier is being transmitted. This can be done by comparing the 11 bit identifier code to a set of codes that the system is accepting. These identities are 0x010, 0x011, and 0x013. If a code is received that does not have this identifier, it will be ignored. After the CAN ID is determined, the task will need to place the appropriate sections of the message into the data variables that will hold the information to be displayed. These variables will be global so that they can be accessed by both the USB Reader Task to change them and the Display Task to display the correct levels on the gauges.

The Window portion of the software will create a window on the desktop of the PC. This window will be full screen on the display to provide the best viewing. Within this window, a static background image provides the layout of the HUD. The thread will then draw different numbers and bars over the image.

Another task will be used to perform conversions on the raw data that is being read in on the USB. The task will use Equation 15 to account for the resolution of the sensor data. This will be necessary to avoid large raw numbers on data that has a high resolution. To avoid having the display update with these raw numbers, a set of priorities for the tasks must be instated. These priorities will ensure that the display does not update before the conversion has been completed for the data. The USB reader will hold the highest priority in order to not miss any data updates. The conversions will be a medium priority so that they preempt the display task which is a low priority.

Artist's Rendition

Figure 113 is a preliminary sketch of what the software could look like. The speed would be displayed right in the center, with the tachometer displayed above. The tachometer was chosen to be a linear gauge, as the exact RPM level isn't as crucial as the general range. In order to help emphasize these ranges, different colors would be implemented in order to give the driver a quick idea what range they are operating the vehicle in. This style gauge would not be as effective for a speedometer, as speed is a more critical value when driving in different circumstances. The black areas on the left and right of the speedometer have been left intentionally blank in order to allow room for additional gauges such as a fuel temperature, oil pressure, or other information considered useful by the team.

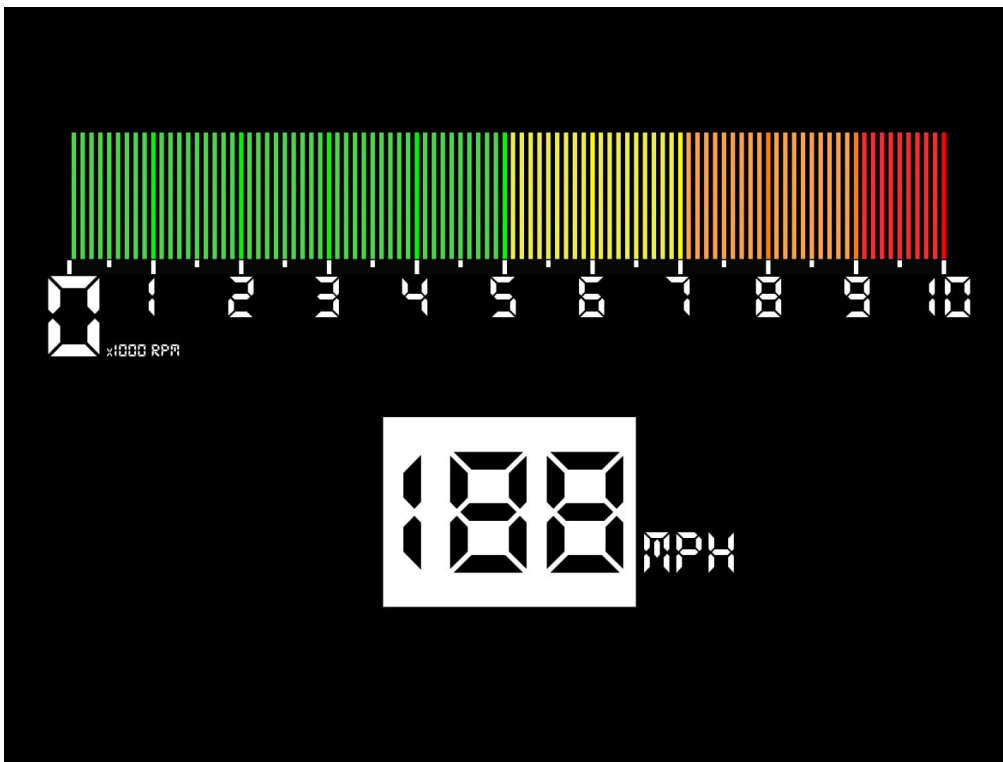


Figure 113: Artist Rendition 1- Digital Dash Display

After discussing with the team, the decision was made to add gauges for Coolant Temp and AFR's. I updated the sketch to reflect how I might implement these gauges in Figure 114.

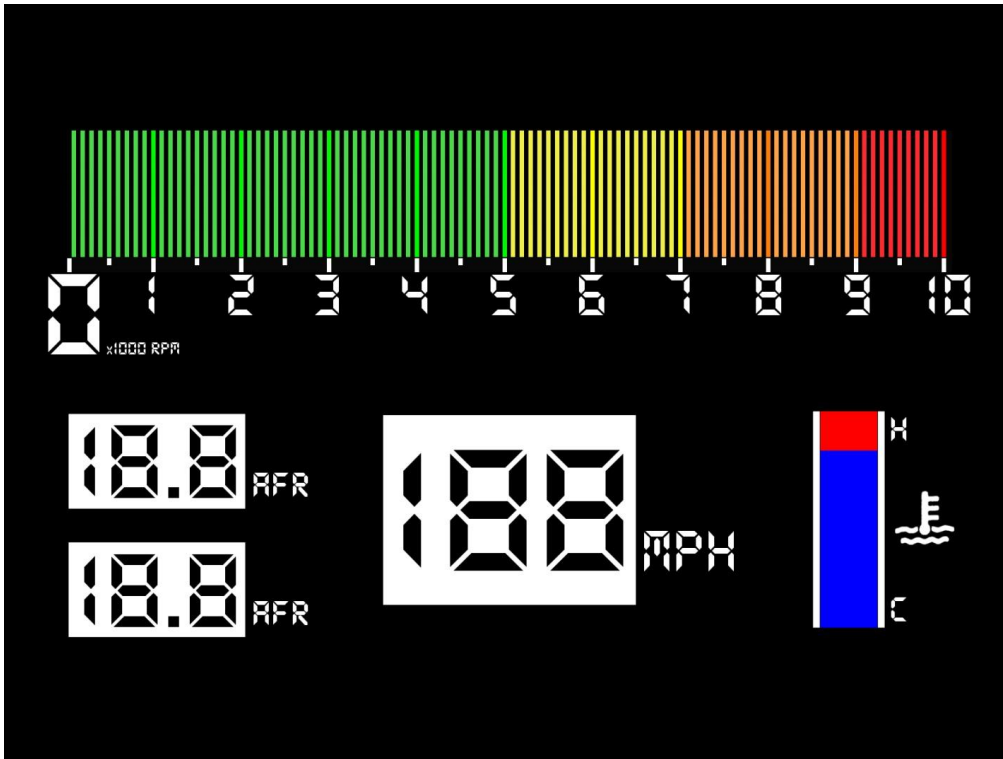


Figure 114: Artist Rendition 2- Digital Dash Display

Implemented Code

The original artist rendition was implemented in a Java application as seen in Figure 115. The implementation is very similar to the Artist's Rendition. The hundredths digit was dropped due to it being impractical for this application, but has been commented out in the Appendix code in case it proves useful for future applications.

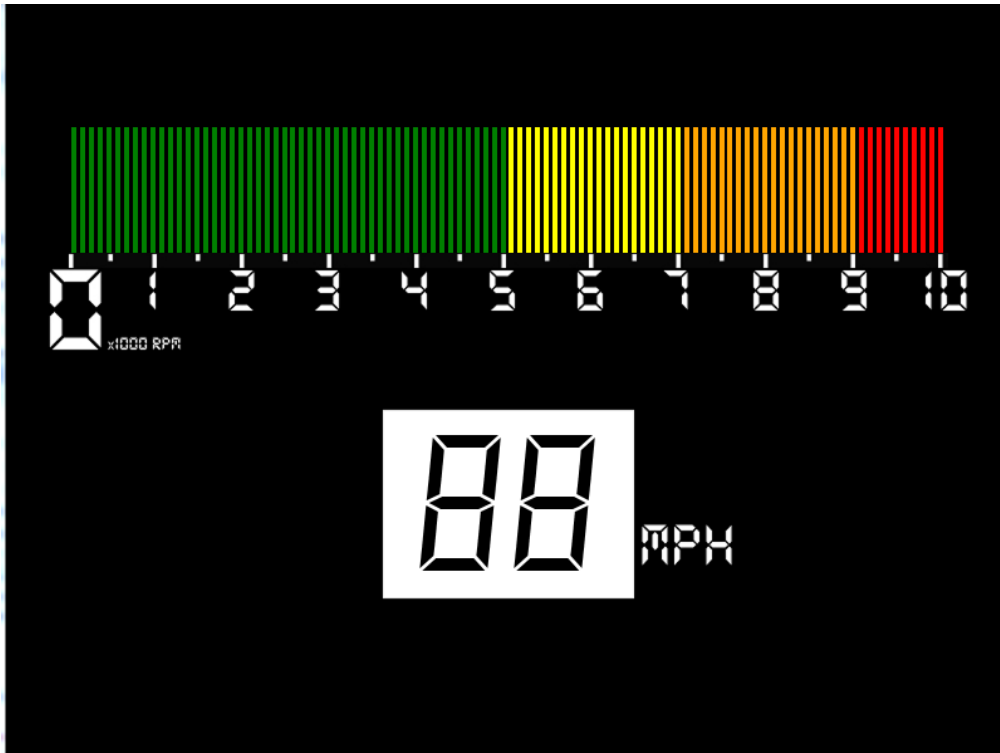


Figure 115: Implemented Code 1- Digital Dash Display

The implementation of the coolant temp and AFR's can be seen in Figure 116.

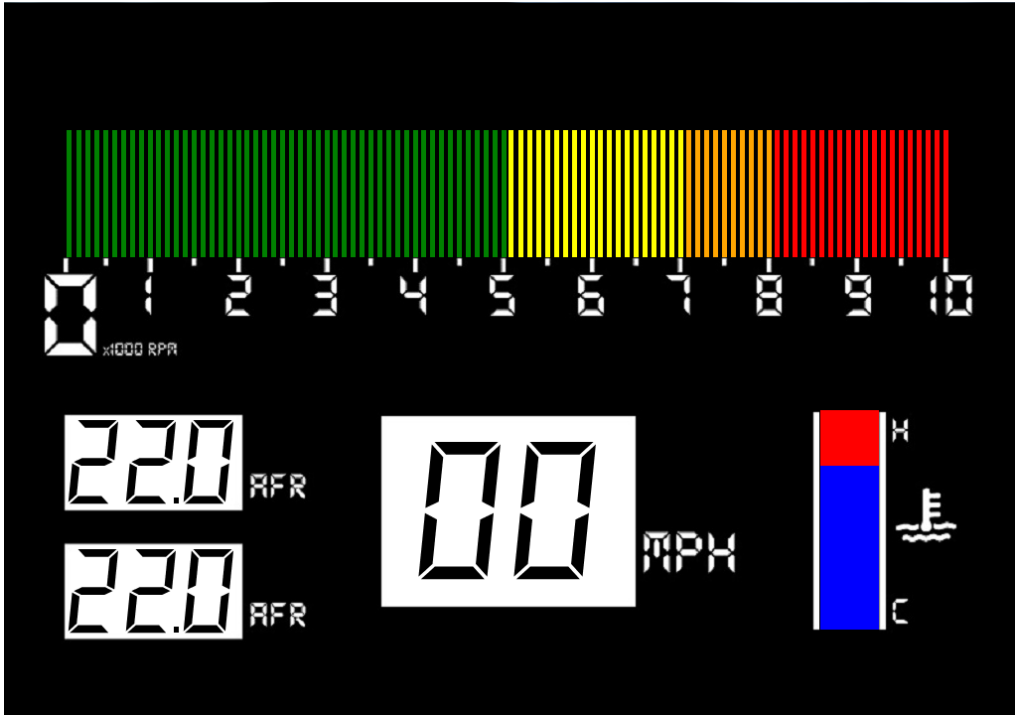


Figure 116: Implemented Code 2- Digital Dash Display

Integration

With all of the connections and interfacing of the CAN bus to the computer, the following circuit diagram can be referenced for system integration.

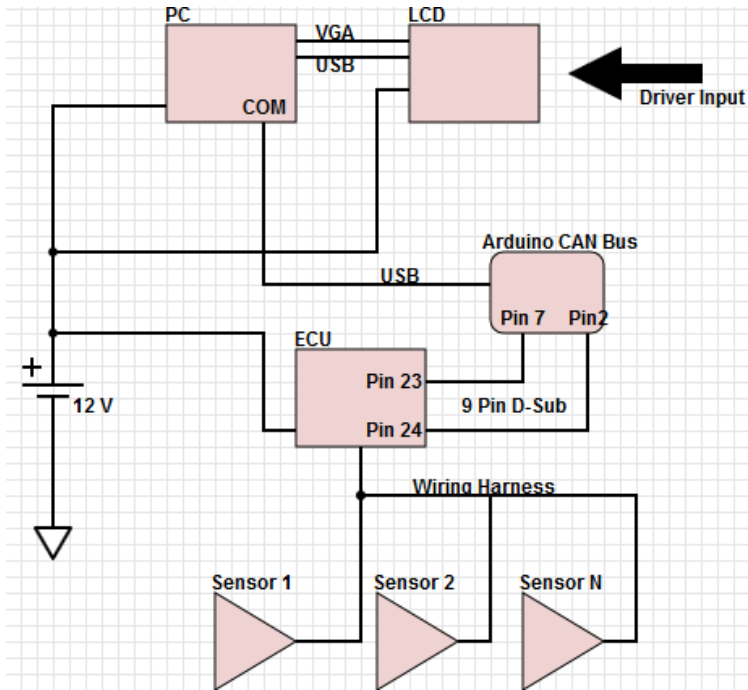


Figure 117: System Interface

The female side of the adapter is a CAN Bus 9 pin D-Sub connector. The CAN High and the CAN Low outputs from the ECU can be wired to a 9 pin connector head so that the connection will be more secure in the automotive environment. These connectors screw together to hold a solid connection. An example of the connector head and its pin layout are shown in Figure 118: Male 9 Pin D-Sub Connector.

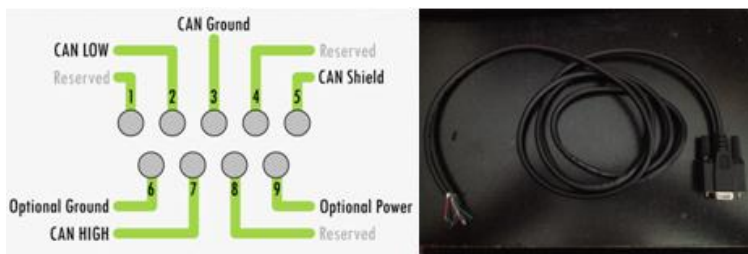


Figure 118: Male 9 Pin D-Sub Connector

Wiring Harness

Overview/Background

As the previous MQP's were focused on the mechanical aspect of the report, little was done for the documentation and cleanliness of the wiring harness on the car. Because of this, the decision was made to replace the wiring harness with a new one and provide documentation.

Initial Condition

The previous wiring harness was left on the car and initially appeared to be in working order. All of the connectors on the harness appeared to be present, but nothing was connected, with the exception of a portion of the front of the car. The wiring harness was removed from the car for testing purposes and to further determine its condition. The wiring harness was traced, using the wiring diagram provided with the Haltech ECU, to identify each of the connectors. For inspection purposes the wiring harness was divided into a front and rear portion.

The rear of the car appeared to be wiring properly with solder joints properly covered with heat shrink tubing. The only visible issues with the rear portion of the harness were that a few of the crimped connections had pulled loose and it was hard to trace because of inconsistency in wire colors. Some of the wires appeared to have been extended with a mid-wire that wasn't the same color.

The front portion of the wiring harness is where the majority of the issues were. This portion of the harness was not done properly; poor soldering took place and electrical tape was used improperly, or not at all, in place of heat shrink tubing. Some components were found to be no longer in working condition, and even obsolete to the current car.

The poor solder joints on the front portion of the harness brought question to the covered solder joints on the rear. It was advised that replacing the entire wiring harness would be ideal in order to eliminate unnecessary components and wires, but at the very minimum the front portion needed to be replaced.

Objective

To rewire the entire car in order to eliminate any doubts about the integrity of the electrical system, obtain an easier to use and diagnose wiring harness, and create proper documentation for future diagnostics and maintenance.

Research and Design

The Haltech ECU has some really nice documentation the came with it, so it was chosen as the basis for the wiring harness that would be used. Haltech provides a wiring diagram for the ECU that includes the 34 Pin and 24 Pin Connectors that groups the pins and wires into logical groups. The added benefit of this is that is also provides wire colors, which were maintained where possible. Based on this information, a general diagram for the wiring harness was made and can be seen in Figure 119. The idea was to have the harness connect to the

ECU and have the sections split closer to the ECU instead of partway through the harness. The reasons for this were to make it easier to debug wiring issues, serviceability, and ease of access.

The wiring harness would have different stages between the ECU and the sensors. The first, to the ECU connectors and split them into the different sections that are shown in Figure 119. For example, some of the pins would get split at the ECU to go to the relay panel, get grounded to the chassis, to the fuse panel, or go into the main harness. After this split, the wires would get split further into the groupings based on the Haltech wiring diagram. For example, the diagram has six pins for the injectors, six pins for the ignition, and two pins for the TPS. These wires would all go into labeled connectors. So even though the car only uses two pins for the injectors and two pins for the ignition because it only has a two cylinder engine, the wiring and connectors will be able to support all six. From there, the mating connector will only have the necessary wires for the current application.

The idea of this is that if an engine with a different number of cylinders was used it would be as easy as crimping pins onto wires and adding them into the blank spots on the connectors. This also would allow individual sections of the wiring harness to be removed and replaced if it ever got damaged, or a component was relocated. In the case of relocation, it would be as simple as ordering the necessary connectors for that section of the harness and making a new one to length, instead of replacing the whole harness.



Figure 119: Concept Layout

The next step in designing the wiring harness was to create documentation that would ease in breaking the harness down further into section. The Haltech wiring diagram was used to create the wiring diagram shown in Figure 120. This broke the wiring harness down into connectors based on the sections discussed previously. The pin label colors represent the

colors of the wires and the node label colors represent the color of stripes on the wires. For solid color wires, such as Pin10 on the ECU Output connector, both the pin label and the node label are the same color, in this case they are both black, which means a solid black wire would be used. For striped wires, such as Pin3 on the ECU Output connector, the pin label is yellow, and the node label is black, so a yellow wire with a black stripe would be used here.

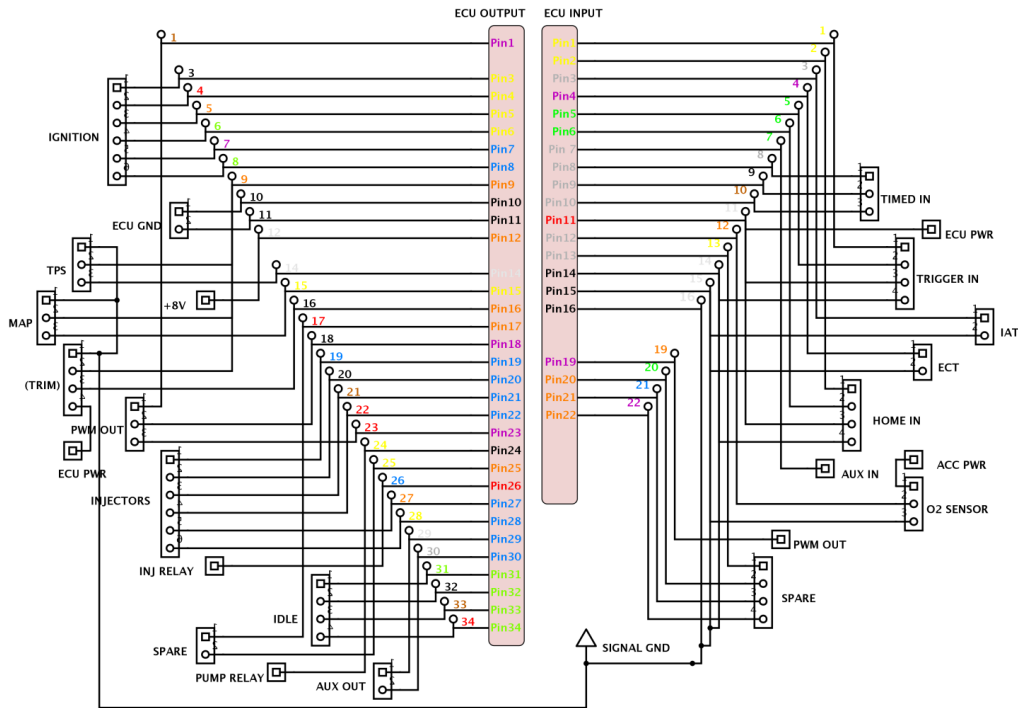


Figure 120: ECU Harness Pigtails

This part of the harness was further broken down on the output and input sides, shown in Figure 121 and Figure 122 respectively.

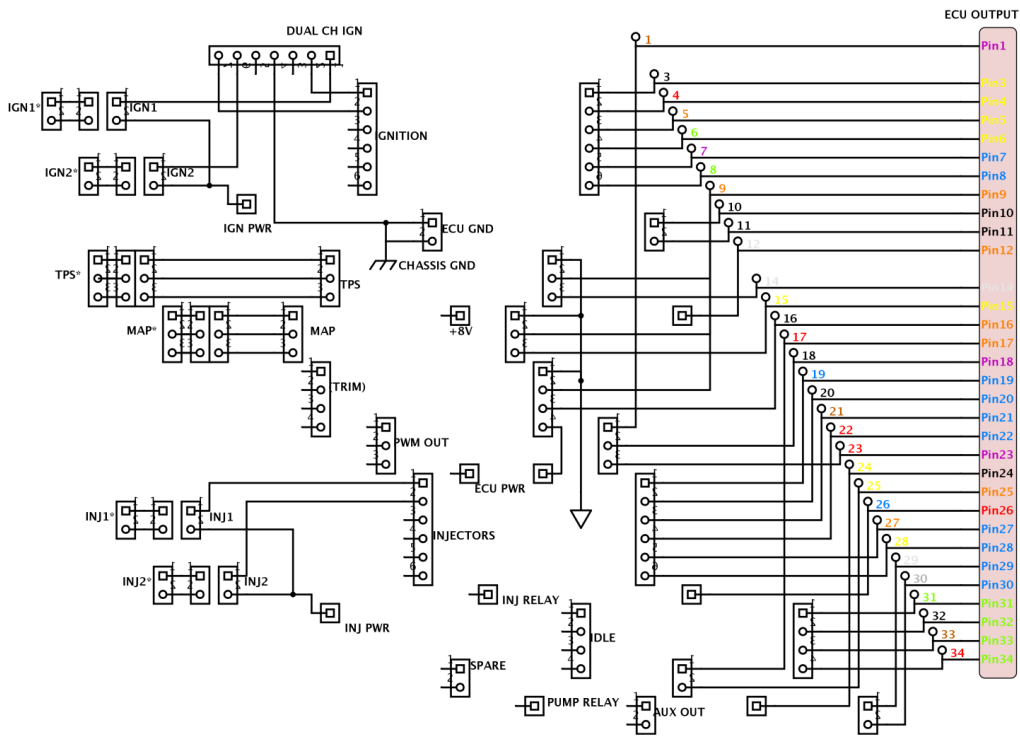


Figure 121: ECU Output Harness Breakdown

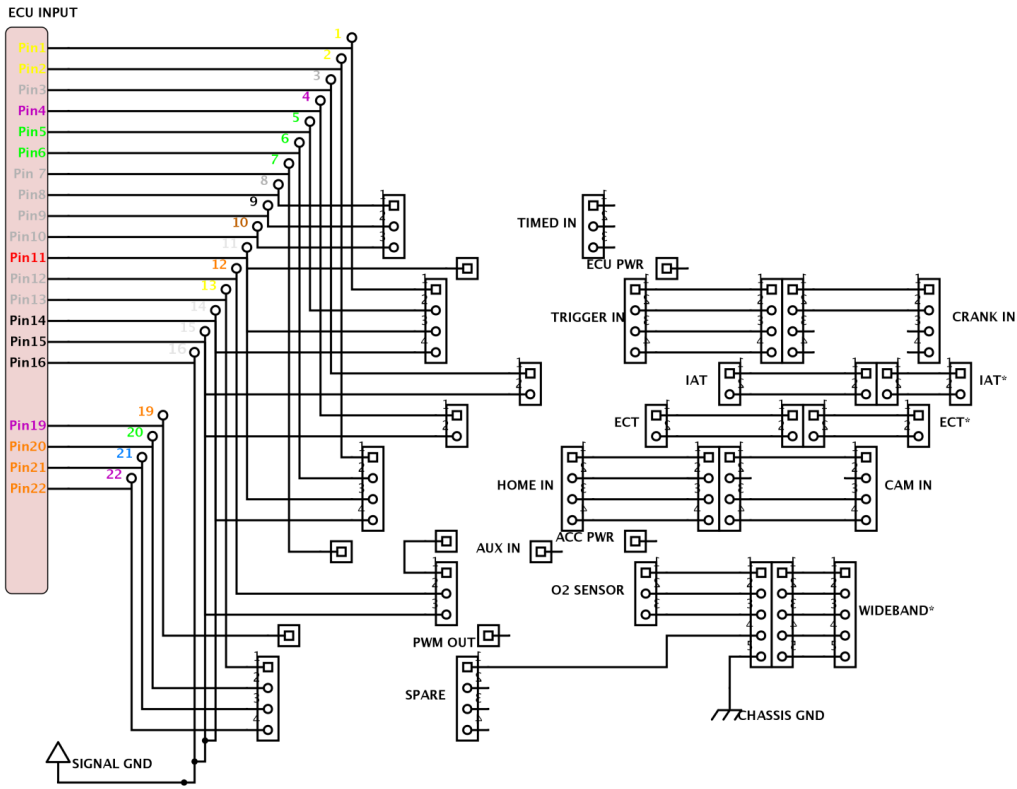


Figure 122: ECU Input Harness Breakdown

These breakdowns were used to order the necessary number of connectors for proper implementation. The labels with the asterisks next to them indicated that terminating connectors for that section would not be ordered because the existing connector would be used. The parts lists with part numbers can be seen in Table 12.

Table 12: Electrical Parts List

| Quantity | Item | Part # | Price | Cost |
|----------|---|-------------------------|--------|---------|
| 100 | S-SEAL SKT 18-16 Cut Strip of 100 | 3-1447221-3 (Cut Strip) | \$0.35 | \$35.00 |
| 1 | 34P PLUG 4 ROW | 4-1437290-0 | \$7.50 | \$7.50 |
| 1 | 26P PLUG 4 ROW | 2-1437285-2 | \$6.50 | \$6.50 |
| 4 | 6P FM BLK CONN ASSY 150 SERIES 14 AMPS | 12052848 | \$1.98 | \$7.92 |
| 4 | 6P MALE BLACK 150 SERIES 14 AMPS | 12124107 | \$1.12 | \$4.48 |
| 10 | 4P FM BLK CON ASSY 150 SERIES 14 AMPS | 12162144 | \$1.62 | \$16.20 |
| 10 | 4P MALE BLACK 150 SERIES 14 AMPS | 12162102 | \$0.90 | \$9.00 |
| 8 | 3P FM BLK CON ASSY 150 SERIES 14 AMPS | 12110293 | \$1.85 | \$14.80 |
| 8 | 3P MALE BLACK 150 SERIES 14 AMPS | 12129615 | \$0.85 | \$6.80 |
| 12 | 2P FM BLK CON ASSY 150 SERIES 14 AMPS | 12052641 | \$1.51 | \$18.12 |
| 12 | 2P MALE BLACK 150 SERIES 14 AMPS | 12162000 | \$0.83 | \$9.96 |
| 9 | 1P CON MP 150 1W FEM | 12047682-B | \$0.36 | \$3.24 |
| 9 | 1P CON MP 150 1W ML | 12047683-B | \$0.36 | \$3.24 |
| 150 | FMALE 150 SERIES TIN CBL RANG 2.80-2.03MM | 12048074-L | \$0.14 | \$21.00 |
| 150 | MALE 150 SERIES TIN CBL RNG 2.78-1.69MM | 12045773-L | \$0.12 | \$17.40 |

Integration

The wiring harness was assembled and integrated with the car. After completion, the harness breakdown was updated to reflect the wiring that is on the car. The updated diagram can be seen in Figure 123, as well as the updated breakdowns in Figure 124 and Figure 125.

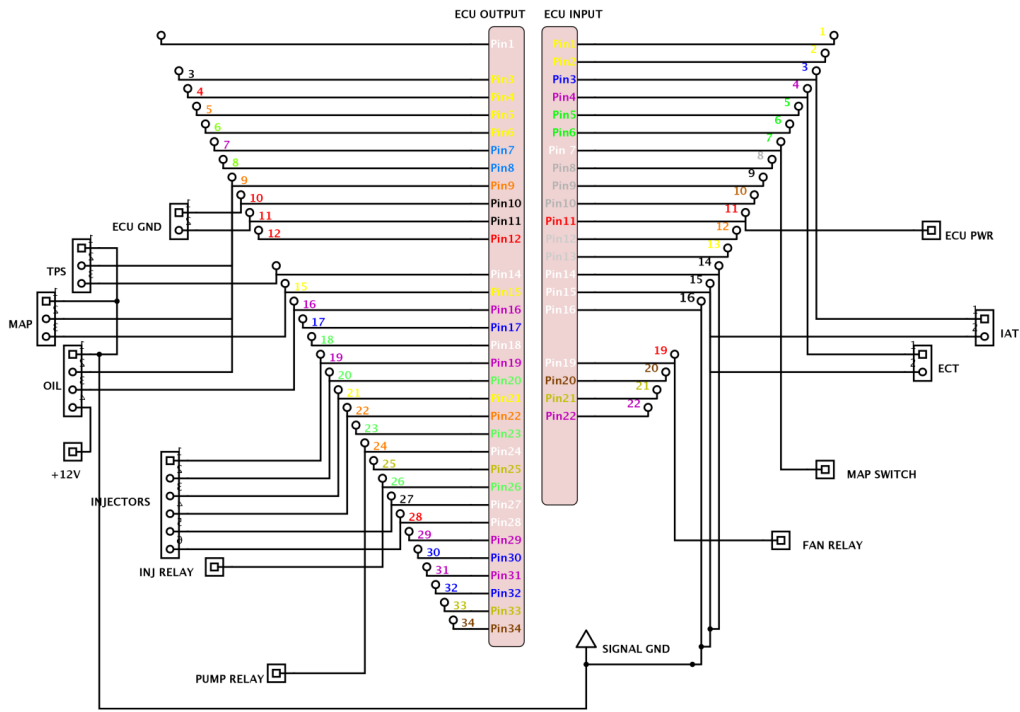


Figure 123: Final ECU Harness Pigtails

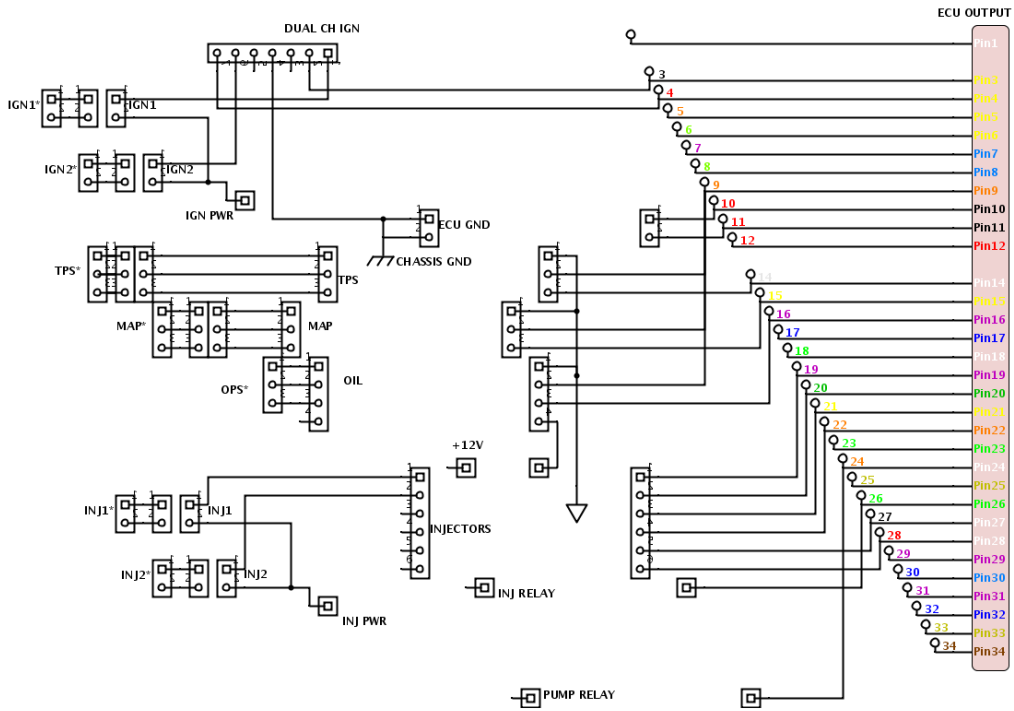


Figure 124: Final ECU Output Harness Breakdown

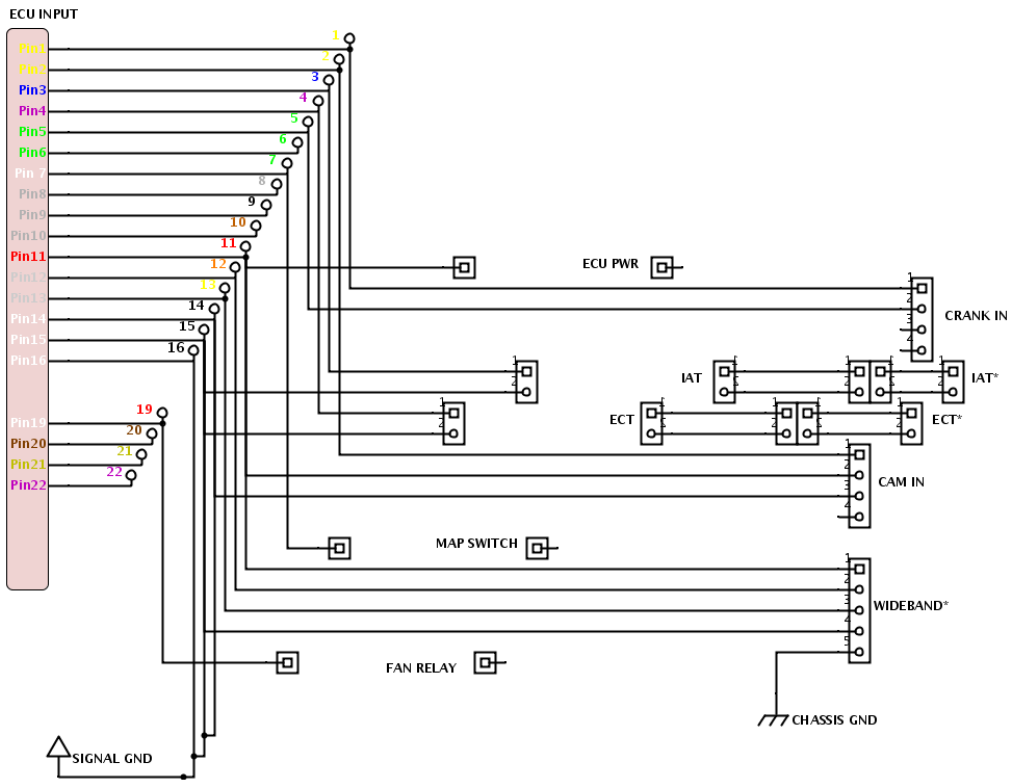


Figure 125: Final ECU Input Harness Breakdown

Table 13: 34-Pin Connector

| Pin # | Wire Color | Connection | Used? |
|-------|---------------------|------------------|-------|
| 1 | - | - | - |
| 2 | - | - | - |
| 3 | Yellow/Black | IGN 1 | Y |
| 4 | Yellow/Red | IGN 2 | Y |
| 5 | - | IGN 3 | N |
| 6 | - | IGN 4 | N |
| 7 | - | IGN 5 | N |
| 8 | - | IGN 6 | N |
| 9 | Orange | +5V DC | Y |
| 10 | Black/Red | CHASSIS GROUND | Y |
| 11 | Black/Red | CHASSIS GROUND | Y |
| 12 | - | +8V DC | N |
| 13 | - | - | - |
| 14 | White | TPS | Y |
| 15 | Yellow | MAP | Y |
| 16 | Purple | OIL PRESSURE | Y |
| 17 | - | - | - |
| 18 | - | - | - |
| 19 | Purple | INJ1 | Y |
| 20 | Green | INJ 2 | Y |
| 21 | Yellow | INJ 3 | N |
| 22 | Orange | INJ 4 | N |
| 23 | - | - | - |
| 24 | White/(Orange/Gray) | FUEL PUMP RELAY | Y |
| 25 | - | - | - |
| 26 | Green | +13.8V INJ POWER | Y |
| 27 | White/Black | INJ 5 | N |
| 28 | White/(Red/Green) | INJ 6 | N |
| 29 | - | - | - |
| 30 | - | - | - |
| 31 | - | - | - |
| 32 | - | - | - |
| 33 | - | - | - |
| 34 | - | - | - |

Table 14: 26-Pin Connector

| Pin # | Wire Color | Connection | Used? |
|-------|-------------------|------------------|-------|
| 1 | Yellow <SHD> | CRANK (+) | Y |
| 2 | Yellow <SHD> | CAM (+) | Y |
| 3 | Blue | AIR TEMP | Y |
| 4 | Purple | COOLANT TEMP | Y |
| 5 | Green <SHD> | CRANK (-) | Y |
| 6 | - <SHD> | CAM (-) | N |
| 7 | White/Green | MAP SWITCH | Y |
| 8 | - | COOLANT WARNING | N |
| 9 | - | | - |
| 10 | - | | - |
| 11 | Red | +13.8V ECU POWER | Y |
| 12 | Gray/Orange <SHD> | O2 INPUT 1 | Y |
| 13 | Gray/Yellow <SHD> | O2 INPUT 2 | Y |
| 14 | White/Black | SIGNAL GROUND | Y |
| 15 | White/Black | SIGNAL GROUND | Y |
| 16 | White/Black | SIGNAL GROUND | Y |
| 17 | - | - | - |
| 18 | - | - | - |
| 19 | White/(Red/Green) | FAN RELAY | Y |
| 20 | - | - | - |
| 21 | - | - | - |
| 22 | - | - | - |
| 23 | - | - | - |
| 24 | - | - | - |
| 25 | - | - | - |
| 26 | - | - | - |

Battery Mount

Overview

The battery on a FSAE racecar is very similar to the battery on an automobile. It is required to start the car and must be able to withstand rigorous tests and be mounted in place without any movement for safety and performance purposes. The mount used to hold such a battery must be carefully designed as to meet all of the criteria necessary for a competitive FSAE car. Due to problems with the current battery, a new battery mount had to be designed and manufactured in order to house a new battery for the 2014 FSAE car.

Initial Condition

The battery used on the previous FSAE car had dimensions of 2" x 4" x 3" and weighed in at only 4lbs. It was mounted to the frame of the car using two pieces of sheet aluminum, which were bent at 90° angles and ran perpendicular to each other, enveloping the battery. This mounting method was sufficient for a battery of such dimensions and weight, but would not be suitable for a larger battery with more mass. While the design of the battery mount had no issues, there was one major problem with the battery itself. A severe acid leak was discovered and the battery could not be used.

Research

The criteria for a battery on an FSAE car are relatively low weight and size (in comparison to an average car battery), the ability to withstand vigorous changes in acceleration, and also have a cold cranking amperage (CCA) of over 160A, which ensures a start in all temperatures. Additionally, according to FSAE rules, the battery installed must be a sealed battery, meaning that the battery acid contained within the battery must be completely sealed and be at no risk of spilling. Batteries that are sealed have this stated on the advertisement and are also usually stated as being "maintenance free."

The FSAE forums were consulted as the next step in the research process. A search was conducted regarding the Yamaha Phazer's Genesis 80FI engine, which is used in the WPI FSAE car, and the batteries that other FSAE teams are using with this engine. The Yamaha Phazer snowmobile is subjected to similar dynamic conditions as an FSAE car and the battery used in a snowmobile meets all of the criteria stated above. The most common battery used by other teams was the Yuasa YTX-14 BS battery, which is an OEM replacement battery for the Yamaha Phazer and has a CCA of 200A. It weighs 10lbs and has dimensions of 8" x 3" x 6". Although it is over twice the size of the previous battery, it offers two major advantages. First, the YTX-14 BS only costs \$40.00, which is a third of the cost of the previous battery. Second, the larger size allows it to be used for testing purposes repeatedly without dying. While testing the engine and electronics, often times the magneto is disconnected or the engine is not running so the battery is not being charged. While the larger size and weight is a disadvantage, it is only a minor disadvantage as it is still a relatively small and lightweight battery, weighing only 8lbs more than the previous battery.

Design

Preliminary Design

Upon shipment of the battery, it was inspected for defects, filled with acid according to the included directions, charged, and tested to read the proper voltage of 12.9V. The design of the mount for the new battery began by defining criteria for the mount. The mount itself had to be rigid and had to prevent the battery from twisting or moving in any direction. Additionally, it had to be lightweight and easy to machine so it could be produced in the machine shop at WPI.

Shown in Figure 126 is the preliminary design for the YTX-14 BS battery mount. It utilizes a piece of aluminum sheet metal, 0.125" in thickness, as the base. Aluminum was chosen due to its low cost, low weight compared to other materials such as steel, and its ease of machinability. It is held in place using tube clamps, which wrap around the frame rails of the car. L-shaped brackets prevent the battery from rotating and threaded rods with a plate on top of the battery (not pictured) push the battery down onto the mount. This design is similar to what is found in most automobiles.

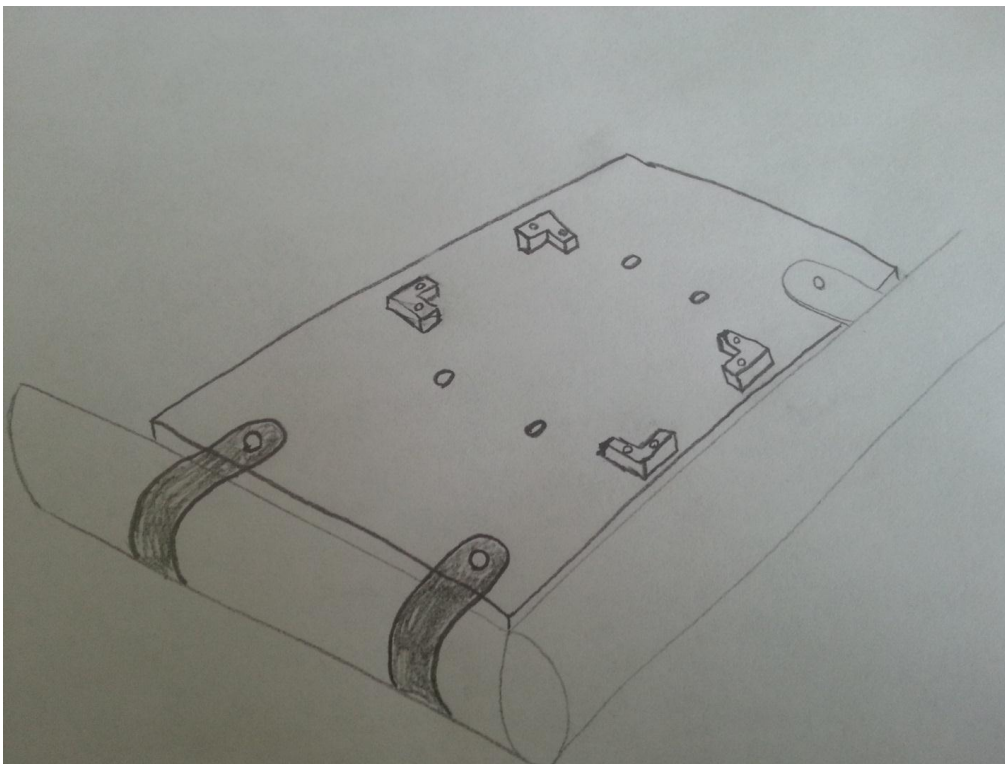


Figure 126: Preliminary Battery Mount Design

Concept Selection

After completion of the preliminary design, a location for the mount to be connected had to be devised. The decision matrix for the mounting location is shown in Table 15. The only location on the car that had enough room to house the battery was under the seat, behind the gas tank. Left, right and central locations are compared in the table.

Table 15: Battery Mount Design Matrix

| Location | Space Available | Frame Rail Support | Mounting height |
|-------------------------|-----------------|--------------------------|-----------------|
| Behind gas tank, left | 5 | 8 | 7 |
| Behind gas tank, center | 9 | 2 | 7 |
| Behind gas tank, right | 9 | 8 | 7 |
| | | | |
| Location | Accessibility | Proximity to Electronics | Total |
| Behind gas tank, left | 7 | 2 | 29 |
| Behind gas tank, center | 4 | 5 | 27 |
| Behind gas tank, right | 7 | 9 | 40 |

Based on the decision matrix, the location on the right side of the car (if viewing from the rear) was chosen as the location for the battery mount. The left side has an issue with the fuel lines coming directly from the gas tank getting in the way of where the mount would be attached. The center lacks supports to connect the mount to, as the left and right sides have two frame rails on the sides and one underneath for the battery mount to rest on. All locations have a low mounting height which is vital to keeping the car's roll center as low as possible. All areas are fairly easy to access. The right side has the advantage of being located closest to the kill switch, which is where the main battery leads attach to. This location allows for the use of short battery leads and also allows one of the fuel tank tabs to be used as a connection to the frame.

Final Design

The final design began by taking measurements of the frame in the area to which the battery mount would be connected. The angle of the frame rails was determined to be 79° and it was also determined that 2" could be cut off the 12" x 12" aluminum plate to allow it to fit behind the gas tank.

The preliminary design consisted of four threaded rods, but the final design was revised to use only two threaded rods to hold the battery to the mount. The reasoning behind this was that the leads on the battery are too close together to allow room for a wide top plate. A thinner top plate could only fit two threaded rods, which is what is used on most automotive battery tie-downs. The design was also modified to include vertical L-brackets instead of the horizontal L-brackets because aluminum vertical L-brackets were found in the FSAE shop and measured to be 1" x 1", which was the ideal size for the application in which they would be used.

Manufacturing

The manufacturing process began by cutting the 12" x 12" piece of aluminum plate to the correct size. It was trimmed to the dimensions and angles, as designed, on a band saw and

sanded down on a belt sander to remove sharp edges. Next, all of the mounting holes were drilled on a drill press using a 9/32" drill bit (to fit 1/4"-20 bolts). The plate was test fitted to the frame to verify that the design was sound and the plate fit as it should.

Next, two 1/4"-20 threaded rods were cut down to a length of 7" and were mounted to the aluminum plate using locking nuts on one side and normal nuts with locking washers on the other side, essentially making the threaded rods part of the plate. The L-brackets were then cut to size, which was 0.500" shorter than the length and width of the battery. Holes were drilled into the L-brackets to be mounted to the plate. Once assembly of the plate was completed, the battery was installed onto the mount using a 2" x 6" piece of aluminum (left over from prior machining to the plate) to hold the battery down onto the mount.

Integration

The completed battery mount assembly was installed onto the frame using two tube clamps and one of the fuel tank tabs to keep the mount in place. The cross member underneath the mount also provided support from underneath to help the mount stay in place and also prevented it from bending under the load of battery's weight. The location of the battery allowed it to be easily integrated into the car's electronics system. The installed battery is pictured in Figure 127 and Figure 128.



Figure 127: Installed Battery (Side View)

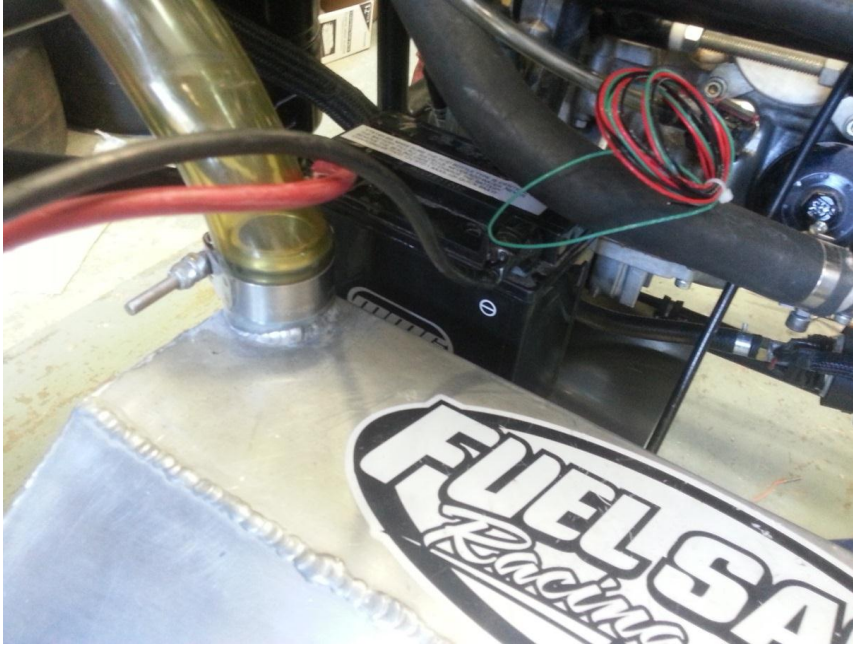


Figure 128: Installed Battery (Top View)

Testing

The battery had already been tested to have a voltage output of 12.9V as expected. Once connected to the electrical system, the car was started and driven without an issue. The battery, which is larger than the battery previously used in the car, has proven its worth by allowing the car to be started repeatedly without giving it enough time to charge, indicating a long battery life.

Conclusion

Summary

Once the small battery that was used previously on the WPI FSAE car was found leaking acid, a new battery was needed. Research was done to determine the best choice of battery; a Yamaha Phazer OEM replacement battery met all of the criteria. A preliminary design was developed that was similar in concept to an automotive battery mount and a location for the battery was chosen based on a decision matrix with the pros and cons of each potential location. A final design was then developed based on the location chosen. The parts for this design were purchased and the battery mount was manufactured and installed on the car. After installation, the battery was integrated into the electronics system of the car and tested in order to verify that the design and construction were both of quality.

Future Recommendations

The battery mount should not need much maintenance, if any. The only recommendation to future MQP teams is to be careful when tightening down the top plate when reinstalling the battery. It is held down with a locking nut on each of the two threaded rods. Tighten these nuts until the top aluminum plate just begins to bend and then stop. This plate does not need to exert a great amount of force on the battery.

Body

The goal of the body design team was to design and produce a fiberglass body that would comply with the FSAE rules. The body protects the driver from road debris. Additionally, the body increases the aesthetic appeal of the vehicle. Fabricating the body out of fiberglass kept costs low while providing necessary performance characteristics to comply with FSAE rules.

Overview

The body of a formula one car is a critical component to the success of the vehicle. The body provides shape and aesthetics that people find synonymous with the concept of a racecar, as well as the downforce and aerodynamics that allow the car to achieve the speeds, acceleration, and handling that exemplify racecars as a whole. The body of the racecar is an important feature that undergoes renovation and optimization frequently to ensure that the car looks the best while it has the best possible performance. Other necessary benefits that are not often associated with the body of a racecar are the passive effects directed towards the driver. The body provides the driver protection against the wind and other minor debris found on a race track.

Initial Condition

The 2013 body was a rushed process; it met the functional requirements of the body, but during the summer storage process it was damaged beyond repair. The 2013 project group spent time ensuring that the body was extremely lightweight and well molded to the frame, to the exclusion of durability, and aesthetics. As shown in Figure 129 and Figure 130, the ribbing used as the structural system for the body was not intact when delivered to the project site. This demonstrated a critical area of improvement for future work. The vinyl plastic wrap used as a primary surface was received in sub-par condition; it was scuffed across the flat surfaces and abraded beyond repair in corners of the structural system. These, when complied together, demonstrated that the 2013 body was unusable and put together as a last minute project.



Figure 129: Body (2013 MQP)



Figure 130: Body Structure (2013 MQP)

Objectives

After the analysis of the 2013 body, it was decided that improvements needed to be made to the durability of the body, while still meeting the functional requirements of the body. The final design requirements of the body were: the body must meet all FSAE rules and regulations, as well as be resilient to road debris and race conditions while maintaining aesthetic features.

Research

Research for the 2014 FSAE body began with materials and common practice for FSAE body building. The two major body materials include carbon fiber and fiberglass. Thus research began with the manufacturing process of fiber reinforced polymers. The FSAE forums were consulted to find the common practice for designing the body. On the forums, there are a number of threads detailing the benefits of different types of fiberglass or comparing fiberglass to carbon fiber. Researching these threads showed that the manufacturing process was the same for both fiberglass and carbon fiber. Many forum posts compared various aspects of the production process. More detail than was needed to develop a basic understanding of the

process from start to finish was provided. In order to find a more basic understanding of the fiberglass manufacturing process, a boat building forum was consulted, as fiberglass is common in boat building. The boat building forums went into great detail about the different forms of fiberglass product manufacturing, often weighing the benefits of the different processes against the intended use of the product. Three methods were discussed on the boat building forum: hand lay-up, vacuum bagging, and spray up. After reading about the hand lay-up method, it was deemed to be the most effective way for the body to be built.

Hand Lay-Up

The hand lay-up method was described in the small boat building forums as well as by several FSAE teams. When creating a fiberglass body using the hand lay-up method, a male mold will need to be created. A surface treatment will need to be applied to the male mold to prepare it for the hand lay-up process. Epoxy is often used as the surface treatment because it provides a firmer surface than foam. A male mold used to make a nose cone of the body is shown in Figure 131.



Figure 131: Nose Mold with Epoxy Stiffener

After the mold is made, fiberglass should be fitted to the mold to ensure that overlap of the fiberglass weave is in appropriate locations to improve stiffness at bends and joints. Then, the epoxy is applied to the fitted fiberglass. This process of fitting the fiberglass weave is repeated until the desired stiffness is achieved. The benefits of this method are the ease of purchase of the components and the low complexity of the construction process. Figure 132 is an advanced bodywork mold that was used by an unidentified FSAE team to create their bodywork.

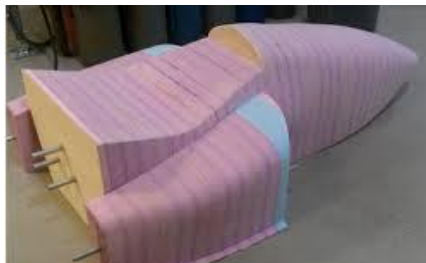


Figure 132: Advanced Bodywork

Vacuum Bagging

Vacuum bagging is a commonly used technique in composite building. Vacuum bagging will give a uniformly distributed compression about the surface of the layup. This helps to minimize any bubbles and wrinkles in the buildup of layers. Bubbles and wrinkles reduce the strength of the product by introducing flaws to the organization of the fibers. When used with a porous substrate made of peel-ply and breather-cloth, it assists in having the optimal ratio of resin to fiber reinforcement, like fiberglass, or carbon fiber, by squeezing out the excess epoxy. It is often used to apply fiberglass to an existing panel or area. Due to the atmospheric pressure developed outside the bag, vacuum bagging reduces the concern of air bubbles generated during the curing process. The downside to vacuum bagging is the need to have a bag that will fit over the mold. This limits the types of molding that can be done to thin pieces like skateboards or side panels.

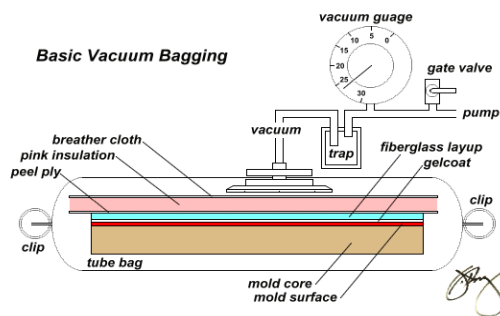


Figure 133: Vacuum Bagging Process

Spray-Up

The final way to apply fiberglass and resin to create a composite product is spray-up. Spray up is the most expensive version to use but it is very effective for large scale projects like boat hulls. Spray up uses a gun that fragments the glass fibers and mixes it with resin before exiting the nozzle of the gun. The gun is effective because the ratio between resin and fiberglass is controlled and regulated. After the fiberglass and resin is sprayed onto the mold, all that needs to be done is compress the fiber and resin together to prevent air bubbles in the mixture. While this method is the fastest in producing fiberglass pieces, it requires the most initial cost and if used with a male mold it is much more difficult to achieve a smooth surface finish. When used with a female mold as shown below, appropriate prep work can be done to improve the surface finish.



Figure 134: Spray-up Molding

Body Design Specifications

After concluding the research, basic ideas were generated about the production of the body. The 2014 FSAE rules were consulted to ensure that any fiberglass body designed would comply with the rules. According to FSAE, the vehicle must be open-cockpit and open-wheeled, with four wheels that are not in a straight line. FSAE defines open-wheeled as being unobstructed when viewed from the top, and side. The wheels are considered obstructed if there is a part of the vehicle within a radius of 2.700" of the outside of the wheel. Specifically, the body must not have openings to the driver compartment from the front of the vehicle back to the main roll hoop. Openings are allowed for the front suspension.

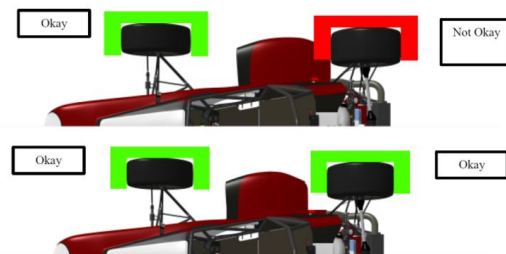


Figure 135: Definition 1 of Open Wheel

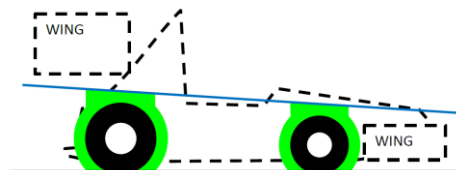


Figure 136: Definition 2 of Open Wheel

Integration with Frame

Common practice for attaching fiberglass bodywork to the car frame is quarter turn fasteners. Quarter turn fasteners are used because they are simple and convenient to incorporate into both the body and the frame. Additional benefits are the ease they provide to the process of adding or removing the body from the frame. Quick release quarter turn fasteners were applied to the fiberglass body in the outside edges at the top and the bottom of the frame. The fasteners were attached using hose clamps to offset the wire used to lock the fasteners in place. If the wire was not offset, holes would be drilled into the frame to create the appropriate room for the fastener to lock securely.



Figure 137: Quick Release Quarter Turn Fastener

Body Design

Keeping the FSAE requirements in mind, it was decided that attempting to create a downforce system with the body work would be too difficult to complete in the time allotted. This decision was reached by analyzing the practical knowledge the team had in working with fiberglass against the complexity of the bodywork done by well-developed FSAE teams. The body was designed to reduce drag, by minimizing the drag coefficient of the car. To determine the ideal body shape, the effects of different shapes in high speed winds were considered. It was calculated that the wind should be treated as incompressible flow because the car will not be traveling faster than 230 mph. Compressible flow is the area of fluid mechanics that deals with fluids in which the fluid density varies significantly in response to a change in pressure. Compressibility effects are typically considered significant if the Mach number (the ratio of the flow velocity to the local speed of sound) of the flow exceeds 0.3. A streamlined body was selected as the goal body shape, due to the low drag coefficient. Due to time constraints, it was decided not to mold past the main roll hoop. The final design meets the FSAE rules regarding open wheel requirements.

Preliminary Design

After concluding the research on the fiber reinforced polymers as well as the manufacturing process of fiber reinforced polymers, a preliminary design was developed. The design process started with a basic shape which was modeled in SolidWorks as shown in Figure 138. The shape took into account the level of skill with fiber reinforced polymers as well as basic aerodynamic concepts relating to incompressible flow. This design was used to generate discussions relating to the look of the final design.

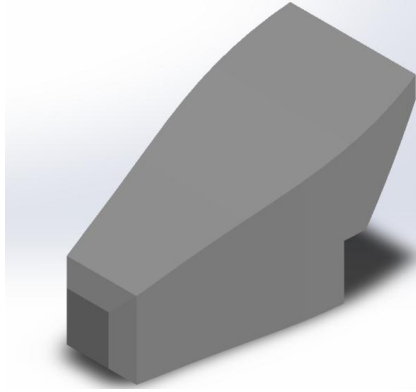


Figure 138: Initial Body Design

Concept Selection

After concluding discussions on the preliminary design as well as the manufacturing process of fiber reinforced polymers, a design matrix was generated weighing the material cost, operational performance, and production cost for carbon fiber and fiberglass. In the matrix below, the material cost, operational performance, and production cost were weighted out of 100. Each subcategory of the design matrix was weighted equally against other subcategories. The differences in cost arose from having fiberglass donated to the SAE Club. In terms of operational performance, carbon fiber out performs fiberglass in every respect. However, the FSAE rules state that body cannot support any load outside its own weight. This reduces the important operational performance characteristics to density and Young's Modulus. Due to the identical manufacturing process, the only significant difference between carbon fiber and fiberglass was the cost of fixing an error caused during the manufacturing process. The difference in cost significantly outweighed the better operational performance of the carbon fiber.

Table 16: Body Design Matrix

| | Fiberglass | Carbon Fiber |
|--------------------------------|------------|--------------|
| Cost | 100 | 68.33 |
| Shipping | 33.34 | 20 |
| Material | 33.33 | 15 |
| Preparation Material | 33.33 | 33.33 |
| Operational Performance | 80 | 100 |
| Density | 40 | 50 |
| Young's Modulus | 40 | 50 |
| Manufacturability | 100 | 86.67 |
| Preparation Time | 33.34 | 33.34 |
| Possibility of Error | 33.33 | 33.33 |
| Cost of Error | 33.33 | 20 |
| Total | 280 | 255 |

Final Design

After finishing the concept selection, the preliminary design was refined to more accurately determine the final weight, shape and integration with frame. The final estimated weight of the body was 19.480lbs and with the fasteners the final weight was 19.710lbs. The final design is shown in Figure 139.

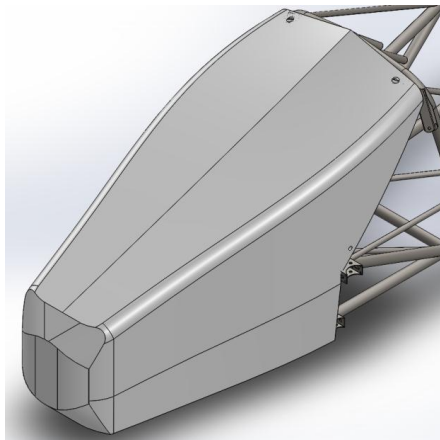


Figure 139: Final Body Design

Manufacturing

In order to create the fiberglass body as it was designed, a male mold for the nose cone needed to be created. In order for the hand lay-up method to be applied, the fiberglass and

resin would have to conform to the mold properly and sanding of the cured fiberglass resin mixture would also be needed.

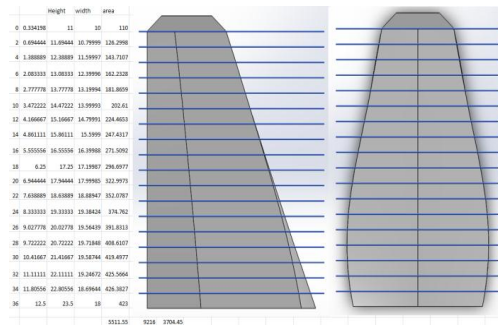


Figure 140: Mold Manufacturing Calculations

Creating the Mold

To create the mold, common practices among the local FSAE teams were researched. It was suggested that the use of rigid insulating foam would be sufficient to create a mold. Extruded polystyrene foam was selected to make the mold. The next step was to determine the amount of foam that was needed to create the mold for the nose cone. The model in SolidWorks was used to measure the height and width of the nose cone in 2" sections. These measurements showed that two 96" x 48" foam panels needed to be purchased. After the foam was purchased, the height and width measurements were used to mark and cut the appropriate rectangles on the foam. The foam was cut using a heat blade and a hacksaw. The heat blade was used to cut long but shallow sections whereas a hacksaw was applicable to the deeper cuts.

After the sections were cut, an adhesive was applied to glue the sections together before sanding began. Sanding was an important step in the mold building process. Sanding allowed the foam to be shaped into the final desired shape of the mold. Sanding eliminated the imperfections that were generated during the cutting of the foam. After sanding the mold into the final shape, an epoxy shell was applied. The epoxy shell was necessary to prevent the foam from being damaged during the hand lay-up process. After the epoxy shell was sanded smooth, the hand lay-up process began.

To begin the process of manufacturing the body, foam insulation was cut into rectangles that were stacked to fit the outline of the body. As shown in Figure 142, a heat blade was used to make long sweeping cuts along the foam. A heat blade is a stretched length of wire that is heated by running an electric current across the wire. This was an effective measure to cut the foam because of the foam's low melting point. The heat blade that was used in this process was almost a meter long; as such, it was impractical to use for small details.



Figure 141: Pre-Sanded Body



Figure 142: Heat Blade

The next step in the shaping process was sanding the foam. Due to the quantity of sanding that needed to be completed, an electric hand sander was used. As shown in Figure 143, the hand sander was used to add a smoother face to the foam mold. Hand sanding was used to add finishing touches to the foam to ensure an appropriate finish to the foam shown in Figure 144. The last test of the mold shaping was a final measurement of the mold against the frame.



Figure 143: Sanding with the Grinder



Figure 144: Initial Shaping Complete

Preparation for Fiberglass Molding

To begin the fiberglass molding process, test pieces of cured fiberglass were developed to determine the effect the exothermic curing process had on the foam. This test was developed due to the use of the heat blade as an effective cutting tool. Shown in Figure 146 is the fiberglass just after the application of the epoxy resin.



Figure 145: Before Curing



Figure 146: Test Piece after Curing

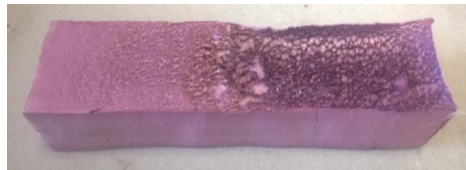


Figure 147: Melted Foam

Figure 147 shows how the test piece was affected by the exothermic process of curing the epoxy. It was determined that the foam melted due to the heat generated and not because of a chemical reaction between the foam and the epoxy. This added a step to the design process of finding an appropriate filler material that would protect the foam from the exothermic process. An autobody filler was chosen as a buffer to the fiberglass molding because of its low exothermic curing process, sanding properties, and ease of application.



Figure 148: Nose Mold with Sanding Complete

As the body filler was applied to the foam, additional sanding shown in Figure 148 was required to achieve the necessary surface roughness to apply the fiberglass and the epoxy to the mold. A mold release wax was applied to the surface to ensure that the epoxy did not bond with the auto body filler.

Fiberglass Molding

The molding of the fiberglass was completed using the hand lay-up process. This was done by cutting sheets of fiberglass weave into appropriate shapes, as shown by Figure 149.



Figure 149: Cut Fiberglass Weave

The sheets allowed the fiberglass to be wrapped around the mold. The wrapping was a critical component because it increased the stiffness of the body in the corners of the mold. Figure 150 shows the applied fiberglass to the mold.



Figure 150: Finished First Layer

After the fiberglass had finished curing, it was removed from the mold. The body was removed in order to effectively correct surface defects on the fiberglass generated during the molding process, shown in Figure 151. The surface defects were corrected using additional body filler as shown in Figure 152.



Figure 151: Body Removed from Mold



Figure 152: Filled Surface Defects

Painting

A final step of the manufacturing process was painting the body to increase the aesthetic appeal of the entire car. Using a spray gun, layers of primer, color and clear were added to the body following the proper use of the spray gun. The final painted body is shown in Figure 153 compared to the unpainted body in Figure 152 to demonstrate the increased aesthetic appeal.



Figure 153: Painted Body

Integration

The last step of the body manufacturing process was to fit the body onto the frame. This was done using quarter turn tabs to ensure that the body could be removed quickly if necessary. The quarter turn tabs were attached to the body using hose clamps. The hose clamps allowed for small adjustments that the body encountered during the test runs of the car. Additional foam was placed on the rails of the frame to reduce the rattling of the body during road testing of the car.



Figure 154: Frame Foam and Mounting Position

Testing

The final testing of the body was limited to the fitting of the body to the frame. Due to time constraints, the overall aesthetic appeal of the body was not effectively calculated. The data sample was too small to accurately predict a result.

Conclusion

In order to improve the body as a whole, many changes would be made in the manufacturing process. The design phase was accurate and complete to the necessary requirements of the body. If more time was able to be spent on the body as a whole, it would be beneficial to run tests on the air flow around the body. These tests were not necessary to the completion of the body but would provide better ways to test the accuracy of the manufactured product to the final design. If more complex shapes are desired, it would be strongly suggested to invest in an outside vendor to manufacture the body; this would reduce errors generated during manufacturing as well as reduce manufacturing time.

Exhaust

Exhaust System

Overview/Background

The purpose of an exhaust system in a commercial vehicle is to carry engine vapors away from the passengers in the vehicle, reduce harmful greenhouse gas emissions, as well as diminish the sound produced by the engine. The requirements are slightly different for an FSAE car, as the emissions of the engine are not as large of a concern as the racecar will not be accumulating nearly as many miles as a commercial car. Carrying the gases away from the passenger and reducing the engine noise are both still concerns.

A proper exhaust system provides efficient removal of the exhaust gases and efficiently silences the engine as well. There are many factors in designing a properly tuned exhaust, ranging from engine displacement, desired RPM, and other factors such as designing for even or odd firing engines.

Initial Condition

The initial exhaust system only included the headers, which are the metal pipes that connect the engine to the mufflers. Since there was no muffler present in the previous year's system, a new muffler setup would have to be purchased or fabricated. The decision on making versus buying the new muffler will be elaborated on later in this section.

Objective

The objective of the new exhaust system was to meet all FSAE noise requirements. The 2014 FSAE rules state the volume of the exhaust must be measured using "a free-field microphone placed free from obstructions at the exhaust outlet level, 0.5m (19.68") from the end of the exhaust outlet, at an angle of 45° with the outlet in the horizontal plane." This was the main design specification as well as the most important one for the exhaust system to meet. Other objectives included properly supporting the mufflers' weight as well as dampening the vibrations output by the system.

Research

Before getting into designing a system, research was conducted. Previous years' MQP reports were referenced as a starting point for the research. Afterward, any terms that were unknown were defined to help understand the exhaust system. (Some terms include mandrel bending, exhaust plenum, cam duration, etc.).

After doing basic system research, direct research was conducted, namely into muffler design. There are two basic types of mufflers; the simpler version is called an absorptive muffler, and the more complex version utilizes a Helmholtz Resonator. Absorptive mufflers utilize a special high temperature material, often fiberglass or steel wool, to physically absorb the sound waves as they travel through the muffler. The other method uses areas of a

calculated size and shape to bounce the waves back towards the engine to dampen the volume of the engine. Most aftermarket exhausts mufflers are the simpler absorptive styles.

Design

Sound Design Analysis

Before designing a completely new system for the Genesis 80FI engine, it was decided to conduct an analysis on the previous system to avoid adding unnecessary work. To begin this design check, the length of the header pipes was measured to ensure they were of proper length for the engine that is being used for the car.



Figure 155: Exhaust Header Pipe



Figure 156: Header Pipe Measurement

The measured lengths of the headers were both 23.500". The calculated length for the headers was 23.410". The difference in the measurements of .090" was likely due to user error in measuring the length, and therefore the header is of sound design.

Preliminary Design/Concepts

Before designing a new system, a decision had to be made whether to purchase a muffler system or to fabricate one. In the case of an MQP, the students only have a single school year to finish their project, so for this reason it was desired to err on the side of caution. By purchasing parts instead of personally manufacturing them, time can be conserved and a given student can still allocate their resources elsewhere.

This was the case for designing a new muffler versus buying a new one. In the end, it was decided to purchase a muffler as this would save time over designing and then fabricating one. Many different muffler options were considered, and after narrowing the results to the top four options, a weighted decision matrix was created to assist in the final decision.

Table 17: Exhaust Design Matrix

| Decision Factor | Weight | Option 1 | | Option 2 | | Option 3 | | Option 4 | |
|----------------------|--------|------------------------------|------------|-------------------|------------|----------------|------------|---------------------|------------|
| | | SuperTrapp Universal Muffler | | Magnaflow Muffler | | Emgo Rev. Cone | | Emgo Shorty Muffler | |
| | | Score | Value | Score | Value | Score | Value | Score | Value |
| Cost | 8 | 6 | 48 | 6 | 48 | 8 | 64 | 10 | 80 |
| Engine Compatibility | 6 | 7 | 42 | 7 | 42 | 5 | 30 | 6 | 36 |
| Mounting Options | 3 | 6 | 18 | 5 | 15 | 7 | 21 | 8 | 24 |
| Noise Reduction | 4 | 8 | 32 | 8 | 32 | 4 | 16 | 4 | 16 |
| Totals | | | 140 | | 137 | | 131 | | 156 |

Cost was a large factor in this decision because the budget for this project was previously set. Therefore it had to be weighed heavier than the other options. For example, the Magnaflow brand of mufflers were about \$200 each which would have cost a total of almost \$400 to purchase one for each of the headers. The second most heavily weighed option was engine compatibility. It was important for the muffler to be capable of being implemented in the current system with minimal changes. Next was the noise reduction. There is a decibel test that all FSAE cars must pass in order to be able to compete, therefore the reduction in the noise produced by the engine was important. The object with the lowest weight was the mounting options. This was because regardless of the type of muffler purchased, it would have to be mounted to the rear subframe. Therefore, whether or not a given muffler had any accessories for mounting (for example an external threaded bolt) that detail was factored in to the decision.

A combination between the cost and the mounting options had the Emgo Shorty Universal Muffler as the best option after the weights had been factored in. A picture of one of the two mufflers can be seen in Figure 157. Also purchased was two Emgo brand header reducer pieces to ensure the inner and outer diameters of the headers properly lined up.



Figure 157: The Two Mufflers and Two Reducers

The next step after purchasing was to connect the mufflers to the headers by utilizing the adapters pictured in Figure 158. Only the smallest piece pictured in Figure 158 ended up being

utilized as it filled the gap between the muffler itself and the header. The next step was to design and implement a bracket to support the weight of the mufflers as well as dampen the vibrations of the exhaust system.



Figure 158: Reducer on the Header Pipe

Designing a Muffler Bracket

The basic goal of this bracket was to be simple yet to be able to support the mufflers as well as dampen the vibrations produced from the exhaust system. The initial design utilized an extruded L-shaped piece of aluminum as the main load-bearing support as seen pictured in Figure 159.

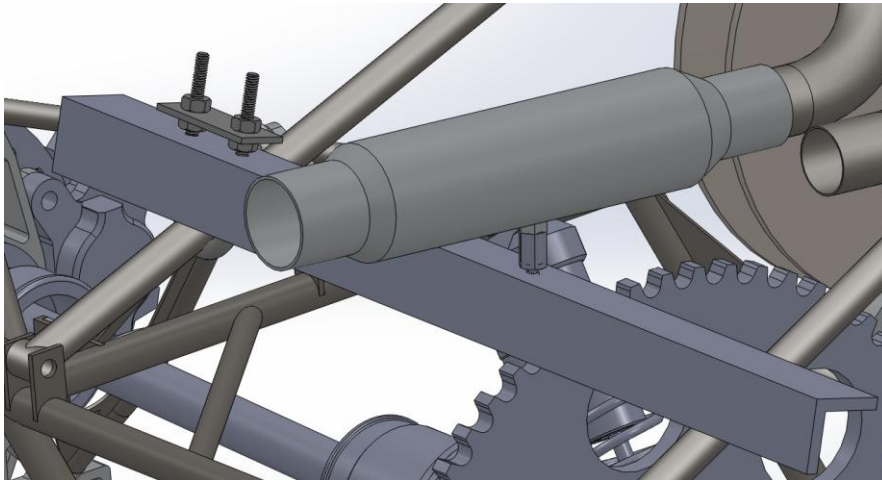


Figure 159: Muffler on the Header

It was later redesigned, however, to use steel to be both more aesthetically pleasing as well as stronger. The bracket had to be constrained to the two bars that connect the “banana” clips to the back of the rear subframe. After searching through McMaster-Carr’s part directories, it was discovered that rubber-coated U-bolts would be perfect for connecting the steel bar to the bars of the rear subframe aforementioned.

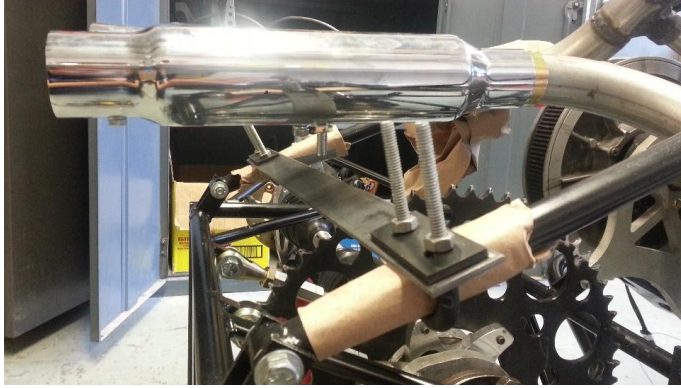


Figure 160: Steel Bar Connected to the Rear Subframe

As seen in Figure 160, there is approximately a 1" gap between the muffler's bolt and the steel bar. The piece that was used to change the muffler's M8 bolt to 1/4"-20, as well as the piece used to dampen the vibrations, called a vibration-dampening sandwich mount, was able to close the gap the amount required.



Figure 161: Vibration Dampening Sandwich Mount

The final two steps in connecting the bracket included welding the muffler adapters on and then drilling the holes directly below the muffler's bolts on. It was critical that the process be done in that order, this way the bolt's position would be finalized before the holes would be drilled. If the order was reversed, the final position of the mufflers could change thus making the holes drilled in the steel bar potentially in the wrong spot.

The final setup performed all desired tasks initially specified and most importantly assisted in dampening the vibrations in the system. After the welding was complete, the bracket was once again bolted to the rear subframe and the two holes were drilled in the steel bar. Finally, everything was bolted together and the exhaust bracket was completed.

Refinement of Design

A few final and minor revisions were made to the bracket. These included mostly aesthetic changes. One of these changes was to cut off the excess external threading of the

rubberized U-bolts to give the bracket a cleaner look. Also, minor changes included adding washers to the bottom side of the steel bar to ensure that the mufflers would stay in place. A picture of the final setup can be seen in Figure 162: Picture of Final SetupFigure 162.



Figure 162: Picture of Final Setup

Conclusion

The goals of the exhaust sub-system were successfully completed throughout this project. The bracket that was designed successfully performed all specifications desired. The mufflers were a cheap and effective solution which in a project with a tight budget is very desirable. The mufflers are slightly small for the size of the engine, therefore a future recommendation is to buy or fabricate another muffler with more absorptive material.

Outside Vendors

While working on a large project in a restricted amount of time, such as the MQP, team members must prioritize their action items in order to meet their corresponding deadlines. In projects that involve any type of product development, team members must organize themselves effectively, perform different tasks in parallel with the other components of the project, and make the best use of their time. Outsourcing some of the workload should always be considered when working on a project of this scale.

Student engineers need to evaluate the pros and cons of performing each individual task themselves versus paying a specialized professional to do it for them. Some of the most common tasks on a FSAE project are not necessarily considered engineering responsibilities. Even though some of these tasks may be crucial for the completion of the project, they are more inclined to the practices of a mechanic or a technician rather than an engineer. These tasks include welding, machining, metal bending, casting, painting, coating, upholstery etc. Students should focus their efforts more on the engineering design component of the project and less on physical work.

Budget calculations, time management, and project management are crucial skills needed when considering outsourcing some of the necessary labor. In the case of the 2014 FSAE MQP team, there were three main components that were done by outside vendors. The rear subframe tubes were manufactured and bent by Cartesian Tubing in Ontario, Canada. Once the tubes were manufactured and shipped to WPI, these were brought to City Welding & Fabrication in Worcester, MA. The company welded the subframe tubes based on the CAD drawings provided by the MQP team. The car's seat was fabricated by New England Trim in Shrewsbury, MA and a wide range of auto parts were purchased from multiple local vendors.

When working with outside vendors, communicating effectively is crucial for the task to be done efficiently. Communicating with engineers, sales people, managers and technicians is not the same and different approaches should be taken. Students must be explicit when requesting a service from a third party not affiliated with WPI. Students need to be aware of the timeframe in which the service needs to be completed and what the cost estimate should be. Assumptions are to be avoided when expecting a deliverable from a vendor and sufficient documentation must be provided early in the process backing up everything that is discussed verbally. A verbal agreement is never enough to support the terms of the agreement.

References

Aho, Christopher, Scott Duncan, Dan Cullen, Dan Swan, Adam Panzica, and Ryan Lehrmitt. 2009 Formula SAE Racecar. Tech. 2009. Print.

Aaen, Olav. Clutch Tuning Handbook. AAEN Performance 2007.

Alspaugh, David, Aquadro, Alessandro, Barnhill, Dylan, Beasley, Nicholas, Bennett, Andrew, Francis, John. Design and Analysis of a FSAE Racecar. Tech. 2012. Print.

Carney, Krysten, Davis, William, Kirschner, Anton, Leith, Jonathan, Piccioli, David. Design and Analysis of a FSAE Racecar. Tech. 2012. Print.

Willis, Christopher Ryan. A Kinematic Analysis and Design of a Continuously Variable Transmission. Blacksburg, VA 2006. http://scholar.lib.vt.edu/theses/available/etd-03312006-91805/unrestricted/Willis_Thesis.pdf

Appendix

Display Code

```
package myMQPapp;

import javafx.animation.KeyFrame;
import javafx.animation.Timeline;
import javafx.application.Application;
import javafx.event.ActionEvent;
import javafx.event.EventHandler;
import javafx.scene.Group;
import javafx.scene.image.ImageView;
import javafx.scene.image.ImageView;
import javafx.scene.paint.Color;
import javafx.scene.Parent;
import javafx.scene.Scene;
import javafx.scene.effect.Effect;
import javafx.scene.effect.Glow;
import javafx.scene.effect.InnerShadow;
import javafx.scene.shape.Polygon;
import javafx.scene.shape.Rectangle;
import javafx.scene.transform.Shear;
import javafx.scene.transform.Scale;
import javafx.stage.Stage;
import javafx.util.Duration;

/**
 * A digital dash application.
 *
 * @author Justin Paprota
 */
public class DigitalDash extends Application {

    private Dash dash;
    public SerialTest STest = new SerialTest();

    private void init(Stage primaryStage) {

        String user = System.getProperty("user.name");

        Group root = new Group();

        //start SerialTest
        STest.initialize();

        //add background
        Image image = new Image("file:C:\\Users\\" + user + "\\Documents\\Digital Dash 2_background.jpg");
        ImageView imageView = new ImageView();
        imageView.setImage(image);
        root.getChildren().add(imageView);
        Scene scene = new Scene(root, 1024, 768, Color.BLACK);
        primaryStage.setTitle("WPI FSAE Digital Dash");
        primaryStage.setScene(scene);
        primaryStage.show();
        primaryStage.setFullScreen(false);
        primaryStage.centerOnScreen();
        for (int i = 0; i < 2; i++) {
            Rectangle rectangle = new Rectangle(175, 498 + (i * 130), 5, 6);
            rectangle.setFill(Color.BLACK);
            root.getChildren().add(rectangle);
        }
    }
}
```

```

// add digital dash
dash = new Dash(Color.BLACK, Color.TRANSPARENT);

// add background to sample
root.getChildren().addAll(dash);
}

public void play() {
    dash.play();
}

@Override
public void stop() {
    dash.stop();
}

public static class Dash extends Parent {

    public int speed;
    public int rpm;
    public int coolant;
    public int afr1;
    public int afr2;
    public int speedoflag = 0;
    public int afrflag = 0;

    //Operating Range values
    public int CTemp_MAX = 100; //Max Coolant level
    public int CTemp_MIN = 0; //Min-Coolant level

    //Threshold RPM/100
    public int RPM_Y = 50; //Yellow threshold value
    public int RPM_O = 70; //Orange threshold value
    public int RPM_R = 80; //Red threshold value
    public int CTemp_Hot = 75; //Hot Temperature value

    private SerialTest ard_data;
    private Digit[] speed_digit;
    private Digit[] afr1_digit;
    private Digit[] afr2_digit;
    private Timeline delayTimeline, secondTimeline;

    public Dash(Color onColor, Color offColor) {
        // create effect for on LEDs
        Glow onEffect = new Glow(1.7f);
        onEffect.setInput(new InnerShadow());
        // create effect for off LEDs
        InnerShadow offEffect = null; //new InnerShadow();

        //create mph digits
        speedoflag = 1;
        speed_digit = new Digit[3];
        for (int i = 0; i < 2; i++) {
            Digit digit = new Digit(onColor, offColor, onEffect, offEffect);
            digit.setLayoutX(i * 96 + 435);
            digit.setLayoutY(442);
            speed_digit[i] = digit;
            getChildren().add(digit);
        }
        speedoflag = 0;

        //create AFR1 digits
        afrflag = 1;
        showAFR1(onColor, offColor, onEffect, offEffect);

        //create AFR2 digits
        showAFR2(onColor, offColor, onEffect, offEffect);
        afrflag = 0;
    }
}

```

```

//create rpm lines
showRPM();

//create coolant level
showCTemp();

// update dash to current data
refreshDash();
}

private void refreshDash() {
//Refresh RPM
Rectangle rectangle1 = new Rectangle(0, 0, 1024, 256);
rectangle1.setFill(Color.BLACK);
getChildren().add(rectangle1);

//Refresh Coolant
Rectangle rectangle2 = new Rectangle(825, 384, 60, 258);
rectangle2.setFill(Color.BLACK);
getChildren().add(rectangle2);

//Read Values from Arduino
speed = SerialTest.new_speed;
rpm = SerialTest.new_rpm;
afr1 = SerialTest.new_afr1;
afr2 = SerialTest.new_afr2;
coolant = SerialTest.new_coolant;

// //Generate Random values for Testing
// int test =randomWithRange(0,20);
// speed = test*5;
// rpm = test*500;
// coolant = test*5;
// afr1 = test*11;
// afr2 = test*21;

// //Set values for Display Testing
// speed = 88;
// rpm = 10000;
// coolant = 100;
// afr1 = 888;
// afr2 = 888;

// Set Digits for Display
speed_digit[0].showNumber(speed / 10 % 10);
speed_digit[1].showNumber(speed % 10);
afr1_digit[0].showNumber(afr1 / 100 % 10);
afr1_digit[1].showNumber(afr1 / 10 % 10);
afr1_digit[2].showNumber(afr1 % 10);
afr2_digit[0].showNumber(afr2 / 100 % 10);
afr2_digit[1].showNumber(afr2 / 10 % 10);
afr2_digit[2].showNumber(afr2 % 10);

showRPM();
showCTemp();
}

public void play() {
//wait till input, then start a timeline to call refreshDash() every second
delayTimeline = new Timeline();
delayTimeline.getKeyFrames().add(
    new KeyFrame(new Duration(1000 - (System.currentTimeMillis() % 1000)), new EventHandler<ActionEvent>() {
        @Override
        public void handle(ActionEvent event) {
            if (secondTimeline != null) {
                secondTimeline.stop();
            }
            secondTimeline = new Timeline();
            secondTimeline.setCycleCount(Timeline.INDEFINITE);
            secondTimeline.getKeyFrames().add(

```

```

        new KeyFrame(Duration.millis(500), new EventHandler<ActionEvent>() {
            @Override
            public void handle(ActionEvent event) {
                refreshDash();
            }
        });
        secondTimeline.play();
    }
}
);
delayTimeline.play();
}

public void stop() {
    delayTimeline.stop();
    if (secondTimeline != null) {
        secondTimeline.stop();
    }
}

public final void showRPM() {
    int X, count = 0, mid;
    if (rpm > 10000) {
        rpm = 10000;
    }
    for (int i = 0; i < (rpm / 100); i++) {
        mid = 0;
        Polygon polygon = new Polygon(69, 128, 74, 128, 74, 256, 69, 256);
        if ((i % 10) == 0) {
            count++;
        }
        if ((i % 50) == 0) {
            mid++;
        }
        X = (i * 9) - count - mid;
        polygon.setLayoutX(X);
        polygon.setLayoutY(i);
        if (i >= 0) {
            polygon.setFill(Color.GREEN);
        }
        if (i >= RPM_Y) {
            polygon.setFill(Color.YELLOW);
        }
        if (i >= RPM_O) {
            polygon.setFill(Color.ORANGE);
        }
        if (i >= RPM_R) {
            polygon.setFill(Color.RED);
        }
        getChildren().add(polygon);
    }
}

public final void showCTemp() {
    int Y, count = 0;
    if (coolant > CTemp_MAX) {
        coolant = CTemp_MAX;
    }
    for (int i = 0; i < (coolant - CTemp_MIN); i++) {
        Polygon polygon = new Polygon(825, 632, 885, 632, 885, 628, 825, 628);
        if ((i % 5) == 0) {
            count++;
        }
        Y = -(i * 2) - count;
        polygon.setLayoutY(Y);

        if (i < CTemp_Hot - CTemp_MIN) {
            polygon.setFill(Color.BLUE);
        } else {
            polygon.setFill(Color.RED);
        }
    }
}

```

```

    }
    getChildren().add(polygon);
}
}

public final void showAFR1(Color onColor, Color offColor, Effect onEffect, Effect offEffect) {
    afr1_digit = new Digit[3];
    for (int i = 0; i < 3; i++) {
        Digit digit1 = new Digit(onColor, offColor, onEffect, offEffect);
        digit1.setLayoutX(i * 58 + 77);
        digit1.setLayoutY(420);
        afr1_digit[i] = digit1;
        getChildren().add(digit1);
    }
}

public final void showAFR2(Color onColor, Color offColor, Effect onEffect, Effect offEffect) {
    afr2_digit = new Digit[3];
    for (int i = 0; i < 3; i++) {
        Digit digit2 = new Digit(onColor, offColor, onEffect, offEffect);
        digit2.setLayoutX(i * 58 + 77);
        digit2.setLayoutY(550);
        afr2_digit[i] = digit2;
        getChildren().add(digit2);
    }
}

/**
 * Simple 7 segment LED style digit. It supports the numbers 0 through
 * 9.
 */
public class Digit extends Parent {

    private final boolean[][] DIGIT_COMBINATIONS = new boolean[][]{
        new boolean[]{true, false, true, true, true, true, true},
        new boolean[]{false, false, false, false, true, false, true},
        new boolean[]{true, true, true, false, true, true, false},
        new boolean[]{true, true, true, false, true, false, true},
        new boolean[]{false, true, false, true, true, false, true},
        new boolean[]{true, true, true, true, false, false, true},
        new boolean[]{true, true, true, true, false, true, true},
        new boolean[]{true, false, false, false, true, false, true},
        new boolean[]{true, true, true, true, true, true, true},
        new boolean[]{true, true, true, true, true, false, true}};
    private final Polygon[] polygons = new Polygon[]{
        new Polygon(2, 0, 52, 0, 42, 10, 12, 10), //top
        new Polygon(12, 49, 42, 49, 52, 54, 42, 59, 12f, 59f, 2f, 54f), //middle
        new Polygon(12, 98, 42, 98, 52, 108, 2, 108), //bottom
        new Polygon(0, 2, 10, 12, 10, 47, 0, 52), //top left
        new Polygon(44, 12, 54, 2, 54, 52, 44, 47), //top right
        new Polygon(0, 56, 10, 61, 10, 96, 0, 106), //bottom left
        new Polygon(44, 61, 54, 56, 54, 106, 44, 96)); //bottom right
    private final Color onColor;
    private final Color offColor;
    private final Effect onEffect;
    private final Effect offEffect;

    public Digit(Color onColor, Color offColor, Effect onEffect, Effect offEffect) {
        this.onColor = onColor;
        this.offColor = offColor;
        this.onEffect = onEffect;
        this.offEffect = offEffect;
        getChildren().addAll(polygons);
        if ((speedoflag == 1)) {
            getTransforms().add(new Scale(1.28, 1.28));
        }
        if ((afrflag == 1)) {
            getTransforms().add(new Scale(0.78, 0.78));
        }
    }
}

```

```

        getTransforms().add(new Shear(-0.1, 0));
        showNumber(0);
    }

    public void showNumber(Integer num) {
        if (num < 0 || num > 9) {
            num = 0; // default to 0 for non-valid numbers
        }
        for (int i = 0; i < 7; i++) {
            polygons[i].setFill(DIGIT_COMBINATIONS[num][i] ? onColor : offColor);
        }
    }
}

// /* TESTING PURPOSES ONLY */
// public static int randomWithRange(int min, int max) {
//     int range = (max - min) + 1;
//     return (int) (Math.random() * range) + min;
// }

@Override
public void start(Stage primaryStage) throws Exception {
    init(primaryStage);
    primaryStage.show();
    play();
}

/**
 * The main() method is ignored in correctly deployed JavaFX application.
 * main() serves only as fallback in case the application can not be
 * launched through deployment artifacts, e.g., in IDEs with limited FX
 * support. NetBeans ignores main().
 *
 * @param args the command line arguments
 */
public static void main(String[] args) {
    launch(args);
}
}

```


Serial Port Code

```
package myMQPapp;

import java.io.BufferedReader;
import java.io.InputStreamReader;
import java.io.OutputStream;
import gnu.io.CommPortIdentifier;
import gnu.io.SerialPort;
import gnu.io.SerialPortEvent;
import gnu.io.SerialPortEventListener;
import java.util.Enumeration;

/**
 *
 * Edited by: Justin Paprota
 */
public class SerialTest implements SerialPortEventListener {

    //Input Speed
    public static int new_speed;

    //Input RPM
    public static int new_rpm;

    //Input Coolant Temp
    public static int new_coolant;

    //Input Air/Fuel Sensor 1
    public static int new_afr1;

    //Input Air/Fuel Sensor 2
    public static int new_afr2;

    public SerialPort serialPort;
    /**
     * The port we're normally going to use.
     */
    private static final String PORT_NAMES[] = {
        "COM12"// Windows
    };
    /**
     * A BufferedReader which will be fed by a InputStreamReader converting the
     * bytes into characters making the displayed results codepage independent
     */
    private BufferedReader input;
    /**
     * The output stream to the port
     */
    private OutputStream output;
    /**
     * Milliseconds to block while waiting for port open
     */
    private static final int TIME_OUT = 2000;
    /**
     * Default bits per second for COM port.
     */
    private static final int DATA_RATE = 9600;

    public void initialize() {
        CommPortIdentifier portId = null;
        Enumeration portEnum = CommPortIdentifier.getPortIdentifiers();

        //First, Find an instance of serial port as set in PORT_NAMES.
        while (portEnum.hasMoreElements()) {
            CommPortIdentifier currPortId = (CommPortIdentifier) portEnum.nextElement();
            for (String portName : PORT_NAMES) {
```

```

        if (currPortId.getName().equals(portName)) {
            portId = currPortId;
            break;
        }
    }
}
if (portId == null) {
    System.out.println("Could not find COM port.");
    return;
}

try {
    // open serial port, and use class name for the appName.
    serialPort = (SerialPort) portId.open(this.getClass().getName(),
        TIME_OUT);

    // set port parameters
    serialPort.setSerialPortParams(DATA_RATE,
        SerialPort.DATABITS_8,
        SerialPort.STOPBITS_1,
        SerialPort.PARITY_NONE);

    // open the streams
    input = new BufferedReader(new InputStreamReader(serialPort.getInputStream()));
    output = serialPort.getOutputStream();

    // add event listeners
    serialPort.addEventListener(this);
    serialPort.notifyOnDataAvailable(true);
} catch (Exception e) {
    System.err.println(e.toString());
}
}

/**
 * This should be called when you stop using the port. This will prevent
 * port locking on platforms like Linux.
 */
public synchronized void close() {
    if (serialPort != null) {
        serialPort.removeEventListener();
        serialPort.close();
    }
}

/**
 * Handle an event on the serial port. Read the data and print it.
 *
 * It also sets the variables to be displayed.
 */
public synchronized void serialEvent(SerialPortEvent oEvent) {
    if (oEvent.getEventType() == SerialPortEvent.DATA_AVAILABLE) {
        try {
            String inputLine = input.readLine();
            String inputBuffer = inputLine;
            char[] inputchar = inputBuffer.toCharArray();
            int i = 3;
            int j = 0;
            while (i <= inputchar.length
                && (inputchar[0] == ':')
                && (inputchar[inputchar.length - 1] == ':')) {
                switch (inputchar[i]) {
                    //for MPH
                    case 'H':
                        i++;
                        char[] mph_buff = new char[inputchar.length - 5];
                        while (inputchar[i] != ':') {
                            mph_buff[j] = inputchar[i];
                            i++;
                            j++;
                        }
                    }
                }
            }
        }
    }
}

```

```

    }
    inputBuffer = String.valueOf(mph_buff);
    System.out.print("Speed: ");
    System.out.println(inputBuffer);
    new_speed = Integer.parseInt(inputBuffer);
    System.out.print("as int: ");
    System.out.println(new_speed);
    System.out.println();
    break;
//for RPM
case 'M':
    i++;
    char[] rpm_buff = new char[inputchar.length - 5];
    while (inputchar[i] != ';') {
        rpm_buff[j] = inputchar[i];
        i++;
        j++;
    }
    inputBuffer = String.valueOf(rpm_buff);
    System.out.print("Tachometer: ");
    System.out.println(inputBuffer);
    new_rpm = Integer.parseInt(inputBuffer);
    System.out.print("as int: ");
    System.out.println(new_rpm);
    System.out.println();
    break;
//for FR1
case '1':
    i++;
    char[] afr1_buff = new char[inputchar.length - 5];
    while (inputchar[i] != ';') {
        afr1_buff[j] = inputchar[i];
        i++;
        j++;
    }
    inputBuffer = String.valueOf(afr1_buff);
    System.out.print("Air/Fuel 1: ");
    System.out.println(inputBuffer);
    new_afr1 = Integer.parseInt(inputBuffer);
    System.out.print("as int: ");
    System.out.println(new_afr1);
    System.out.println();
    break;
//for FR2
case '2':
    i++;
    char[] afr2_buff = new char[inputchar.length - 5];
    while (inputchar[i] != ';') {
        afr2_buff[j] = inputchar[i];
        i++;
        j++;
    }
    inputBuffer = String.valueOf(afr2_buff);
    System.out.print("Air/Fuel 2: ");
    System.out.println(inputBuffer);
    new_afr2 = Integer.parseInt(inputBuffer);
    System.out.print("as int: ");
    System.out.println(new_afr2);
    System.out.println();
    break;
//for ECT
case 'T':
    i++;
    char[] coolant_buff = new char[inputchar.length - 5];
    while (inputchar[i] != ';') {
        coolant_buff[j] = inputchar[i];
        i++;
        j++;
    }
    inputBuffer = String.valueOf(coolant_buff);

```

```

        System.out.print("Coolant: ");
        System.out.println(inputBuffer);
        new_coolant = Integer.parseInt(inputBuffer);
        System.out.print("as int: ");
        System.out.println(new_coolant);
        System.out.println();
        break;
    default:
        i++;
        break;
    }
}

} catch (Exception e) {
    System.err.println(e.toString());
}
}
// Ignore all the other eventTypes, but you should consider the other ones.
}

public static void main(String[] args) throws Exception {
    SerialTest main = new SerialTest();
    main.initialize();
    Thread t = new Thread() {
        public void run() {
            //the following line will keep this app alive for 1000 seconds,
            //waiting for events to occur and responding to them (printing incoming messages to console).
            try {
                Thread.sleep(1000000);
            } catch (InterruptedException ie) {
            }
        }
    };
    t.start();
    System.out.println("Started");
}
}
}

```

Arduino Code

```
//FSAE MQP CAN Bus Receive Data
//Camden Mallette
//WPI 2013-2014

#include "mcp_can.h"
#include <SPI.h>
#include <stdio.h>
#define INT8U unsigned char

unsigned char Flag_Recv = 0;
unsigned char len = 0;
unsigned char buf[8];
char str[20],HexString;
int data;

void setup(){
  CAN.begin(CAN_500KBPS); // init can bus : baudrate = 500k
  attachInterrupt(0, MCP2515_ISR, FALLING); // start interrupt
  Serial.begin(115200);}
void MCP2515_ISR()
{ Flag_Recv = 1;}
int HextoDec(UpperBit,LowerBit){
  int sum = UpperBit*256 + LowerBit;
  return sum;}
void loop(){
  if(Flag_Recv){ // check if get data
    Flag_Recv = 0; // clear flag
    CAN.readMsgBuf(&len, buf); // read data, len: data length, buf: data buf
    char ID = getCanId();
    if(ID=0x360){ // check if message contains RPMs
      Serial.println("We have RPMs!"); //Visual to say which gauge should be updating.
      data = HextoDec(buf[0],buf[1]);
      Serial.println("");}
```

```

Serial.println("RPM");
Serial.print(data);
Serial.println(";"); }

if(ID=0x370){ // check if message contains roadspeed
Serial.println("We have Speed!"); //Visual to say which gauge should be updating.
data = HextoDec(buff[0],buff[1]);
Serial.println(";");
Serial.println("MPH");
Serial.print(data);
Serial.println(";"); }

if(ID=0x3E0){ // check if message contains coolant temp
Serial.println("We have Coolant Temp!"); //Visual to say which gauge should be updating.
data = HextoDec(buff[0],buff[1]);
Serial.println(";");
Serial.println("ECT");
Serial.print(data);
Serial.println(";"); }

if(ID=0x368){ // check if message contains coolant temp
Serial.println("We have Air Fuel Ratios!"); //Visual to say which gauge should be updating.
data = HextoDec(buff[0],buff[1]);
data *= 14.7; //Convert lambda 1 value to AFR value
Serial.println(";");
Serial.println("FR1");
Serial.print(data);
Serial.println(";");
data = HextoDec(buff[2],buff[3]);
data *= 14.7; //Convert lambda 2 value to AFR value
Serial.println(";");
Serial.println("FR2");
Serial.print(data);
Serial.println(";"); } }

```